Investigations into Parameters Affecting Purity in the Oscillatory Baffled Crystallizer and Stirred Tank Crystallizer

Hannah Ruth McLachlan

Thesis submitted for Doctor of Philosophy

Heriot Watt University

Department of Chemical Engineering

January 2017

ACADEMIC REGISTRY

Research Thesis Submission

Name*:*	Hannah McLachlan		
School/PGI:	School of Engineering and Physical Sciences, Institute of Mechanical, Process and Energy Engineering		
Version: *(i.e. First, Resubmission, Final)*	Final	Degree Sought (Award **and** Subject area)	Doctor of Philosophy in Chemical Engineering

Declaration

In accordance with the appropriate regulations I hereby submit my thesis and I declare that:

1) the thesis embodies the results of my own work and has been composed by myself
2) where appropriate, I have made acknowledgement of the work of others and have made reference to work carried out in collaboration with other persons
3) the thesis is the correct version of the thesis for submission and is the same version as any electronic versions submitted*.
4) my thesis for the award referred to, deposited in the Heriot-Watt University Library, should be made available for loan or photocopying and be available via the Institutional Repository, subject to such conditions as the Librarian may require
5) I understand that as a student of the University I am required to abide by the Regulations of the University and to conform to its discipline.

* *Please note that it is the responsibility of the candidate to ensure that the correct version of the thesis is submitted.*

Signature of Candidate*:*		Date:	

Submission

Submitted By *(name in capitals):*	HANNAH MCLACHLAN
Signature of Individual Submitting:	
Date Submitted:	

For Completion in the Student Service Centre (SSC)

Received in the SSC by *(name in capitals):*			
Method of Submission *(Handed in to SSC; posted through internal/external mail):*			
E-thesis Submitted (mandatory for final theses)			
Signature:		Date:	

Abstract

Previously completed industrial trials suggested that the purity of crystals which were produced in an oscillatory baffled crystallizer (OBC) had a higher purity than those produced from the stirred tank crystallizer (STC). The results from these trials were obtained when the vessels were operated at similar experimental conditions and power densities. This thesis work initially aimed to confirm these results for a model compound (urea) and find possible scientific reasons for the noted purity differences between the two vessels. Following this the effect of the addition of a specific impurity (biuret) was investigated to see whether the OBC would still produce higher purity material and how the impurity affected the monitored system parameters.

It has been shown from the work included in this thesis, that the OBC produces higher purity crystals than the STC under comparable experimental conditions. Investigations into these purity improvements were monitored using an in-situ FTIR system and the resulting data indicated that a lower supersaturation was required to induce nucleation in the OBC. This lower supersaturation corresponded to a higher nucleation temperature within the OBC. It has been proposed that the higher supersaturation in the STC leads to an increased nucleation rate consequently producing smaller single crystals which are more likely to agglomerate. In the STC this increase in the number of agglomerates led to a decrease in purity, as more mother liquor or impurity could become trapped within the crystals.

This agglomeration in the STC was apparent at all three impurity levels investigated, with it being particularly apparent with 0 % added impurity. At this level of added impurity there was only evidence of mother liquor entrapment. Experiments completed with 5 wt. % added impurity also indicate impurity incorporation as well as mother liquor entrapment, leading to the production of more ‘cubic’ crystals with lower purities as well as agglomeration in both vessels.

Nomenclature

All symbols utilized in this thesis are presented below.

AI = Added impurity [%]

ANT = Average nucleation temperature [°C]

ATR = Attenuated total reflectance

c = Solute concentration [g ml^{-1}]

c* = Saturation or equilibrium concentration [g ml^{-1}]

C_D = Orifice discharge coefficient

CCP = Controlled cooling profile

CED = Diameter of perfect circle with equivalent area from Morphologi G3 [µm]

CSD = Crystal size distribution

D = OBC column diameter [m]

D_O = Baffle orifice diameter [m]

D_S = STC impeller diameter [m]

D_{10} = Equivalent diameter of 10 % of CSD sample [µm]

D_{50} = Equivalent diameter of 50 % of CSD sample [µm]

D_{90} = Equivalent diameter of 90 % of CSD sample [µm]

f = Frequency of oscillation [Hz]

F = Statistical ratio of two mean square values used for analysis

FBRM = Focused beam reflectance measurement

FTIR = Fourier transform infrared analysis

h = Statistical factor describing process ability to accept or reject a null hypothesis

IR = Infrared light source

L = Longest crystal projection on the major axis from Morphologi G3 [µm]

LCP = Linear cooling profile

MSZW = Metastable zone width [°C]

N = Number of baffles per unit length [m^{-1}]

N_S = Agitator (or impeller) speed [RPS or s^{-1}]

NaN = Not a number; utilized in statistical analysis

NT = Nucleation temperature [°C]

NCP = Natural cooling profile

P = Statistical probability factor

P_{KS} = Kolmogorov-Smirnov statistical probability factor

P_{KW} = Kruskal-Wallis statistical probability factor

P_o = Power number of impeller

P/V = Power density (or mixing intensity) [W m^{-3}]

Re = Reynolds number

Re_n = Net-flow Reynolds number

Re_O = Oscillatory Reynolds number

S = Supersaturation ratio

St = Strouhal number

SD = Standard deviation of averaged results

SE = Standard error of averaged results

SEM = Scanning electron microscopy

S1 = Impeller 1

S2 = Impeller 2

T_{cryst} = Nucleation (or crystallization) temperature [°C]

T_{sat} = Dissolution (or saturation) temperature [°C]

T1 = Central internal vessel temperature [°C]

u = Superficial mean velocity [m s^{-1}]

Urea1 = Initial batch of urea [89 % pure]

Urea2 = Second batch of urea [95 % pure]

V_{ST} = Volume of fluid in stirred tank [m^{-3}]

W = Crystal width – longest crystal projection on minor axis from Morphologi G3 [µm]

x_O = Oscillation amplitude [m]

α_1 = Baffle free area ratio

Δc = Concentration driving force [g ml^{-1}]

ρ = Fluid density [kg m^{-3}]

σ = Relative supersaturation

μ = Dynamic viscosity [Kg m^{-1} s^{-1}]

μ_s = Fluid viscosity [Ns m^{-1}]

ω = Angular frequency of oscillation [rad s^{-1}]

Statistical Analysis

$\bar{x}$ and $\bar{y}$ = the sample means for Students' t-test

S_x and S_y = the sample standard deviations for Students' t-test

n and m = the sample sizes for Students' t-test

y_{ij} = an observation linear model in a one-way ANOVA

i = the observation number of indicator variable *y*

j = indicative of the different group of indicator variable *y*

α_j = the population mean for the *j*th group for one-way ANOVA

ε_{ij} = the random error which is independent and normally distributed for the one-way ANOVA

D = EDF test statistic

*F*1(x) and *F*2(x) = Separate steps for Komolgorov-Smirnov statistic

H = test statistic from Kruskal-wallis Test

SS_B' = the sum of squares between groups using the ranks instead of raw data.

Acknowledgements

The author would like to thank Professor Xiong-Wei Ni for his support and input during this PhD project. Dr Cameron Brown and Dr Craig Callahan for their technical assistance during the initial stages and continuing support throughout.

Thanks to EPSRC Centre for Innovative Manufacturing in Continuous Manufacturing and Crystallisation (CMAC) for funding and equipment support. [Grant: EP/I033459/1]

The author would also like to thank her friends and family for emotional support when things got tough.

Publications

An investigation into parameters affecting crystal purity of urea in a stirred tank and an oscillatory baffled crystallizer, Co-Author – Published by Chemical Engineering Communications, 23rd February 2016

On the effect of added impurity on the crystal purity of urea in the oscillatory baffled crystallizer and stirred tank crystallizer, Co-Author – Published by Journal of Crystal Growth, March 2016

Contents

Chapter 1 Introduction

Crystallization has many important functions as a unit operation: in addition to its use as a separation process, it is also an important purification tool, particularly in the pharmaceutical and fine chemical industries (1, 2). Crystallization is broadly defined as the separation of crystalline solid particles from solution (3) and there are several different types, with cooling crystallization and anti-solvent crystallization being among the most popular in the pharmaceutical sector. In cooling crystallization, the solution temperature is lowered beyond its saturation point to induce nucleation. Whereas in anti-solvent crystallization, a second solvent is added into the system to reduce solubility and initiate nucleation. Cooling crystallization is the most common method used in industry, as it is fairly easy to control, and is consequently the focus of this project. In cooling crystallization, the rate of crystallization is often controlled by many parameters such as the mixing intensity, cooling rate, concentration, impurity profile and temperatures, to name but a few.

The use of crystallization as a purification tool is advantageous because it removes impurities from the system before any downstream processing stages occur, e.g. filtration. The production of crystals with a high purity is important in the pharmaceutical industry as any unwanted impurity can cause either side-effects (3) or a reduction in the bioavailability of a compound (4). Consequently, identifying the reasons for any decrease in purity is an essential step in research and development and production. Generally, a decrease in crystal purity is caused by mother liquor being included in product crystals (5) either through inclusion within the growing crystal or by becoming trapped between agglomerating single crystals (5). Another function of crystallization is its use in modifying the shape of the crystals produced: the removal or addition of certain impurities has been shown to alter the crystal habit of the product. This could be a useful outcome for further crystal processing within the system, e.g. improving filterability (6).

Traditionally, crystallization has been carried out in a stirred tank crystallizer (STC) which is generally a large jacketed vessel fitted with an impeller to mix the contents. This system normally runs as a batch process which can easily be operated and controlled. Depending on the type of impeller used, the STC can be prone to poor mixing and heat transfer, often due to the formation of dead zones (7) and thermal gradients. The presence of a thermal gradient means that the solution nearer the jacket is at a different temperature to the solution nearer the centre of the vessel. This leads to inconsistent crystallization environments, in turn crystal properties and problematic scaling up of crystallizers.

The implementation of both efficient mixing and improved heat transfer can lead to better temperature control and in turn cooling crystallisation processes. Both can be achieved in the oscillatory baffled crystallizer (OBC) (8-10) which is a viable alternative to the STC. The OBC is a tubular device which can be run, on a laboratory scale, as either a moving baffle or moving fluid system and be linearly scaled up to an industrial scale. Confidential results obtained from trials using industrial compounds (11) showed that when crystallization was carried out under comparable conditions, the OBC produced higher purity crystals than the STC. The motivation and aim of this PhD project is to verify these confidential results and then to seek scientific explanations for any differences observed.

The structure of the thesis is as follows; a literature review looking at the theory of crystallization and the types of crystallizers used is presented in Chapter 2, Chapters 3 and 4 discuss the experimental set-up of the systems and the analytical methods utilized for this work, Chapters 5 to 8 present and discuss the results from the research, with conclusions and possible further work related to this project presented in Chapter 9.

.

Chapter 2 Literature Review

In this chapter the background of crystallization science will be outlined including the important factors affecting nucleation and crystal growth which are relevant to this work. The previous studies on crystal purity will also be reviewed. The main features of the crystallizers will also be discussed.

2.1 Crystallization

Crystallization is an important separation process and purification tool utilized in many different industries. As a unit operation it can be used to remove impurities from a chemical system, to change the shape of crystals formed and to influence the size distribution of crystals produced. In general, control of crystallization processes requires the control of either the nucleation or growth of the crystals, or both simultaneously (12). These mechanisms are linked to the supersaturation of the solution, i.e. the driving force (13). There are different ways of achieving supersaturation, e.g. cooling, evaporative and anti-solvent crystallization; the focus for this work is cooling crystallization.

2.1.1 Supersaturation

Supersaturation is defined as the "degree of solid dissolved in a solution above the saturation level of the solution at a given temperature" (14). There are several common equations for calculating the supersaturation of a solution; these are shown below in equations 2.1 - 2.3 (15) for the concentration driving force [Δc], the supersaturation ratio [S] and the relative supersaturation [σ] respectively. The supersaturation ratio is the most commonly used term and will be adopted in this work.

$$\Delta c = c - c^* \text{ [g ml}^{-1}\text{]} \qquad (2.1)$$

$$S = {}^{c}/_{c^*} \qquad (2.2)$$

$$\sigma = {}^{\Delta c}/_{c^*} = S - 1 \qquad (2.3)$$

Where c is the solute concentration (g ml^{-1}) and c* the saturation (or equilibrium) concentration (g ml^{-1}) at a given temperature.

Supersaturation is an important parameter which can be optimized under certain system conditions, although this often occurs through a compromise with other variables. For example, a high supersaturation level gives high nucleation rates, resulting in smaller crystals

(16). This suggests that in order to produce large crystals with better filterability a lower supersaturation level is required. In fact, Doki et al. (17) noted that in systems of a low supersaturation profile, there was less evidence of secondary nucleation regardless of the cooling mode used. Maintaining a crystallizer at a temperature range which ensures low supersaturation and large crystals would minimise the yield obtained by reducing the supersaturation consumed, when in fact a high crystal yield is often required for industrial production.

The saturation (or equilibrium) concentration is the point at which the solid added becomes fully dissolved in the solvent and is often presented as the weight of solid over the volume of solvent (g ml^{-1}) (3). Generally, when the system temperature increases the weight of solid which can be dissolved in a set volume also increases (14). The saturation concentration is specific to a given temperature as well as the purity of the compound, the addition of impurity often has an effect on the saturation concentration (15) by often increasing the concentration required for nucleation. An example of a saturation curve (C*) and a MSZW curve are shown in Figure 2.1. Having knowledge of both the saturation concentration and temperature, i.e. the solubility profile, is essential to allow for control and analysis of the system. Prior to any experimental work, it is customary to confirm the saturation information in the form of a solubility curve specific to the system employed.

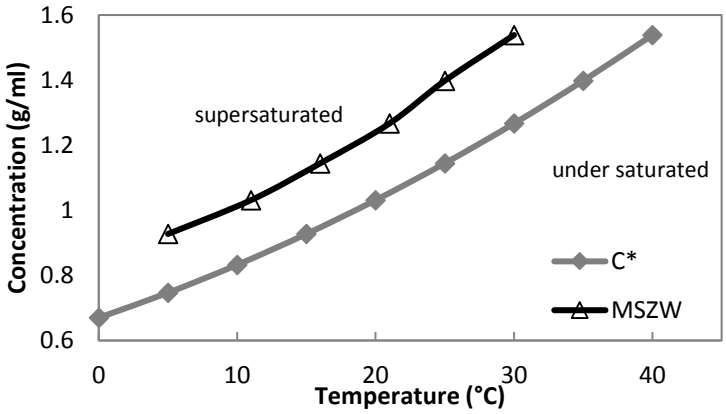

Figure 2.1 – An example concentration saturation curve (C*) and the corresponding MSZW curve

Ideally, both nucleation and crystal growth should take place within the boundary between solubility and supersolubility, i.e. the metastable zone width (MSZW) (Figure 2.1). The MSZW (equation 2.4) is the difference between the nucleation temperature [T_{cryst}] and the

dissolution (or saturation) temperature [T_{sat}] of a saturated solution, resulting from the specific characteristics of nucleation (18).

$$MSZW = T_{sat} - T_{cryst} \ [°C] \qquad (2.4)$$

When a crystalline product is created from chemical reactions and is then dissolved in solvent/solution, it is necessary to cool the solution below its saturation temperature until the critical supersaturation is reached to separate the crystal solids from the solution. At this point, the amount of solid being held in solution becomes too much and the excess solid begins to precipitate out of the solution as crystals, this point is known as the nucleation temperature. The dissolution temperature is taken as the point where the crystal solids are fully dissolved during heating. The measurement of the MSZW is mainly carried out by the polythermal method (3), in which nuclei are detected visually or instrumentally. The method of visual detection is made more difficult as nucleation is a stochastic phenomenon; meaning the probability of observing the first nuclei is very low (19). Therefore, the MSZW is often determined using a turbidity meter or FBRM, discussed in later chapters. It should be noted that it is impossible to detect true nucleation using any modern tools because the event of nucleation is too fast and the concentration of primary nuclei is too low. Consequently, only post nucleation events are monitored. The parameters which affect the MSZW include external temperature, solution concentration and history (3), cooling rate, presence of impurity and mixing (20). Supersaturation and MSZW are important factors often used to study the product specifications from industrial crystallizations through their contributions to nucleation and crystal growth. These product specifications include crystal size, size distributions (CSD), shape and polymorph (18). Two steps are involved in the formation of crystals from a saturated solution, the first is the formation of minute crystalline aggregates (nuclei), which then must grow (21).

2.1.2 Primary and Secondary Nucleation

The control of the crystallization process requires the understanding of both nucleation and growth (12). Nucleation is the process of the creation of minute particles of a new phase, i.e. nuclei, within a supersaturated homogeneous phase (14); in this case a supersaturated aqueous solution. Due to its critical location at the beginning of the crystallization process, both primary and secondary nucleation are very important within the overall crystallization process, as nucleation has been shown to determine many of the crystal properties of the emerging crystalline phase (22) including the specific polymorph of the crystals produced. It has also been noted that the speed at which nucleation occurs can have an effect on the number and final size of crystals formed. When the nucleation process is fast, many small crystals are produced simultaneously, this fast appearance depletes the supersaturation and may lead to the

termination of nucleation during the later stages of the process (23). An advantage of this is the production of a narrow, uni-modal size distribution. On the other hand, a slow nucleation rate leads to fewer crystals nucleating at the same time and therefore, the drop in supersaturation is slower. The main consequence of this is the continuous nucleation of crystals throughout the process, leading to a wide size distribution of crystals showing various sizes (22). There are two main types of nucleation: primary and secondary. Primary nucleation is the initial step in all nucleation mechanisms; secondary nucleation is generally seen as a second step and has several possible mechanisms. Nucleation can occur spontaneously within a system or it can be induced (15), for example through seeding.

Primary nucleation is defined as the formation of nuclei within a system in the absence of previously formed crystals (13) or crystalline surfaces. It can split into two different types: homogeneous and heterogeneous nucleation. Homogeneous nucleation occurs in systems where there are no solid or foreign particles present. In reality, homogeneous nucleation is very rare due to the existence of dissolved impurities and physical vessel features such as crystallizer walls and mixing apparatus (3), which can produce heteronuclei. On the other hand, heterogeneous nucleation usually occurs when dissolved impurities and dust are present within the solution. In this case it has been observed that a lower supersaturation is required for nucleation (3) than in the homogeneous system. In both cases, nucleation occurs spontaneously in the bulk of a supersaturated solution when the critical supersaturation has been reached and the metastable limit has been crossed (13). However, as previously mentioned, this metastable limit varies according to the type of nucleation, with homogeneous nucleation having a higher limit than heterogeneous, as is emphasised in Figure 2.2 (20). Therefore, the MSZW is an important parameter in the crystallization of unseeded and highly supersaturated solutions (18) where spontaneous nucleation must be considered. Several factors can affect the nucleation rate attained within the primary nucleation step, such as temperature, supersaturation, interfacial tension (15) and impurity concentration, with several affecting both homogeneous and heterogeneous. However, it should be noted that no overall trends can be drawn about the parameter effects, as the influence of each factor varies with individual systems.

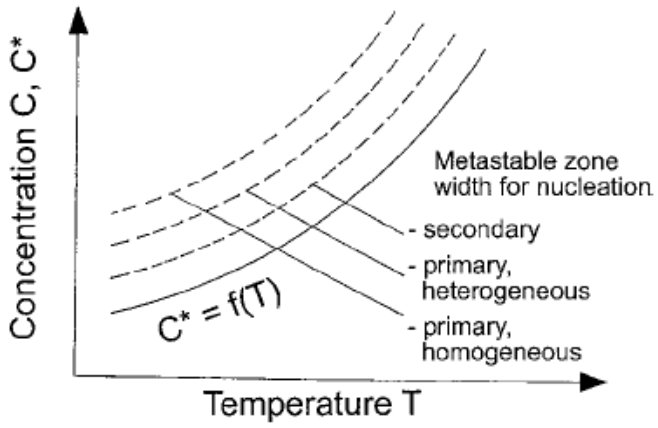

Figure 2.2 – Example of effect of nucleation method on MSZW (20)

The rate of nucleation is a very important concept that relates the number of nuclei formed to the time and volume of the system (15). This rate equation is well defined in the classical nucleation theory (15, 24) and has been shown to have a non-linear response to changes in the supersaturation, with small changes in the supersaturation inducing large changes in the nucleation rate obtained. If a fast nucleation rate is obtained, for example under high levels of supersaturation (25), this leads to the production of a large number of small crystals which depletes the supersaturation stunting crystal growth. In contrast if a slower nucleation rate is achieved, i.e. through slow cooling and a low supersaturation, fewer crystals are likely to be produced and due to a larger supersaturation available for crystal growth, will produce larger crystals. Control of this nucleation rate, through control of the supersaturation, is a key stage in achieving the correct product quality required (20).

Secondary nucleation is a heterogeneous process and is often seen as the second step in nucleation as it involves the formation of nuclei in the presence of already formed crystals or nuclei (13). In an industrial crystallizer, secondary nucleation is known to be the dominant mechanism for generating particles (26). This type of nucleation occurs at supersaturations which would not normally induce spontaneous nucleation, i.e. at temperatures within the MSZW (Figure 2.2) and is mainly induced by mechanical impacts on the crystals already suspended in solution via initial surface breeding, needle fracture, shear and attrition or collision breeding. Initial surface breeding only occurs when a crystal is first introduced into a solution and has been attributed to the presence of crystal dust on the surface which is then 'washed' off and grows as a new individual crystal (27). Needle fracture generally transpires in highly supersaturated solutions (27) and occurs when new nuclei are formed by growths, called needles, detach from the surface of already formed crystals (13) as a result of mixing, etc. Shear breeding produces nuclei through shear effects on the crystal surface, e.g. by flowing the

solution past a crystal face at a sufficient enough rate to produce secondary nuclei through shear forces (14).

The final type of secondary nucleation introduced here is collision or attrition breeding. This type of nucleation takes place readily in agitated solutions, where a crystal collides with another solid body in a supersaturated solution (27) causing direct crystal breakage leading to the production of several small, often rough, crystals which offer more sites for crystal growth. For the systems used within this research, these 'solid bodies' include the vessel walls, any stirrers and baffles present for mixing, as well as any other crystals within the solution (14). In fact, for materials of high solubility within agitated vessels, collision breeding has been recognised as the most significant nucleation mechanism (14). It should be noted that the exact source of the secondary nuclei produced is very difficult to identify (3), as several of the aforementioned mechanisms could occur simultaneously. The rate of this secondary nucleation is controlled by several processes including generation of secondary nuclei on or near a solid phase, removal of clusters and growth to form a new phase (3). These processes are mainly affected by the supersaturation, with the rate of cooling, impurity concentration and degree of agitation also having an effect.

The main means to induce secondary nucleation in industrial processes is through direct seeding of the system. This generally involves adding relatively pure 'seed' crystals into a supersaturated solution at a temperature where nucleation would not normally occur (3). One of the main advantages of this mechanism is that the supersaturation of the solution is kept constant post-seeding (28), which can help to stabilise the system and reduce batch-to-batch variations (29). Seeding has been shown to effectively remove the primary nucleation step in crystallizers (30) and this can lead to more control over the crystallization process, e.g. the preferential production of specific polymorphs (31) and improvements in the size distribution (28, 32) and shape of the crystal produced, in turn leading to an increase in the purity achieved.

2.1.3 Crystal Growth

Some understanding of crystal growth is important along with a comprehension of nucleation as it often controls the final crystal size distribution of the system. The conditions and rate of crystal growth also have a significant effect on the product purity and crystal habit produced (3). Once stable nuclei have been formed in a supersaturated or supercooled system, by primary or secondary nucleation, they begin to grow into crystals of visible size through crystal growth mechanisms. It is generally believed that direct control of nucleation is difficult, especially if primary nucleation is the main mechanism; therefore controlling the crystal growth stage is

important (12). The main mechanisms for controlling crystal growth are through secondary nucleation by seeding and again, through the control of the supersaturation of the solutions.

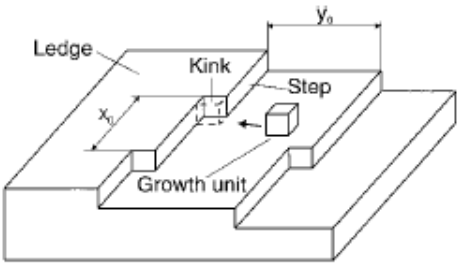

Figure 2.3 – Schematic of crystal growth faces (3)

As crystal growth proceeds, supersaturation is consumed by the growing crystals present in the solutions (28). In these supersaturated solutions, a crystal surface is exposed and growth units present in the solution are in constant flux moving towards and away from this surface; for crystal growth to occur the number of growth units joining the surface must be higher than those leaving (14). These growth units can be atoms, ions or molecules. In a three dimensional crystal, there are three types of faces (3) to which a growth unit could attach, as shown in Figure 2.3: the kinked faces, which contain three possible intermolecular bonds; the stepped faces, which consist of two possible bonds and are moving layers of monatomic height; and the flat (or ledge) face which comprise of just one surface bond (15). In addition to these sites, there are likely to be loosely absorbed growth units on the crystal surface as well as vacancies in the surfaces and steps (15). Growth units are more easily incorporated at the kink sites due to the availability of three possible intermolecular bonds and as more growth units are added, the kink sites move along the step surface unit, until the crystal face has completely been covered (33).

With ideal crystal growth, the number of growth units attaching to each surface are assumed to be equal. This suggests that all crystal faces will grow at an equal rate and that the final crystal will have exactly the same habit as the initial crystal produced; an example of this is shown in Figure 2.4. This is unlikely to happen, particularly under industrial conditions which have been shown to produce crystals with different surface growth rates than those produced at a lab scale (34).

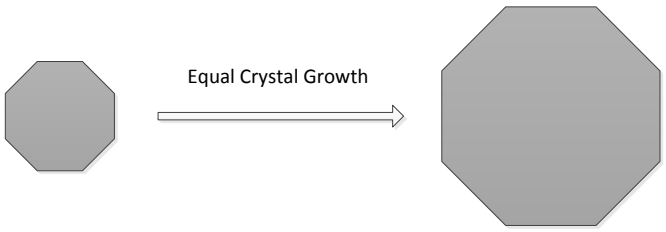

Figure 2.4 – Ideal crystal growth

The main mechanisms behind crystal growth are based on adsorption layer theories (15) which imply that when growth units arrive at the crystal face they are not immediately integrated into the crystal lattice. Instead, they are free to move over the whole crystal face leading to a loosely adsorbed layer of growth units at the interface between the bulk solution and the crystal surface. This adsorption layer can play an important role in both crystal growth and secondary nucleation.

The main methods of crystal growth include continuous growth, surface nucleation and spiral growth. Continuous growth occurs when the energy required to roughen the surface is low, which suggests that the surface of the crystal contains several kink and step sights for growth. This indicates that every growth unit which arrives at the surface will find an available growth site (14). When surface nucleation is present, the roughness of the crystal surface decreases and therefore, some growth units arriving at the crystal surface are unable to find a suitable growth site. The growth units which cannot find a suitable site either return to the fluid phase or join other previously absorbed units to form surface 'islands' (14). The final type of crystal growth discussed here is spiral growth which is thought to occur when the crystal surface is initially flat and contains no growth sites. Therefore growth can only take place through exploitation of some in-built crystal lattice defect, often due to screw dislocations. Most crystals contain dislocations (15) which are often the result of stresses that occur during crystal growth, particularly around liquid inclusions (14). The dislocation then results in one part of the crystal lattice becoming misaligned, screw dislocations then emerge on the growing crystal face. These are characterised by steps which can then be used as addition sites for growth units (14). For this mechanism to succeed the emerging step must only cover a section of the surface and during growth it should wind up into a spiral, creating a growth 'hillock', see Figure 2.5. Since a completely smooth face never appears under spiral growth, the crystal behaves as if its surface were covered with kinks (15). Therefore growth continues uninterrupted until the supersaturation has depleted and no further growth can occur.

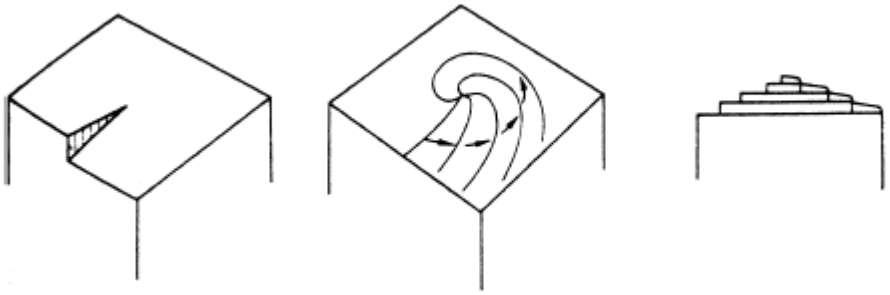

Figure 2.5 – Development of spiral growth (15)

Certain aspects of crystal growth from aqueous solutions are well known and agreed upon; these include the fact that a crystal which grows under constant external conditions, i.e. supersaturation and cooling rate, remains very nearly, geometrically similar to its original shape (21). It is however important to note that different faces of the same crystal usually have different growth rates. Although determining the exact mechanism and the order of attachment for a particular face is difficult, it has been noted that the rate of growth is a function of the supersaturation of the bulk solution in direct contact with that face at any given time (21). For the growth of perfect crystals it is important that no un-wanted impurities are present within the system. The presence of these impurities could lead to the crystal growth mechanisms acting on them instead of the nuclei formed through nucleation. They may also affect the crystal growth rate which will be discussed later in the section on impurity.

The crystal growth rate generally measures the rate at which either its mass or one of its dimensions changes with time (14) and to differentiate between the different crystal faces which may change at different rates it is common to give this rate relevant to a specific face. As with the nucleation rate, the growth rate is dependent on the supersaturation available, with the growth rate increasing as the supersaturation level increases (35). However, the mechanism of crystal growth can also have an effect on the growth rate of the system (20). As the growth rate obtained is often face specific, it can be utilized to give an idea of crystal shape as discussed above.

As mentioned, crystal growth is an important factor due to its use in controlling the crystallization process and its effect on crystal habit, yield and size distribution. Hence, the crystal growth and supersaturation can be used as methodologies to obtain the ideal outcomes of these crystal attributes.

2.1.4 Effect of Cooling Profile

In cooling crystallization, the driving force for separation is the difference in concentration between the current temperature and the saturation temperature (36), i.e. the supersaturation. A predetermined temperature profile is commonly utilized in cooling crystallization (13) and it has been proved that different cooling profiles imposed onto a solution control the supersaturation generated (37). As well as the cooling profile, the rate of cooling has an effect on the crystallization (25). The vessel temperature in a batch crystallizer is usually controlled by the temperature and flow rate of a coolant moving through a jacket (38) which means that the cooling rate is a function of both flow rate and temperature.

2.1.4.1 Type of Cooling Profile

The cooling profile is defined as the variation of the temperature of the crystallizing medium over time (37) and is generally applied in a predetermined manner. For cooling crystallization, three types of cooling profiles are routinely used: the natural cooling mode (NCP), the controlled cooling mode (CCP) and the linear cooling mode (LCP), an example of each is shown in Figure 2.6.

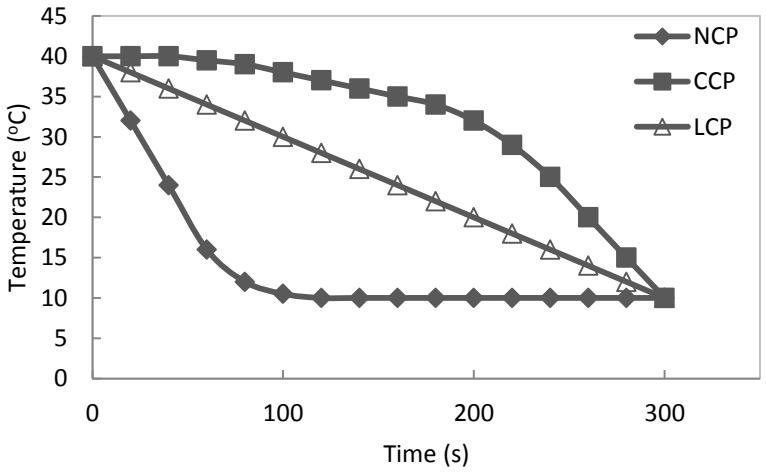

Figure 2.6 – Examples of different cooling profiles; natural cooling (NCP), controlled cooling (CCP) and linear cooling (LCP)

Natural cooling is the simplest and one of the most common cooling modes used, as it requires no external temperature control (39). An example of a natural cooling profile is shown by the NCP curve in Figure 2.6. However, the crystallization is generally uncontrolled (40) and it has never been believed to be optimal for obtaining the desired large crystals (17). This is probably due to the large supersaturation peak produced at the start of the crystallization (39) when the temperature drops quickly and then as the temperature stays constant at a lower

value, the supersaturation remains unchanged. This high supersaturation peak increases the nucleation rate throughout the process and leads to a bi-modal crystal size distribution (CSD) with large numbers of both small crystals (39) and larger crystals. As there is no control over the temperature drop or supersaturation produced, a natural profile is undesirable when the primary objective is to obtain the optimum CSD and crystal yield.

Controlled cooling has long been thought to be the optimal cooling profile for batch crystallization (17). When employing this profile, the temperature drop initially occurs very slowly and then the cooling rate increases (CCP in Fig. 2.6) as time proceeds and the crystal surface area in the suspension increases (41). This cooling profile is carried out to ensure that the supersaturation level is kept at a low and almost constant level, with the concentration kept within the metastable zone throughout crystallization. One disadvantage of this cooling profile is that it is could lead to a bi-modal CSD; however unlike the natural cooling CSD, the controlled system is likely to contain an increased number of large crystals, because secondary nucleation can more effectively be supressed (17) due to the lower supersaturation available in the seeded systems tested. Another feature of this cooling profile is that primary nucleation has been observed to occur at a much lower supersaturation level than when using a linear or natural cooling profile (42). In fact due to the very low initial cooling rate the supersaturation profile increases very slightly at the start, it then remains constant as the temperature is slowly reduced, before decreasing quickly when the final faster temperature drop occurs (39). While this profile has been shown to be optimal in terms of supersaturation levels, it is very hard to control and difficult to implement in industry, therefore it is rarely used and will not be applied within this research project.

The final approach to cooling, which will be used in this research, is the linear cooling profile (LCP in Fig. 2.6). In linear cooling the temperature is decreased at a constant pre-determined rate throughout the process with respect to time (40). This means that as the temperature drops at a constant rate (39), so does the corresponding dissolved solids concentration. Since the solubility curve of the solution is rarely a straight line, this leads to an initial high supersaturation level which in unseeded systems may cross the metastable limit to produce many small nuclei (36), though this high level is lower than that produced under the natural cooling profile (39). It should be noted that this 'peak' in supersaturation cannot be avoided in unseeded crystallization, but its height can be minimised through use of either the linear or controlled cooling profile (36). As the small nuclei are produced, this consumes the supersaturation, which leads to reducing the supersaturation profile, i.e. the concentration re-entering the metastable zone and remaining there (37) until the end of the experiment, an example of such a concentration profile is shown in Figure 2.7. This profile produces a uni-modal

CSD which contains small amounts of both small and larger crystals, with the majority of crystals being the same medium size. This cooling profile gives more control over the process and better results than the natural profile but is not as good as the controlled cooling system in terms of the supersaturation profile produced.

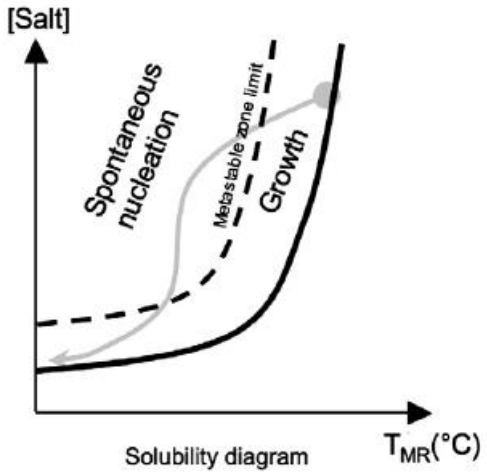

Figure 2.7 – Concentration profile (Grey line) of an example linear cooling profile

2.1.4.2 Effect of Cooling Rate on Varying Supersaturation Levels

In cooling crystallization, the supersaturation of a pre-prepared solution is generated by the degree of cooling to be applied; the rate of cooling can determine how long the solution spends in or out of the metastable zone. In highly supersaturated solutions the nucleation rate is generally predominant over the growth rate (37), when a fast cooling profile is applied to these solutions, this promotes spontaneous primary nucleation, giving small crystals. To try and reduce the number of small crystals produced, a slow cooling rate is preferable to limit the amount that the concentration crosses the metastable limit (37), thus minimising the supersaturation peak. These slow cooled systems were shown to crystallize more rapidly and were less likely to agglomerate than similar rapidly cooled systems (43). The production of single crystals shortens the time required for downstream processing and also leads to a narrower crystal size distribution often with larger mean crystal sizes. These single crystals are also purer with fewer inclusions.

In systems with a low supersaturation level, less secondary nucleation was observed regardless of the cooling rate or profile used (17). In fact if the supersaturation level is low enough, secondary nucleation can be neglected altogether, as the concentration profile never leaves the metastable zone after the first crystals have appeared (17). This low supersaturation

results in the slow growth rate of crystals and long batch times, meaning that the cooling rate must be decreased to allow any significant level of crystal growth (44).

Cooling rate can also have an effect on the purity of crystals to be harvested. When a higher cooling rate is used, the purity of the crystals has been shown to decrease compared to those produced with slower cooling rates (25, 45). This effect is especially pronounced in the stirred tank crystallizer (STC), when compared to the oscillatory baffled crystallizer (OBC). The reasons for this difference are largely unknown and have formed the main focus of this research.

2.1.5 Purity

One of the most important requirements for commercial crystal production is purity (46), in the pharmaceutical industry any unwanted impurity could cause either side-effects (3) or reduction in the bioavailability of a compound (4). Therefore it is important to understand the effects impurities can have on the crystallizing system, as well as some knowledge of possible ways to enhance the purity.

2.1.5.1 Effects of Impurities

There are two main types of impurity; the first type is impurities which are undetected within the system and are often formed when mother liquor adheres to crystal surfaces and becomes trapped within the growing crystals, these are frequently impossible to remove from the crystal (5), lowering the crystal purity. The second type of impurity is those which are intentionally added into the system to affect the growth and to investigate specific impurity effects. This is the type of impurity work which is commonly discussed in literature. Given the importance of crystal growth on the system, it is important not only to identify the sources of any impurities present, but also to understand the mechanisms behind their role in the crystal growth process (47).

It has been noted that the growth rate of a crystal can dramatically be reduced by trace amounts of certain additives or impurities (33, 48, 49) leading to an increased process time, as well as the production of non-ideal crystals which affect the downstream processing of the product, e.g. by lowering filterability. The habit of the crystal, which is the overall external shape of the crystal, can also be disrupted by impurity addition due to specific impurity effects on individual crystal faces. Impurity addition also has an unwanted effect on the MSZW, making the MSZW either wider or narrower (50), depending on the type and amount of impurity being added into the system.

Adsorbed impurity molecules are often not the only type of impurity present within the system; even when no solid impurity is added into the system, crystal growth can still be inhibited by trapped mother liquor. Crystals generally contain foreign impurities of some sort, whether solid, liquid or gas. These pockets of impurity are called 'inclusions' (15), with specific added impurity molecules known as solid inclusions, while trapped mother liquor are known as liquid inclusions. There are two types of inclusions, type 1 and type 2 (5), shown in Figure 2.8. Type 1 inclusions occur when a foreign molecule, either an impurity or mother liquor, adsorbs onto the crystal surface and stays there, eventually becoming incorporated into the crystal (33). Type 2 inclusions take place when the foreign molecule becomes trapped between several primary crystals which are joined together by agglomeration (51), generally this inclusion type is randomly distributed throughout the crystal (15). Inclusions happen more regularly in fast growing or large crystals than slowly grown or smaller scale crystals (15). Often these inclusions cannot be removed from the product crystals and the impurities become part of the newly formed crystals.

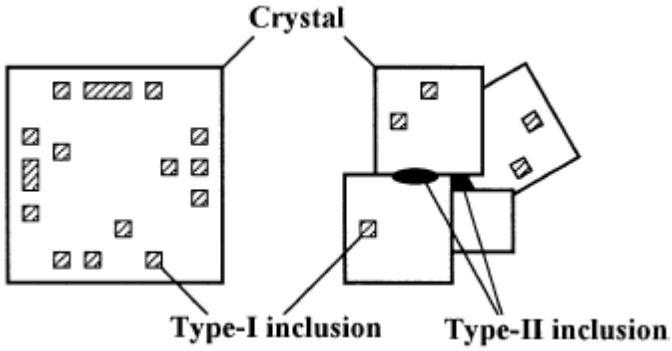

Figure 2.8 – Graphical representation of the two different types of inclusions formed during crystallization (5)

This aforementioned effect on crystal growth rate is thought to be due to the adsorption of impurities onto the crystal surface. As discussed in Section 2.1.3, during growth from pure solution solute molecules reach the crystal surface and stay there for a certain length of time before they re-dissolve into the solution. However, during the adsorption process of impurities, the impurity molecules constantly collide with the solute molecules on the crystal surface and their movement is somewhat restricted (52). This means that the impurity molecules spend longer at the crystal surface effectively blocking the growth sites and inhibiting the crystal growth. The same preferred kink and step sites are used for the adsorption of both the solute molecules and the impurity molecules (52), often leading to modification of the crystal habit

(47). The growth suppression characteristics of an impurity are expected to depend on the size, shape and orientation of the impurity molecule compared to the crystal surface (48). This is a stereochemical effect and has a direct impact on the effectiveness of the impurity particle. For example, if an impurity particle with the exact size, shape and orientation of the growth site adsorbs onto the crystal surface, the blocking effect of that impurity would be greater than if a particle with different characteristics was adsorbed. If the adsorption of these impurity molecules onto the crystal surface is irreversible, these molecules will be incorporated into the growing crystal lattice (50), shown as Type 1 inclusions in Figure 2.8. As a result, inclusions, both type 1 and 2, are frequent sources of problems in industrial crystallization (15).

The habit of a crystal can play an important role in the processability of product crystals especially in pharmaceutical raw materials (53). In industry selected impurities have been used to change the shape of crystals and to consequently improve the quality of the crystalline products, powders or granular materials (48). In some cases even minute traces cause large changes in the crystal habit (54). This occurs because the concentration of active growth sites on the crystal surface is low and therefore any additives or impurities added can exert significant effects even at low concentrations (14). However this is not always the case, sometimes habit modification only occurs in the presence of large quantities of impurity in the crystallizing system, for example in the system with dissolved urea and biuret (the impurity), more than 5 wt. % of the impurity must be added to change the habit of the urea crystals from needle-like to cubic (54).

The morphology and shape of a crystal depend greatly on the growth rates of the different individual faces of the crystal; this is governed by the crystal structure and defects present on that particular growing face, as well as the conditions of the growth medium used (15). The change in morphology when impurity is present can arise due to the selective adsorption of impurity components onto a particular face (14). The result of such surface-specific adsorption processes is often a change in the morphology of the crystal. The difference in impurity effects between different crystal faces takes place due to the differences in growth rates of specific crystal faces. Some crystal faces show very fast growth and have little effect on the growth form, unless these are inhibited and the growth is slowed. This is because the slow growing faces exert much more influence on the crystal morphology (15). Specific adsorption onto the fastest growing faces is shown in Figure 2.9, where the modification of crystal habit from a needle crystal to one of a more equal shape is observed. This habit modification is similar to that occurring in urea with the addition of the impurity biuret; the compounds used in this research, which will be discussed later in Section 3.3. It has been noted that a crystal surface

almost completely covered by impurity molecules results in the complete retardation of growth (50).

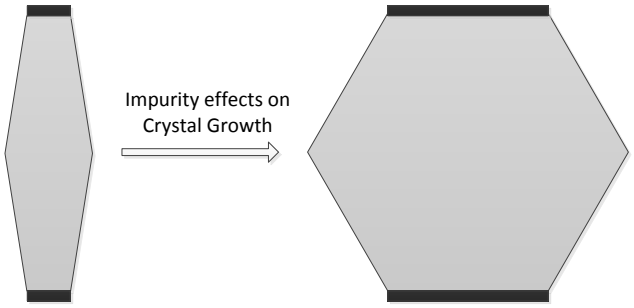

Figure 2.9 – Example of the change in crystal habit following the addition of impurity

2.1.5.2 Methods to Enhance Crystal Purity

When unwanted impurities are present in a crystallizing system, certain measures can be put into place to minimise impurity uptake and enhance the crystal purity. Success has been achieved in the enhancement of crystal purity through control of process variables such as mixing intensity and cooling rate (45). The mixing intensity has been shown to have an effect on purity through the processes of agglomeration and crystal breakage, which is discussed later. When a low stirrer speed was used it was observed that crystal agglomeration occurred, trapping mother liquor and impurities within the agglomerating crystals (25), i.e. type 2 inclusions (5). When the agitation was increased to a moderate rate, the agglomerates formed were smaller in size and contained fewer single crystals. This suggested that the amount of mother liquor trapped was reduced, indicating that increasing the agitation rate leads to a decrease in impurity uptake (25). Upon further agitation however the resulting crystals showed a decrease in purity, as the mother liquor became unavoidably stuck to the smaller and broken crystals with larger and rougher surface areas (25). This implies that within each system there is an optimal mixing intensity which produces agglomerates at a minimum size, but does not lead to excessive crystal breakage.

Along with the mixing intensity, the rate of supersaturation generation through cooling has an effect on the purity of crystals produced. It has been shown that the formation of crystal inclusions (type 1) and the entrapment of mother liquor (type 2) increased as the cooling rate increased, which led to a drop in crystal purity (45). This increase was possibly due to the increased rate of supersaturation generation noted at the higher cooling rate.

As well as keeping the supersaturation low, the possibility of controlling type 1 inclusions through control of the solubility has been investigated (45). This involved the use of chemical variables to affect the solubility and cause changes in the solution thermodynamics of dissolved species (45). By changing or modifying the mother liquor to one which has a higher solubility value for the impurity than the wanted product, the wanted product should become less soluble and therefore 'salt-out' or leave the dissolved state before the impurity under the process conditions. In this type of system the impurity often stays dissolved in the mother liquor until it is removed at a later stage post-crystallization.

It can be concluded that the manipulation of crystallization process variables is a viable tool in limiting the unwanted impurity levels with the crystallizing system. This occurs through control of the supersaturation, the amount of agglomeration and solubility behaviour. It should be noted that in this research project control of the supersaturation through the cooling rate and agglomeration through mixing intensity are investigated as process variables. Furthermore, any "optimum" conditions identified for limiting impurity uptake depend strongly on the particular system being used.

2.2 Crystallizers

Batch crystallizers are widely used vessels in crystallization, generally having a simple flexible design and often requiring less capital investment than continuous units (14). In batch processes external mixing must be provided in order to promote heat or mass transfer, or even simply to maintain uniform conditions for crystallization (9).

In this research project an oscillatory baffled crystallizer (OBC), as well as a traditional stirred tank crystallizer (STC) will be utilized to investigate the differences in crystal purity at various operating conditions. This section aims to outline the fundamental principles of these crystallisers and associated parameters.

2.2.1 Stirred Tank Crystallizers

A stirred tank crystallizer (STC) is generally designed as a round bottomed vessel where heating and cooling is often applied through a jacket (15). Mixing is achieved through the addition of a stirrer unit, frequently an over-head stirrer, which is attached to an impeller shaft to mix the fluids within the vessel; a schematic is shown in Figure 2.10. The main challenges in a traditional batch STC include obtaining good mixing and heat transfer (9), as the circulation rate must be high enough to maintain total suspension of any crystals present (3) but not too high to cause vortices and lead to excessive crystal breakage, as mentioned in Section 2.1.5.2. Mixing can be promoted by the addition of static baffles in STC (9). However, non-uniformity has been shown to occur even when turbulences are achieved in the STC; and get worse when the vessel size increases, giving rise to large mixing gradients during industrial operation (55). The use of continuous STCs is often used in industry is generally through either several tanks in series or a MSMPR system. MSMPR is mixed-suspension, mixed-product removal system where after a hold time, the products are removed and the reactants inputted into the vessel at the same rate.

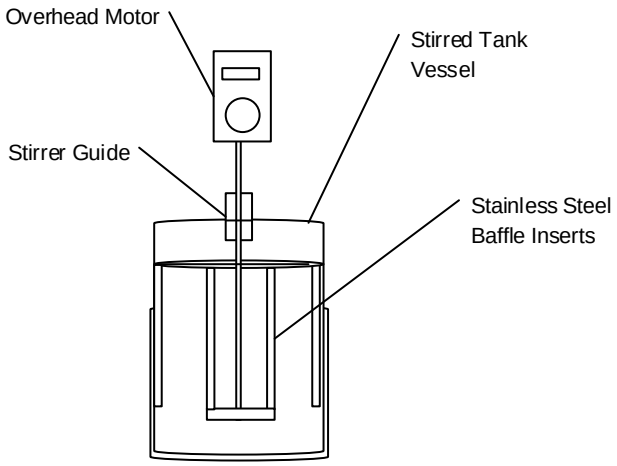

Figure 2.10 – Schematic of a typical stirred tank crystallizer

Poor heat transfer within the vessel is another consequence of this non-uniformity and this means that the outer edges of the reaction liquid (those nearest the jacket) are generally at a different temperature to the centre of the vessel (56); transferring the heat produced from the jacket into the centre is not easy with any real speed (45). A lag time can consequently occur elongating the crystallization time and disrupting the crystallization, e.g. nucleation may occur around the outer edges of the vessel before the centre (57), which depending on vessel size could lead to unwanted seeding of the supersaturated solution (28).

It has be shown that when a higher stirrer speed is used in the STC, the number of impurity inclusions present in the product crystals are higher than in crystals produced using lower stirrer speeds (46, 58). As the stirrer speed is increased within STC, the energy input for crystal-crystal, crystal-impeller and crystal-wall collisions is high, which then raises the nucleation rate (58) through collision breeding. This would lower the MSZW; the potential effect of this is likely to be unwanted nucleation of a system when temperature variations exceed the MSZW boundary.

Within the STC the controlling dimensionless number is the Reynolds number, equation 2.5, which is related to the impeller. This number influences the fluid friction and heat and mass transfer within the system; with a higher value indicating improvement in these parameters as the system enters the turbulent mixing regime.

$$Re = \frac{\rho N_S {D_S}^2}{\mu_S} \qquad (2.5)$$

Where ρ = fluid density [kg m^{-3}], N_s = agitator speed (RPS or s^{-1}), D_s = impeller diameter [m] and μ = the fluid viscosity [Ns m^{-2}].

In order to compare the performance of different vessels, mixing conditions for both vessels were selected so that the power density or dissipation rate is approximately equal. The power density of a crystallizer is defined as the "time averaged power dissipation divided by the system volume" (8). For the STC determinations of this have been well documented (59), and can be calculated using equation 2.6.

$$\frac{\mathrm{P}}{\mathrm{V}} = \frac{\mathrm{P_O}\rho \mathrm{N_S^3 D_S^5}}{\mathrm{V_{st}}} \quad [\mathrm{W\ m^{-3}}] \qquad (2.6)$$

Where P/V = the power density or mixing intensity [W m^{-3}] and V_{ST} = the volume of fluid within the stirred tank [m^3]. P_O = the power number of the impeller (60), which varies with the impeller type and is obtained from literature. It should be noted that the other parameters are the same as those used in equation 2.5.

The STC has been utilized for crystallization for many years and consequently there is a large body of research in connection with the nucleation, growth and purity effects in the STC. Within un-seeded systems, nucleation has been shown to occur sporadically (31). Due to this, large batch-to-batch variations can occur (61) leading to a serious problem (62) especially in industry. The rate of production of these primary nuclei also has an effect on the secondary nucleation and consequently the growth rate of the system. Due to the differences between vessel and impeller diameter, mixing gradients can occur within the vessel when the region close to the impeller is 'better' mixed than the outer edges, any nuclei located here are likely to undergo more crystal breakage than those in the poorly mixed regions (3). This could lead to a higher rate of secondary nucleation at the centre producing smaller crystals throughout the process. Another consequence of the mixing gradient is the production of agglomerates in the poorly mixed outer edges. Here, single crystals are likely to 'stick' together during the process as they are in close contact and are not likely to be moved apart (51), resulting in a large size distribution. This large size distribution is generally unwanted (63) and often has an effect on the final purity, generally lowering the value obtained. This is probably due to a combination of effects, with the smallest crystals having a rough surface to which impure mother liquor often sticks (3, 25) and the largest agglomerates trapping mother liquor between the single crystals (25).

The addition of seeds is a widely used methodology for minimising primary nucleation (20). The addition of seeds lowers the supersaturation required to nucleate (20) and therefore reduces the effect of the cooling rate and supersaturation on the system, adding a degree of control to the crystallization process.

2.2.2 Oscillatory Baffled Crystallizers

An oscillatory, or pulsed, flow system offers improvements to the traditional stirrer unit, in terms of heat and mass transfer, multiphase mixing and particle suspension (9).

The OBC is a form of mixing technology in which the fluid is oscillated inside a cylindrical, tubular vessel containing several periodically spaced orifice baffles (64). By combining the oscillating fluid with the periodically spaced baffles, baffle spacing is often 1.5 times the tube diameter (1.5D). This vigorous eddy mixing can be achieved between the baffles at any given time, as shown in Figure 2.11 (65). These periodically formed vortices (eddies) can then be controlled through a combination of geometrical and operational parameters, including baffle diameter, spacing and oscillation frequency and amplitude (66). This then leads to conditions similar to plug flow mixing in a continuous system, while more uniform mixing is obtained in a batch system. (67). An advantage of the OBC is that control of the mixing can be achieved independently, through variation of the amplitude and frequency of the oscillation, which is separated from the bulk flow rate of any moving fluid in a continuous system (9, 65).

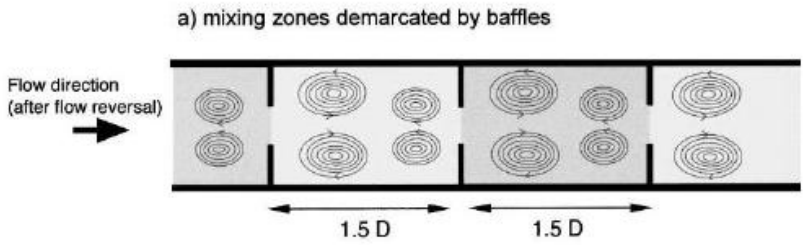

Figure 2.11 - Possible location of eddy formation in OBC (65)

Oscillatory flows are often characterised by a set of three different dimensionless numbers: the oscillatory Reynolds number (Re_o) and the Strouhal number (St), which are used in both batch and continuous modes; and the net flow Reynolds number (Re_n) which is only utilized in the continuous oscillatory baffled crystallizer (COBC). The oscillatory Reynolds number, equation 2.7, governs the fluid mechanical conditions for a specific baffle geometry, assuming a sinusoidal velocity profile is present (66). Essentially, it describes the intensity of mixing being applied to the column.

$$Re_o = \frac{\rho D x_o \omega}{\mu} \qquad (2.7)$$

Where D = the column diameter [m], ρ = the fluid density [kg m^{-3}], μ = the dynamic viscosity [kg m^{-1} s^{-1}], ω = the angular frequency of the oscillation [rad s^{-1}] = 2πf (where f = the frequency of oscillation [Hz]), and x_o = the oscillation amplitude [m].

The Strouhal number is the ratio of column diameter to stroke length, Equation 2.8 (65), and is a measure of the effective eddy breeding (66). The Strouhal number, along with the oscillatory Reynolds number, controls the fluid mechanical conditions within the OBC.

$$St = \frac{D}{4\pi x_o} \qquad (2.8)$$

Where D = the column diameter [m] and x_o = the oscillation amplitude [m].

For batch OBC systems, there are two methods of generating oscillation: the moving baffle and the moving fluid. In the moving baffle system (mb-OBC), oscillation is obtained by moving a set of orifice baffles up and down the column through a stationary fluid. In contrast, within the moving fluid system (mf-OBC) the fluid is moved through a set of stationary baffles by a motor and bellows unit located at the base of the column.

It has been shown that the addition of oscillatory flow to a baffled tube can significantly enhance the heat transfer obtained in both the batch and continuous systems (9, 68). In the OBC, this heat transfer is actually better than that achieved under turbulent flow in the STC for a given power input (10, 68, 69). This improved heat transfer means that obtaining a linear cooling rate in crystallization is easier in the OBC.

As a result of the improved mixing and heat transfer within the OBC, a reduction in the MSZW is obtained in this system (70) compared to the STC at comparable conditions. It has also been shown that the OBC system is easier to control than the STC, generally producing crystals with more consistent properties (9), e.g. smaller size distributions, improved purities, crystals with fewer defects and a greater regularity in shape (70). These improved properties lead to higher purity crystals than those containing defects and agglomeration (14, 25, 45, 63). However there is one disadvantage to the batch OBC system, due to the higher surface area of solution in contact with the walls and mixing apparatus, high mixing intensities can lead to increased crystal breakage through constant mixing of the system, especially in a batch system. This can lead to a reduction in the mean crystal size which could lower the purity produced by increasing the crystal surface area available for impurity attachment (25).

As mentioned above, to allow direct comparison between the STC and the batch OBC similar values for the power density (mixing intensity) will be utilized. For the batch OBC the power density can be calculated from equation (2.9) (8).

$$\frac{P}{V} = \frac{2\rho N(1-\alpha_1)^2}{3\pi C_D^2 \alpha_1^2} x_o^2 \omega^2 \quad [W\ m^{-3}] \qquad (2.9)$$

Where P/V = the power density or the mixing intensity [W m^{-3}], ρ = the fluid density [kg m^{-3}], N = the number of baffles per unit length [m^{-1}], C_D = the orifice discharge coefficient (which is usually 0.6) and α_1 = the baffle free area ratio, which is the ratio of the effective baffle orifice area to the tube area $\left(= \left({}^{D_o}/_{D}\right)^2\right)$ where D_o = the orifice diameter [m] and D = the column diameter [m]. The other specific oscillation parameters required are x_o = oscillation amplitude [m] and ω = the angular frequency [rad s^{-1}]; ω = 2πf, where f = the frequency of oscillation [Hz]. The oscillation amplitude is the centre-to-peak amplitude of the baffle string.

The continuous OBC (COBC) operates in a similar method to the moving fluid batch system, but with an input and output. The net flow component effectively 'pushes' the solution through the system (9) and near plug-flow mixing can be achieved in the COBC (9). The oscillatory Reynolds number (Eq. 2.7) and Strouhal number (Eq. 2.8) together with net flow Reynolds number, Eq. (2.10), are relevant for the continuous mode and the latter is defined as (65).

$$Re_n = \frac{uD}{\mu} \qquad (2.10)$$

Where u = the superficial mean velocity [m s^{-1}], D = column diameter [m] and μ = the dynamic viscosity [kg m^{-1} s^{-1}].

In the COBC, for the full effect of the eddy cycle to be realized it is usually necessary for the oscillatory flow to be the dominant flow, $Re_o > Re_n$ (65).

Utilizing continuous modes of crystallization has many advantages over batch operation, including more efficient use of compounds, energy and space as well as minimising reactor downtime due to cleaning (55). For the best results from the COBC the conditions should be set so that the space between each pair of baffles is operating as a well-mixed individual stirred tank (55). It is therefore apparent that the operation of many stirred tanks in series produces conditions which are much closer to plug-flow (55). Previous work using the COBC for crystallization (55, 71) has shown improvements in control over the system and consequently shorter experimental durations. This additional control has led to the production of consistent

crystal size and morphology along with improved CSDs when compared to the STC system. In this work, a batch STC and a batch OBC will be used.

Chapter 3 Experimental Set Up and Procedures

3.1 Experimental System

Both the Oscillatory Baffled Crystallizer (OBC) and the Stirred Tank Crystallizer (STC) were utilised in this work and were operated in batch mode.

3.1.1 Oscillatory Baffled Crystallizer

As shown in Figure 3.1, the OBC employed the 'moving baffle' method to mix the contents and consisted of a jacketed glass column with an internal diameter of 76 mm, with a total volume of 1 L and a working volume of 0.5 L. To generate the mixing two stainless steel orifice baffles were connected by metal rods to form a baffle string; this was attached to a linear actuator at the top of the vessel. The oscillation motion within the column was delivered via a control box connected to the actuator, providing the different oscillation amplitudes and frequencies to be used. The outer diameter, the orifice diameter and the spacing of the baffles were 72 mm, 35 mm and 52 mm respectively, which gave an overall surface area of the baffle string of 13320 mm^2. To control the temperature accurately within the vessel, water was circulated through the jacket via a water bath (Grant Instruments GP 200/R2); enabling different cooling rates to be applied.

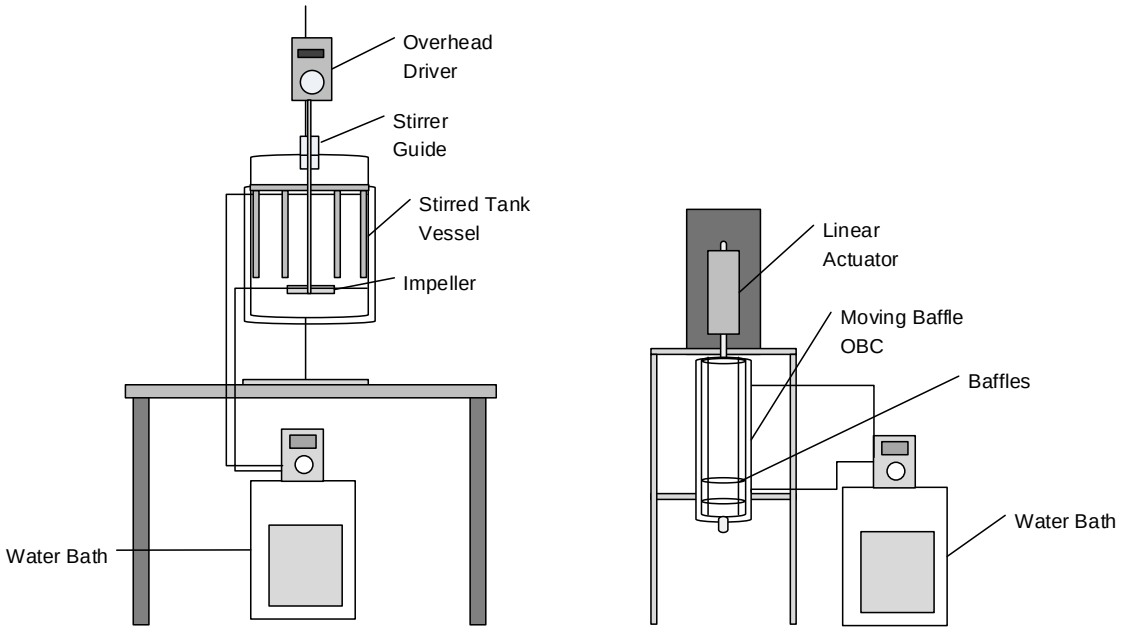

Figure 3.1 – Graphical illustration of STC and OBC set-Up

3.1.2 Stirred Tank Crystallizer

Similarly the STC is a jacketed glass vessel, which has an internal diameter of 90 mm, a total volume of 1 L and a working volume of 0.6 L. For the initial work in this vessel a stainless steel two-blade flat-paddle impeller (impeller S1), 60 mm in diameter, was used to generate the mixing and was centrally aligned within the vessel. The impeller was attached to an overhead stirrer to control the rotation speeds. To reduce the vortices produced when using this type of impeller, four stainless steel wall-baffle inserts were added into the system to aid mixing. These inserts essentially work by breaking up the rotating vortices, enhancing vertical motions. The total surface area of the impeller and wall baffles in direct contact with solution is 3070 mm^2. Temperature control was identical to that used in the OBC, shown in Figure 3.1, with a similar water bath being used to control the internal vessel temperature.

As impeller type has been known to affect mixing within the STC (7), a second impeller (impeller S2) was trialled at certain conditions. This was a four pitched-blade impeller, which had an overall diameter of 50 mm. The total surface area of this second impeller together with wall baffles was 2952 mm^2. This type of impeller was chosen as it has been shown to improve the mixing and heat transfer within the STC (72).

3.2 Experimental Conditions

To enable valid comparison of performances of two different vessels, power densities or dissipation rates of both the STC (59) and the OBC (73) are used where:

$$\left(\frac{\mathrm{P}}{\mathrm{V}}\right)_{STC} = \frac{\mathrm{P_O}\rho \mathrm{N_S^3 D_S^5}}{\mathrm{V_{st}}} \quad [\mathrm{W\ m^{-3}}] \qquad (3.1)$$

$$\left(\frac{P}{V}\right)_{OBC} = \frac{2\rho N(1-\alpha_1)^2}{3\pi C_D^2 \alpha_1^2} x_o^2 \omega^2 \quad [W\ m^{-3}] \qquad (3.2)$$

The detailed definitions of each parameter were given in section 2.2 under Crystallizers.

The mixing intensities were kept the same for both the OBC and STCs, with the mixing conditions for each crystallizer and impeller type outlined in Table 3.1.

Table 3.1 – Mixing conditions utilized and the corresponding target mixing intensities

Mixing intensity ($W\ m^{-3}$)	OBC			STC	
	Set frequency [f] (Hz)	Angular frequency [ω] ($rad\ s^{-1}$)	Centre-to-peak amplitude [x_o] (mm)	Stirrer speed (S1) [N_{S1}] (RPM)	Stirrer speed (S2) [N_{S2}] (RPM)
20	0.6	3.77	10	104	154
170	1.2	7.54	10	201	318
750	2	12.57	10.5	351	450

As well as the three different mixing intensities shown in Table 3.1, three different cooling rates were also tested from 0.25 °C/min (the low rate) to 0.50 °C/min (the medium rate) through to 0.75 °C/min (the high rate which was limited by the maximum cooling rate achievable by the water bath). The effect of cooling rates on process parameters and purity was conducted at a fixed mixing intensity (170 W/m^3 the medium level). Likewise the effect of mixing intensity was undertaken at a fixed cooling rate (the highest rate). For the work with no impurity (the 'verification' work) and with the second impeller, the high mixing (750 W/m^3) was also used with the medium linear cooling rate (0.50 °C/min), which was suggested by previous trials to be a condition which produced interesting results.

3.3 Experimental Compound

Following a review of several possible model compounds, urea was selected for this research because it is relatively safe, highly soluble in water (74, 75), stable and has only one known polymorph under normal process conditions. The chemical structure is shown in Figure 3.2 and technical grade urea was sourced from VWR with an average initial urea purity of 95 %. The urea purchased contained traces of impurity, including biuret and ammonia.

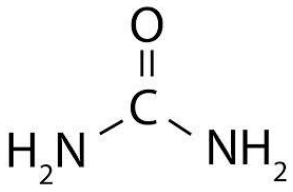

Figure 3.2 – Chemical structure of urea

Urea is an organic compound and while it is mainly used in the fertilizer and plastics industries (76), it has recently found applications as a material for frequency shifters of high power lasers in a wide spectral range (77). As can be seen from the chemical structure in Figure

3.2, the main attachment mechanism of the individual urea molecule is through strong hydrogen bonding, resulting in a chain-like crystal lattice (78). When urea crystallizes as a pure compound, it generally forms long, needle-like crystals, which can have a large length to breadth ratio, often exceeding 50:1 (76). This crystal habit is distorted when impurity is present within the crystal (79) and leads to the formation of a more cubic shape crystal as the impurity value increases towards 5 wt. %. This change in habit can be used to verify whether any impurity is being incorporated into the product crystal.

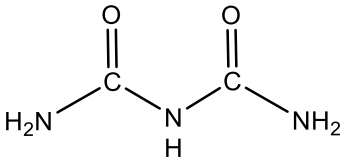

Figure 3.3 – Chemical structure of biuret

The impurity which will be used in this work is biuret, sourced from Acros Organics with a high purity (97 %); the chemical structure of which is shown in Figure 3.3. Biuret is a condensation product of two urea molecules and has therefore many properties very close to that of urea. It is known that biuret often exists as a hydrate containing an intermolecular hydrogen bond (79) and has a much lower solubility in water than urea (80, 81). It is thought that biuret interferes with the hydrogen bonding of the pure urea by attaching itself to two of the urea molecules, effective blocking them and stopping the growth in this direction as biuret contains its own intermolecular bond stopping further attachment at this site. This is shown quite well in a diagram by *Scott and Black* (79), a copy of which is shown in Figure 3.4. When the biuret is present within the growing crystal at a high enough concentration (above 5 % impurity), the crystal habit of the urea becomes distorted and more cubic in nature, which can clearly be observed through crystal imaging.

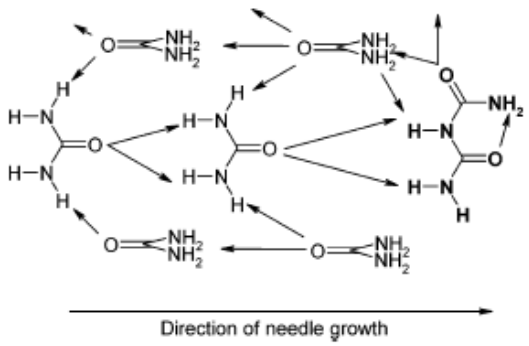

Figure 3.4 – Diagram of hydrogen bonding in urea and the disruption caused by the addition of biuret (central molecules) (79)

In this work, both 1 % and 5 % biuret will be used to study the effect of impurity on crystal purity and compare the purity data from the two systems.

3.4 Procedures and Final Temperatures

3.4.1 Procedures

3.4.1.1 - 'Pure' Experiments

The terminology of the 'pure' system is one without addition of biuret as the impurity. A copy of the solubility curve for urea produced by Speyers (74) is shown in Figure 3.5, along with the experimentally confirmed data points from this work. To confirm the solubility, set amounts of urea were accurately weighed and a set volume of distilled water added. This slurry was then heated to a set temperature and left mixing for around 1 hour. The slurry was then filtered and the weight of solid recovered measured and used to calculate the concentration at each temperature point.

For each experiment, a certain amount of technical grade urea was weighed using an electronic balance, according to the previously confirmed solubility curve (74). The solid urea particles were then poured into each vessel using a funnel to minimise loss and to this the required volume of distilled water was added. This gave a final solution with a supersaturation of 1.05 at a saturation temperature of 30 °C for both systems. The exact amounts utilized in making up the solutions in each system are shown in Table 3.2. The solution was then heated to 40 °C until all the solid had dissolved and was held at this temperature for one hour under the specific mixing conditions. The solution was then cooled at a given cooling rate to a final temperature of 24 °C, as shown in Table 3.2. Once the final temperature had been reached, the solution temperature was held for 30 minutes to allow the crystals to grow.

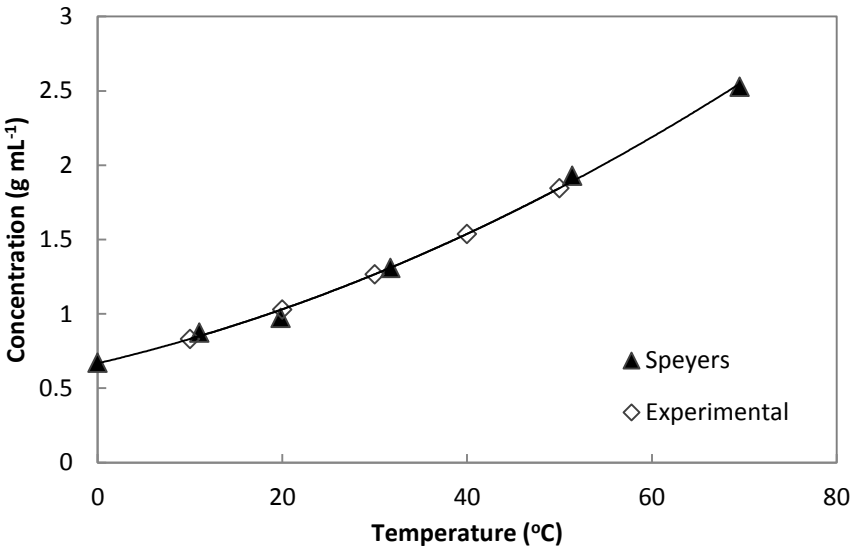

Figure 3.5 – Solubility curve of urea in distilled water

Table 3.2 – Components added to the systems and system temperatures

System	Weight urea added (g)	Volume distilled water added (ml)	Concentration (g ml^{-1})	Supersaturation at 30 °C saturation temperature	Initial temperature (°C)	Final temperature (°C)
OBC	332.5	250	1.33	1.05	40	24
STC	399	300	1.33	1.05	40	24

3.4.1.2 – 1 wt. % Added Impurity Experiments

When 1 wt. % impurity was added into each system the basic procedure was the same as that of the 'pure' trials; this is termed as '1 wt. % added impurity'. The specific amounts of urea and distilled water were measured out in the same quantities shown in Table 3.2; to this 1 wt. % biuret was added before all solid particles were poured into each vessel using the funnel. As previously mentioned biuret has a much lower solubility in water than the urea within the experimental temperature range (Figure 3.6), therefore care was taken to ensure that the amount of biuret added was well below the biuret saturation point in both vessels. The required volume of distilled water was then added into each vessel, recovering any solid stuck to the vessel walls. Table 3.3 gives the exact quantities of components and crystallization temperatures. The solution was again heated to 40 °C to ensure the solid was fully dissolved and held at this temperature under the specific applied mixing conditions for one hour. The solution was then cooled at the given cooling rate to a final temperature of 24 °C. Once the final

temperature had been reached, the solution temperature was again held for 30 minutes to allow the crystals to grow, before the crystals were removed for downstream filtration and washing.

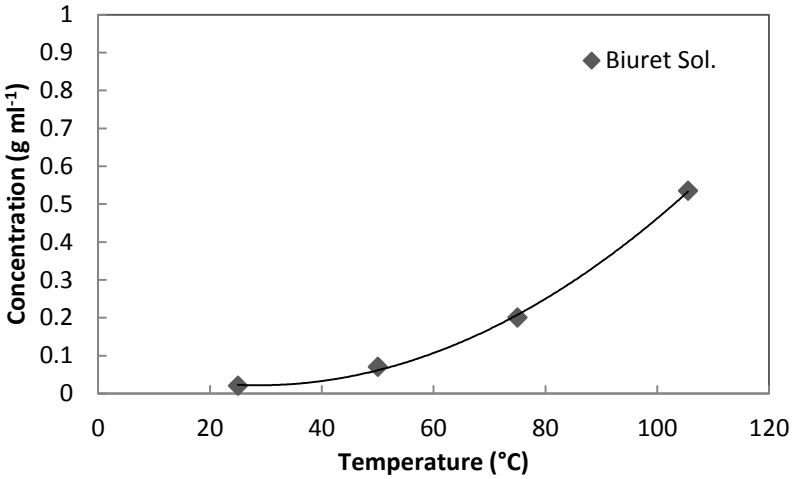

Figure 3.6 – Solubility curve for biuret in water (81)

Table 3.3 – Components added to the 1 wt. % added impurity system and system temperatures

System	Weight urea added (g)	Volume distilled water added (ml)	Weight biuret added (g)	Added impurity [on weight basis] %	Initial temperature (°C)	Final temperature (°C)
OBC	332.5	250	3.3	1	40	24
STC	399	300	4	1	40	24

3.4.1.3 – 5 wt. % Added Impurity Trials

The procedures for preparing trials are identical to that of the 1% impurity system, except the amount of biuret was increased, see Table 3.4.

Table 3.4 – Components added to the 5 wt. % added impurity system and system temperatures

System	Weight urea added (g)	Volume distilled water added (ml)	Weight biuret added (g)	Added impurity [on weight basis] %	Initial temperature (°C)	Final temperature (°C)
OBC	332.5	250	16	4.8	40	20
STC	399	300	19	4.8	40	20

It should be noted that the final temperature was lowered by 4 °C in these experiments, this was due to the effect of the added impurity on the nucleation temperature (79). When the amount of added impurity was increased the nucleation temperature dropped (23, 49), while this effect was observed in the 1 wt. % impurity trials, the decrease in temperature was small.

The final temperature of 24 °C was selected for all 'pure' experiments; however crystallization had not completely finished at this temperature. To investigate whether the final temperature could have an effect on purity and yield, tests were carried out on a 'pure' trial system with further cooling to 20 and 14 °C at a fixed mixing of 750 W/m^3 and a fixed cooling rate of 0.25 °C/min in the OBC. A total of three repeats were conducted at each of the final temperatures and the data are given in Table 3.5, with all values being an average of the three trials.

Table 3.5 – Yield and purity results for various final temperatures for the 'pure' trials

Run	Final temperature (°C)	Urea concentration added (g ml^{-1})	Cooling rate (°C min^{-1})	Overall yield (%)	% Purity achieved
1	24	1.33	0.25	13.96	96.2
2	20	1.33	0.25	15.50	96.0
3	14	1.33	0.25	24.78	96.1

It can be seen from Table 3.5 that while the overall yield was improved as the final temperature was lowered, there was very little change in crystal purity. In addition, excessive solids were noted in each crystallizer with lower final temperatures; this led to a detrimental effect on the capability of mixing of both systems. Large deposits of solid collected at the bottom of the vessel which could form agglomerates with time. As a consequence of this, 24 °C was chosen as the best compromise in terms of purity study and better overall mixing within both vessels for the 'pure' system.

A similar test was carried out with 1 wt. % added impurity and the same outcome was established, while 20 °C was chosen as the final temperature for the 5% impurity tests, this is due to the lower nucleation temperature noted in these tests, as impurity led to the retardation of crystal growth (14), the mixing provided in the two systems is still high enough to avoid excessive solid concentration within either vessel.

3.5 Filtration and Washing Protocols

3.5.1 Filtration

Following the completion of each experimental run, the crystal slurry from the crystallizer was transferred into a pre-warmed beaker, before being taken to a temperature controlled box for filtration and washing. To recover the crystals from the mother liquor, the crystal slurry was filtered using a Büchner filter which was attached to a vacuum pump. This was completed in the specially built 'temperature controlled box', which delivers precise and constant temperature throughout the filtration and washing process. The box as shown in Figure 3.7 was fitted with a standard heat lamp and thermocouple, as well as a fan connected to the temperature controller so that the final crystallization temperature can be maintained. The main purpose was to minimise any additional nucleation which may occur due to any fluctuation of room temperature varying from 10 °C in winter, to 25 °C in summer during the filtration and washing processes. Any additional nucleation after the end of the experiment is problematic, as the mother liquor attached to the crystal surface could crystallize prior to washing, lowering the purity.

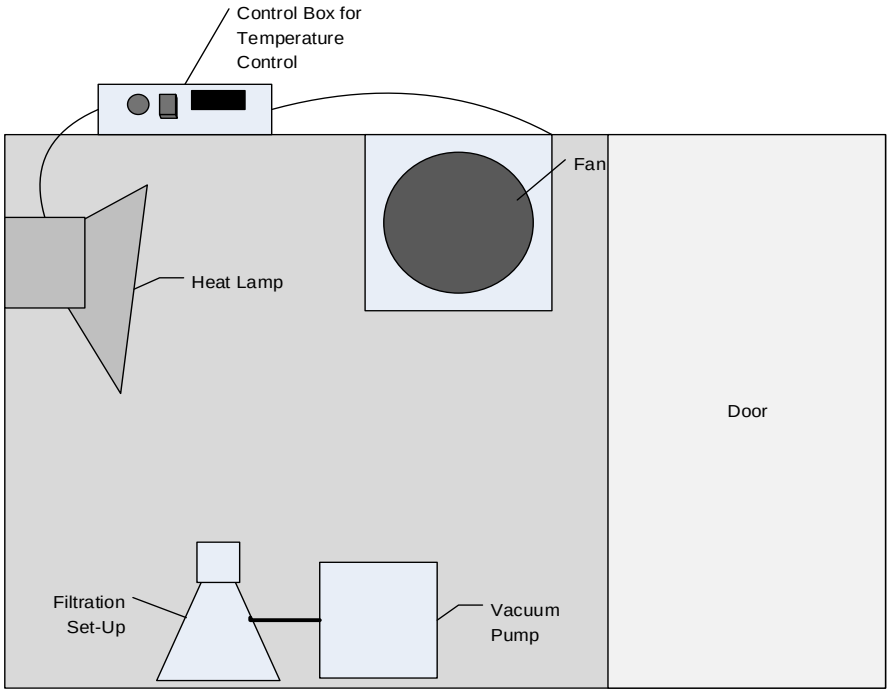

Figure 3.7: Diagram of filtration system and temperature controlled box

To ensure no 'extra' crystallization occurred during the slurry transfer, the beaker used was also pre-warmed to the box temperature and removed just before the slurry was to be

transferred. This transfer was completed as quickly as possible. In addition, the flow in the jacket of the crystalliser was left on throughout the transfer procedure in order to maintain the final temperature within the vessel. All due care was also taken to avoid any spillage or loss of slurry. Once the slurry had been moved to the box it was immediately and carefully poured into the Büchner filter with the vacuum pump already turned on, drawing the solution through the filter paper and into the collection vessel. It should be noted that all glassware used for the filtration was pre-warmed to the box temperature and was thoroughly cleaned after each use and replaced in the box to maintain its temperature.

3.5.2 Washing

Following the initial separation of mother liquor, the crystals collected were washed. The washing step is to remove any mother liquor which is adsorbed onto the crystal surface as well as within the voids of the filtration cake owing to capillary attraction (15). Traditionally washing is carried out using solvents of varying concentrations in several stages in industry (15). As a result, the selection of washing solution/solvent and the establishment of the washing protocols are important. Due to the high solubility of urea in water and many other readily available organic solvents (82), isopropanol (purity > 95 %) was identified as the most suitable wash liquor. Several possible solvents and washing arrangements were identified and trialled, see Table 3.6. Each trial was carried out as three replicate experiments to establish the statistics.

Table 3.6 Possible washing methodologies

Trial Number	Washing temperature (°C)	Wash solvent used	Number of washes	Volume solvent per wash (ml)
1	24	None	N/A	0
2	24	Isopropanol	1	100
3	24	Isopropanol	2	50
4 (step 1)	24	Saturated urea solution	1	127
4 (step 2)	24	Isopropanol/Water mix	1	127
5 (step 1)	24	Saturated urea solution	1	100
5 (step 2)	24	Isopropanol	2	50

To allow comparison between the different washing protocols, a base run was carried out with no washing. The purity was determined using the off-line FTIR solution analysis system (Section 4.1.3) and the yield calculated was related to the expected mass of solid recovered at

the final temperature. Table 3.7 shows the yield and purity results corresponding to the washing methodologies listed in Table 3.6.

Table 3.7: Results from washing trials

Trial number	Test 1			Test 2			Test 3			Average yield (%)	Average final purity (%)
	Yield (%)	Initial purity (%)	Final purity (%)	Yield (%)	Initial purity (%)	Final purity (%)	Yield (%)	Initial purity (%)	Final purity (%)		
1	68.0	87.6	96.4	87.6	87.6	96.3	86.4	87.6	95.9	80.7	96.2
2	50.0	87.6	96.7	57.5	87.6	96.6	64.0	87.6	96.7	57.2	96.7
3	47.0	87.6	96.8	55.8	87.6	97	58.4	87.6	96.7	53.7	96.8
4	10.6	87.6	96.6	-	-	-	-	-	-	10.6	96.6
5	53.0	87.6	96.9	55.5	87.6	96.8	55.3	87.6	95.5	54.6	96.4

As can be seen in Table 3.7, the application of washing has opposite effects on the purity and yield, when any washing is applied, the average yield obtained from the crystallization falls while the purity increases. This is likely due to a combination of the removal of any extra mother liquor present on the crystal surface and the probable loss of solid due to the solubility of urea in isopropanol (3.17 g/100g at 25 °C (82)). Note that the Trial 4 was only carried out once due to the heavy loss of solid, this was because of the high solubility (47.6 g Urea/100 g solvent at 25 °C (82)) of the urea in the isopropanol/water mix (2/3 IPA to 1/3 H_2O). Subsequently this solvent mixture was disregarded.

In Trial 5 where the saturated urea solution and isopropanol were used to wash the crystals in sequence, the best results of yield and purity were obtained. However the preparation of the saturated urea solution was done batch wise, not only was this time consuming, but it was also difficult to ensure the consistency of the solution. To make up the solution, high purity urea (99.5 % pure) must also be used. In order for the solution to not dissolve the crystal samples, excess urea was added into the solution which was then left for one hour at the set box temperature for full dissolution. The solution was then filtered to remove any undissolved urea and then kept in the box for a further 20 minutes until use. Unpredictability could occur where sometimes the solution would re-crystallize or the solution would dissolve the sample crystals during application. On balance it was decided to discard this method.

This left the two 'pure' isopropanol washing systems to be considered. As can be seen from Table 3.6, the only difference between these two systems is how the 100 ml of isopropanol was delivered. Trial 2 just had one isopropanol wash of 100 ml, while Trial 3 split this volume into two 50 ml washes. It was decided that the Trial 3 method gave more control over the even dispersion of the solvent across the surface of the filter cake and was consequently adopted as the washing methodology and applied to the rest of the work. It should be emphasized that the purities of washed and unwashed crystals, as well as of both the mother liquor and the wash liquor were also analysed to ascertain that the mother liquor and impurity from the wet cake were washed away as thoroughly as possible. The results indicated that the impurity was contained within the mother and washing liquors and that the amount of impurity left on the crystals was negligible. This justifies the methodology that was established and is also in line with the GMP operation in GSK.

3.6 Post Filtration and Washing Steps

To complete every experimental test, several steps and procedures were put in place to ensure consistent crystal drying and bottling, minimising any post-filtration variations in conditions affecting the purity obtained.

After the washing steps, the crystals were left in the filter under vacuum for 30 minutes at the set temperature, ensuring that as much of the mother liquor and wash solvent as possible had been removed from the crystals. If any excess solvent was present in the filter cake, this could lead to either further nucleation or loss of solid during the drying stage, depending on if solvent was still attached to the crystals. The length of time under vacuum was established when it was found that crystals filtered and dried straight after washing were more likely to form large lumps which showed evidence of further crystallization from the isopropanol. In contrast leaving the slurry filtering for longer than 30 minutes had no extra benefits, with similar results of purity and yield as those only filtered for 30 minutes, this time of 30 minutes was therefore applied throughout this work.

After filtration, the crystals were removed from the filter and placed in a dish that was moved quickly and carefully to the pre-heated oven, at a temperature of roughly 65 °C for drying overnight. Following this the dish was removed from the oven and left for a further hour at room temperature before being weighed and bottled. This final hour would allow the crystals to cool before being bottled, so no condensation would occur within the sample bottle. The

condensation could lead to water or solvent collecting in the sample bottles and this has been known to have a detrimental effect on the yield and purity of the product.

Note that the filtration, washing and drying procedures and protocols are directly taken from the GSK GMP practices.

3.7 Effect of Initial Solid Purity

Two different sources of urea were initially utilized within this research; an initial batch from Prolabo UK with an average purity of 89 % (Urea1) and a second batch of industrial grade urea sourced from VWR with an average initial purity of 95 % (Urea2). All initial purities were confirmed in house using the offline FTIR solution method described in Section 4.1.3.

The urea starting purity was thought to be an important factor with a possible effect on nucleation and growth; this must be verified before valid comparisons could be commenced. Consequently several experiments were undertaken using the 'pure' system. Following that the tests were repeated with 1 % added impurity.

3.7.1 Results and Discussion

The first results to be compared are the nucleation temperatures obtained in the 'pure' trials, Table 3.8 presents the average nucleation temperature from both urea sources in the OBC, with the standard deviation and Kolmogorov-Smirnov Statistical Probability factor (P). Further discussion of the statistical analysis is provided in Section 4.2. A 'P' value of less than 0.1 is considered to be statistically significant.

Table 3.8 – Average nucleation temperatures (NT) for the OBC system with varying initial urea purity, were n = 3

NT ± standard deviation [°C]		Cooling rate (°C min^{-1})								
		0.25			0.50			0.75		
		Urea1	Urea2	P	Urea1	Urea2	P	Urea1	Urea2	P
Mixing intensity (W m^{-3})	20							24.59 ± 0.30	28.44 ± 0.72	0.03
	170	25.57 ± 0.30	29.95 ± 0.75	0.03	24.64 ± 0.36	29.55 ± 0.78	0.03	24.77 ± 0.18	28.59 ± 0.24	0.03
	750							24.48 ± 0.12	29.84 ± 0.15	0.03

As can be seen in Table 3.8, the nucleation temperatures for the crystallization of Urea1 is statistically lower than that for Urea2 at every condition investigated. This suggests that the lower the initial urea purity, the lower the nucleation temperature and the larger the MSZW. ensure that the cooling rates are similar, examples of the temperature cooling profiles are shown in Figure 3.8 at a specific cooling rate of 0.50 °C/min and a mixing intensity of 170 W/m^3. These curves show a similar cooling slope with the Urea1 having a peak, indicating nucleation at a lower temperature than Urea2. The curves are consistent for all conditions investigated above.

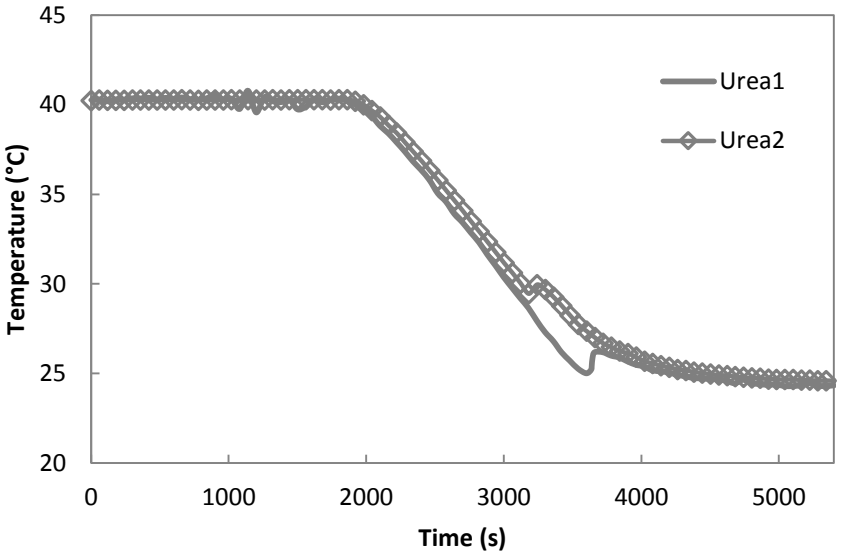

Figure 3.8 – Temperature profiles obtained with a cooling rate of 0.50 °C min^{-1} and mixing intensity of 170 W m^{-3} for the crystallization of Urea1 and Urea2 in the OBC

To ensure that the nucleation temperature differences noted are due to the initial purity and are not vessel dependent, the same analysis was repeated in the STC. The average nucleation temperatures achieved are shown in Table 3.9, along with the Kolmogorov-Smirnov test result and the standard deviations.

Table 3.9 – Average nucleation temperatures (NT) for STC with varying initial urea purity where n = 3

NT ± standard deviation [°C]		Cooling rate (°C min^{-1})								
		0.25			0.50			0.75		
		Urea1	Urea2	P	Urea1	Urea2	P	Urea1	Urea2	P
Mixing intensity (W m^{-3})	20							25.15 ± 0.09	28.20 ± 0.27	0.03
	170	26.32 ± 0.27	29.88 ± 0.48	0.03	25.00 ± 0.18	29.17 ± 0.57	0.03	25.37 ± 0.03	29.34 ± 0.36	0.03
	750							25.14 ± 0.42	29.48 ± 0.42	0.03

The results again indicate that the urea with the higher initial purity (Urea2) nucleates at a statistically higher temperature than the lower starting purity (Urea1). The consistent trend obtained here suggests that the initial purity of the crystallizing solid has an effect on the nucleation temperature.

Following completion of these comparisons for the 'pure' systems, it is important to verify that this trend is still present in an 'impure' starting environment. Therefore, crystallization was carried out for both starting urea purities (Urea1 at 89 % and Urea 2 at 95 %) with the addition of 1 % biuret. Table 3.10 shows the nucleation temperatures at five conditions for the OBC, while Table 3.11 shows the results for the STC under the same conditions. Again these values are the average of at least three trials and are shown with the Kolmogorov-Smirnov probability factor and the standard deviations.

Table 3.10 – Average nucleation temperatures (NT) for1 % AI from the OBC system with varying initial urea purity where n = 3

NT ± standard deviation [°C]		Cooling rate (°C min^{-1})								
		0.25			0.50			0.75		
		Urea1	Urea2	P	Urea1	Urea2	P	Urea1	Urea2	P
Mixing intensity (W m^{-3})	20							20.83 ± 1.05	24.41 ± 0.60	0.03
	170	22.44 ± 0.27	27.77 ± 0.39	0.03	21.05 ± 0.33	26.53 ± 0.33	0.03	20.73 ± 0.33	26.74 ± 0.93	0.03
	750							20.68 ± 0.54	27.15 ± 0.60	0.03

Table 3.11 – Average nucleation temperatures (NT) for 1 % AI from the STC system with varying initial urea purity where n = 3

NT ± standard deviation [°C]		Cooling rate (°C min^{-1})								
		0.25			0.50			0.75		
		Urea1	Urea2	P	Urea1	Urea2	P	Urea1	Urea2	P
Mixing intensity (W m^{-3})	20							20.85 ± 0.36	24.38 ± 1.11	0.03
	170	22.02 ± 1.11	27.50 ± 0.33	0.03	21.65 ± 0.90	26.68 ± 0.27	0.03	20.72 ± 0.51	25.57 ± 0.09	0.03
	750							21.13 ± 0.51	26.90 ± 0.15	0.03

Both Tables 3.10 and 3.11 have the same trend as the 'pure' systems with Urea2 showing a much higher nucleation temperature than the lower initial purity system (Urea1). Therefore the starting purity of the compound affects the nucleation temperature obtained in this system, independent of the experimental condition and added impurity level.

The previously noted trends of decreasing nucleation temperature with increased cooling rate (70) are still apparent in Tables 3.10 & 3.11, as are the trends with increasing mixing intensity (31). Table 3.12 shows the nucleation temperature differences calculated from the average values between 'pure' and 'impure' trials, in both the OBC and STC using both Urea1 and Urea2.

Table 3.12 – Differences in average nucleation temperatures [ANT] between 0 and 1 % AI

Differences in ANT [°C]		OBC – 0% to 1% AI		STC – 0% to 1% AI	
Cooling rate [°C min^{-1}]	Mixing intensity [W m^{-3}]	Urea1	Urea2	Urea1	Urea2
0.25	170	3.13	2.18	4.31	2.37
0.50	170	3.59	3.02	3.34	2.49
0.75	20	3.77	4.03	4.30	3.82
0.75	170	4.04	1.84	4.66	3.77
0.75	750	3.80	2.69	4.02	2.57

The data presented in Table 3.12 shows that the differences between the 'pure' and 'impure' systems are generally larger for the lower initial purity urea (Urea1). When we compare the solid FTIR traces, Figure 3.9, of both compounds we can see that while the two profiles

appear similar, there are subtle differences as the material possibly contains different impurities. This could have led to the larger difference from Urea1, possibly due to extra nucleation retardation thorough the addition of impurity. Explanation of how these spectra were produced can be found on section 4.1.3.

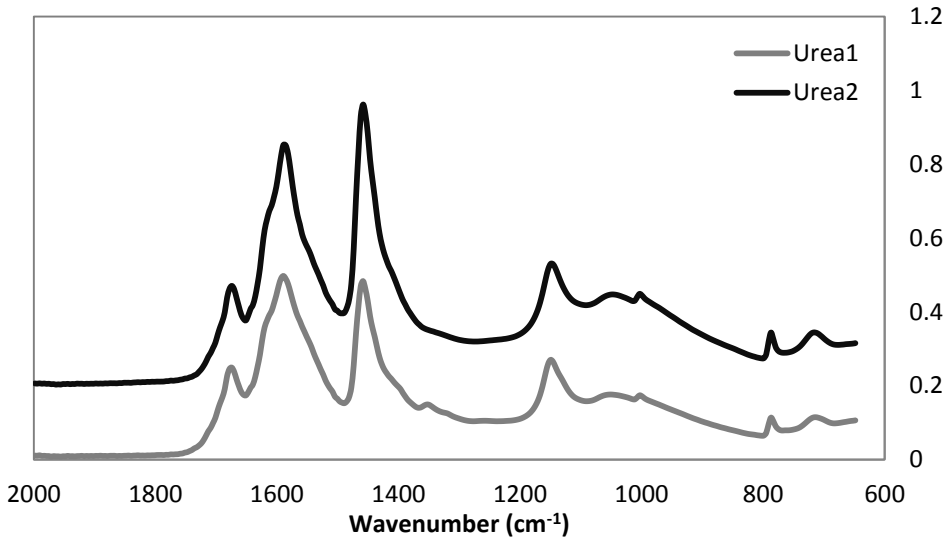

Figure 3.9 – FTIR spectra of Solid Urea1 (grey line) and Urea2 [+0.2 Absorbance offset] (black line)

3.7.2 Conclusion

In conclusion, the initial purity of the compound has an effect on the nucleation temperature obtained, with a lower nucleation temperature being noted with a lower starting purity. This trend is verified as independent of the applied cooling rate and mixing intensity effects.

The addition of a specific impurity lowers the nucleation temperature regardless of the initial purity. It has also been noted that a lower initial purity leads to a larger temperature drop when impurity is added, this is most likely due to the variation in impurity profile between the urea sources. The trends are confirmed for all cooling rates and mixing in both vessels. These results highlight the importance of knowing the initial purity of the substance. Note that all experiments presented in the remaining thesis were completed using Urea2.

Chapter 4 Analysis Techniques and Methodologies

4.1 Experimental Parameter Analysis

In order to analyse the various parameters and crystals produced in this work, several different analytical techniques have been utilized, for instance, the nucleation temperature, the solution concentration and supersaturation were monitored and analysed using a thermometer, turbidity probe and infrared probe. In this section each technique will be discussed respectively and methods or calibrations will be described.

4.1.1 Temperature Measurement

One of the most important parameters to be monitored within cooling crystallization is the temperature. As stated previously, supersaturation is the driving force and the best way to achieve the required supersaturation is through the control of the temperature (36). Since the temperature within the vessel is controlled by flowing a hot/cold medium through the jacket, accurate measurements of the temperatures within the vessel and from the water bath are required. The water bath used was a R2/GP200 system sourced from Grant Instruments. Labwise software was supplied to control and record the bath temperature and set cooling rates. For the internal vessel temperature a stainless steel PT 100 probe, sourced from HEL group, was placed in the centre of the vessel. Both temperature and turbidity reading were taken every 20 seconds to ensure a complete picture was obtained of the crystallizing system. An example of the temperature probe location is shown in Figure 4.1.

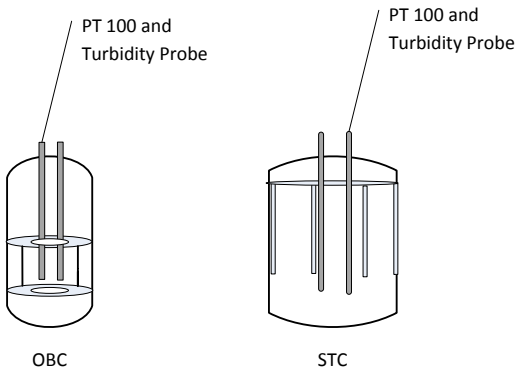

Figure 4.1 – Probe locations for the OBC and STC systems

An example of the temperature profile (T1) obtained during cooling is shown in Figure 4.2. This shows that temperature was unchanged during the dissolution and the holding period, then decreased linearly with time and that a temperature spike was noted when nucleation

occurred. This is due to the exothermic nature of the urea crystallization process, and the nucleation temperature is thus taken as the temperature obtained directly before the temperature spike. The temperature then levelled off as the final temperature was reached. For accurate temperature measurement multiple readings were taken and errors were calculated as shown below in Table 4.1 at three temperature points. To ensure reliability of the measurements the same water bath and probe systems were used for all experiments.

Table 4.1 – Error values noted in the temperature probe systems

Set temperature (°C)	HEL PT 100 error (°C)	Labwise error (°C)
-20	± 0.10	Below lowest applicable temperature
20	± 0.10	± 0.50
200	± 0.25	± 1.00

4.1.2 Turbidity Analysis

As mentioned in Section 2.1.1, knowledge of the temperature at which nucleation occurs is important in gaining insight into the crystallizing system. This temperature can directly be compared with those of other trials and also allows the determination of the metastable zone width (MSZW) (18). To do this a turbidity probe is used in conjunction with temperature measurement. Turbidity itself is the measure of how opaque or clear a solution is in the presence of solid particles (83). This makes it ideal for referencing the onset of nucleation.

The turbidity probe consists of a stainless steel casing which contains two optical fibres. When connected to a light source, the light passes down one fibre, reflects from a polished mirror at the bottom and then travels back through the other fibre to a control box which converts the amount of reflected light to a voltage output and can then be presented as % transmittance. The turbidity probe was purchased from the HEL group and the signal was recorded using the CrystalEyes software.

There are several ways in which the signal produced can show turbidity, the method described below is the one used in this research although others are equally valid. To measure the solution the turbidity probe is placed within a fully dissolved solution (Figure 4.1). When the solution is clear, the signal displayed in the software is low; this is because there are few/no particles present to block the reflectance of light. As the temperature falls and the solution crystallizes, the signal obtained from the system increases as there are now several particles present in the solution which block the mirror and lead to an increase in the signal. T_{cryst} can be

calculated as the temperature where the turbidity signal changes by 10%. An example of the temperature and raw turbidity signals is shown in Figure 4.2, from which it can be noted that there is a very clear change in the turbidity signal upon nucleation. This gives a good indication of the nucleation temperature.

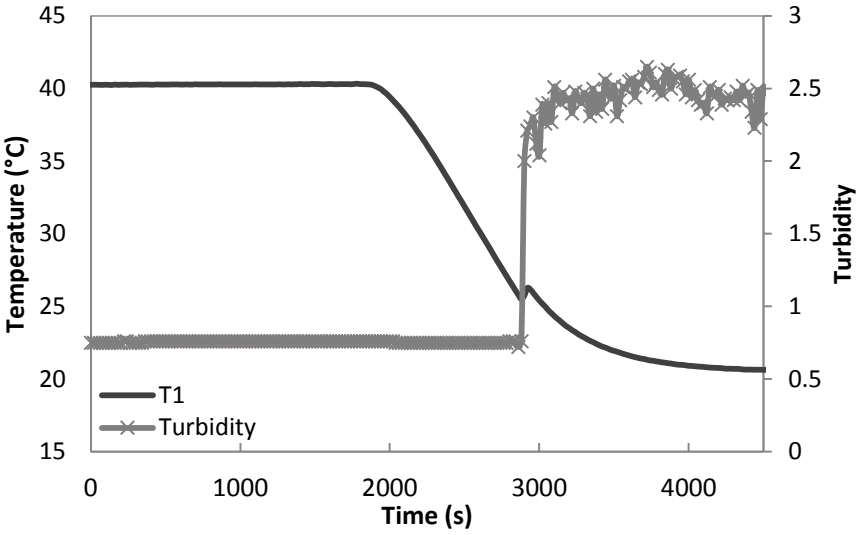

Figure 4.2 – Example of temperature profile and raw turbidity results obtained from the Crystaleyes monitoring system

In theory, a calibration curve could be obtained which links the solid concentration to the turbidity signal (70). In practice however, this becomes challenging as different solution concentrations have to be made at specific temperatures; it is difficult to know the exact concentration of solid when crystallization is taking place. The turbidity data is very useful in determining the nucleation temperature as shown in Figure 4.3, the nucleation temperature is taken when the signal has dropped by at least 10 %.

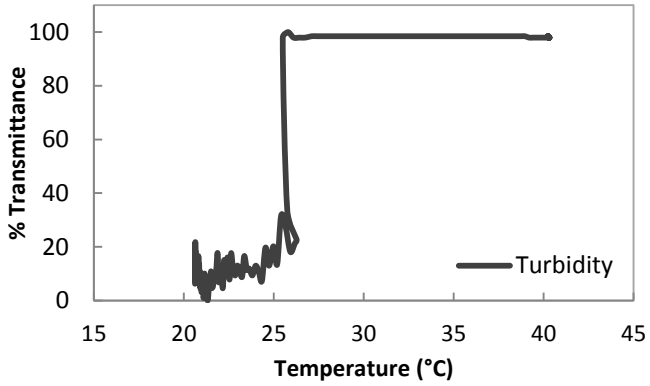

Figure 4.3 – Example of the turbidity profile obtained through cooling

4.1.3 Analysis Using Fourier Transform Infra-Red Spectroscopy

The IR instrument itself consists of a bench-top Shimadzu Prestige-21 FTIR base unit into which either the off-line SPECAC ® analysis module or the on-line PIKE FlexIR™ hollow waveguide probe accessory can be inserted. Both can be used to measure solids, liquids and powders (84). ATR stands for attenuated total reflectance (85) and works by letting the infrared light bounce through the ATR crystal and into the sample in contact with this surface, as illustrated in Figure 4.4 (86). From the spectra produced, specific FTIR peaks can be followed over time using the LabSolutions IR software, which allows direct analysis of the system over time, independent of the system conditions.

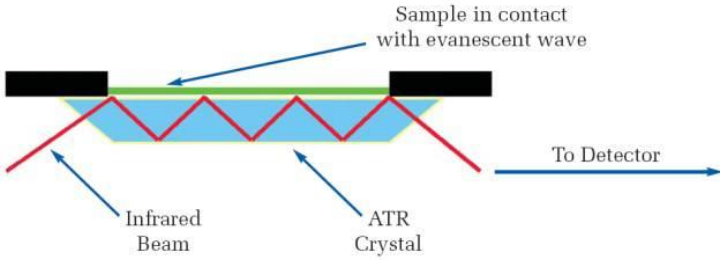

Figure 4.4 – Illustration of FTIR beam within ATR crystal (86)

4.1.3.1 Off-line IR measurement

To quantify the purity of crystals produced, off-line Fourier transform infra-red (FTIR) spectroscopy was used for both solution and solid analyses. This was carried out using the SPECAC® module fitted into the FTIR which contains a diamond embedded in the surface of a stainless steel analysis plate, this allows comparison of many different types of sample with little preparation required (85). One of its main advantages is that it has a relatively short optical path length which minimizes the loss of IR signal providing strong outputs with little interference (87).

Solid analysis can be used to confirm that the crystals produced are mainly urea by comparing the obtained spectra against the Shimadzu® compound library, the sample analysed achieved a sample score of 977 out of 1000. However, it is impossible to calculate the sample purity from the solid samples as the signal intensity varies greatly, often depending on the amount of solid which is in direct contact with the ATR crystal surface. This is shown by Figure 4.5, which presents the spectra obtained from the same sample of urea analysed twice and emphasises the difference in the peak heights obtained. This variation can lead to problems, as

a poor connection between the sample and analysis space could give either an overly high or very low signal leading to incorrect purity results.

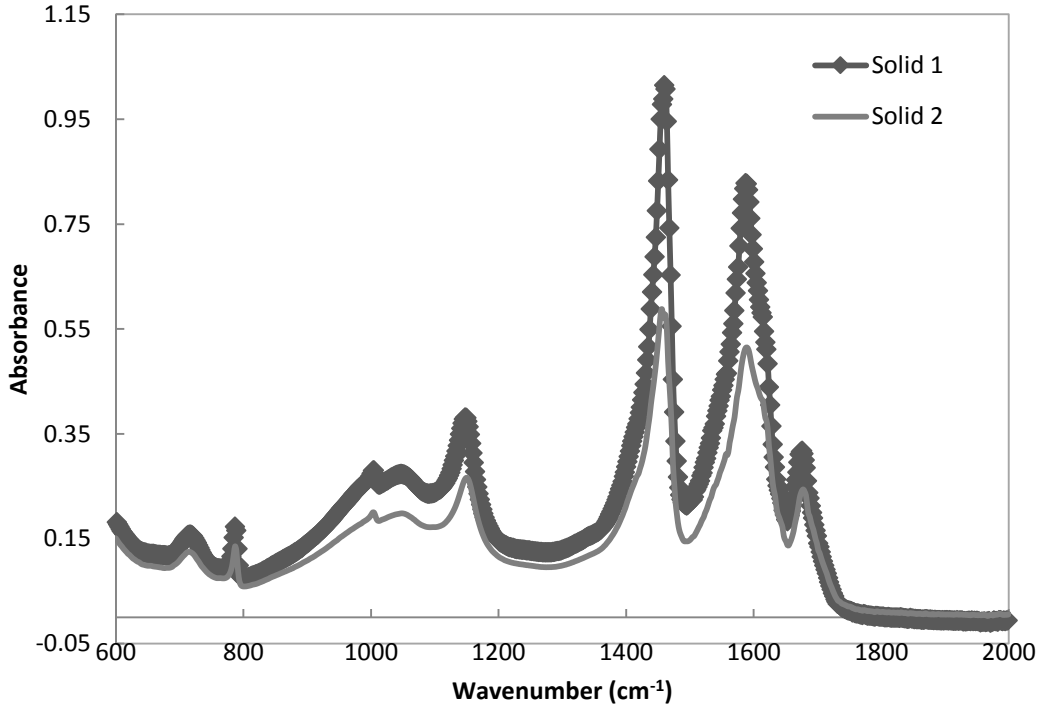

Figure 4.5 – Example of solid urea spectra produced through off-line measurement

To solve these problems a solution sample was used and this was completed by dissolving the exact weighed sample in a specific volume of distilled water. By doing this the issues relating to contact between the sample and crystal are removed, as long as the crystal is fully covered by the sample solution and no air bubbles are present to disrupt the contact. Care is also taken to ensure that the ATR crystal is clear of any contamination before the analysis of the sample is completed.

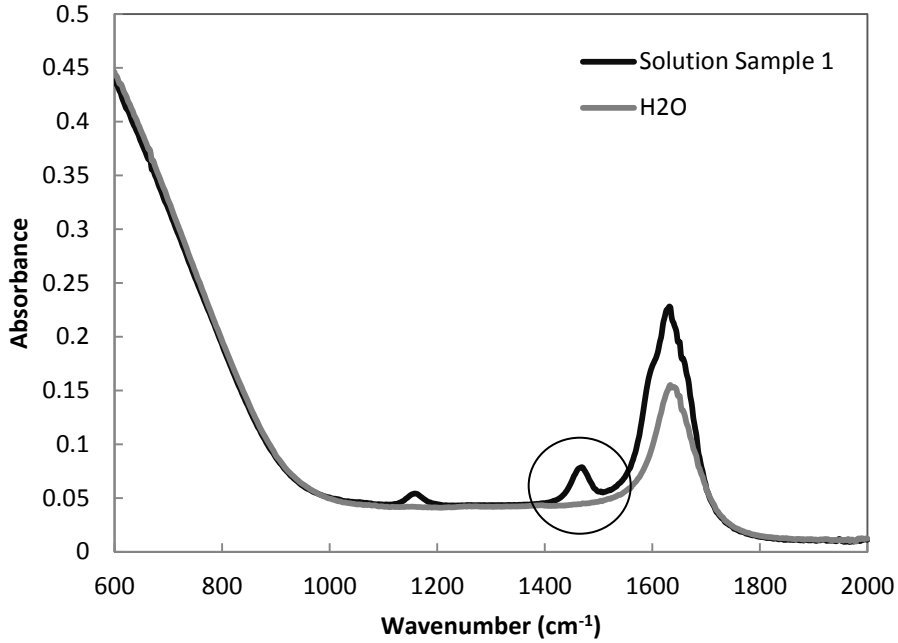

Figure 4.6 – Example FTIR spectra from 0.1 g ml^{-1} urea solution (Solution Sample 1) and 'pure' water (H2O)

Figure 4.6 shows the spectra obtained using the solution method which is slightly different to the solid spectra presented in Figure 4.5. There appears to be fewer peaks within the solution system but this is merely due to the dilute nature of the sample and the presence of the strong O-H water bonds shown in Figure 4.6. Other than the water bonds the main peak shown is at a wave number of around 1460 cm^{-1} (circled in Fig. 4.6), this relates to the N-C-N asymmetric bond stretching of the urea molecule (88) and is observed in both the solid and solution samples (Figs. 4.5 and 4.6). During the trials this peak was the clearest indication of urea concentration and the peak height increases as the urea concentration is increased.

4.1.3.2 Calibration for off-line purity measurement

Prior to purity analysis, a calibration curve was established by dissolving high purity urea (99.5% pure) in distilled water to form a series of solutions with known concentrations. Once fully dissolved, a small amount of the sample was placed on the analysis plate and peak absorbance measurements were taken. This was repeated with all prepared samples and using the in-built Shimadzu quantification package, a calibration curve was produced. The off-line calibration curve is shown in Figure 4.7 (open squares) with the initial point obtained by measuring a sample of the distilled water only.

Once the calibration curve has been established, each individual sample from experiments can then be analysed. The procedure for determining the purity of each run is as follows: a specific amount of every dry sample was weighed (to 4 decimal places) and the weight was recorded before the distilled water was added. Once the entire sample had been dissolved, 0.5 ml of the solution was placed on top of the embedded diamond in the off-line plate and the peak height was registered. The corresponding urea concentration was then determined using the calibration curve. To ensure the repeatability of the urea concentration measurements, three repeats for each sample were performed and the diamond thoroughly cleaned between each run. A background scan was also taken between tests to ensure that any residue present from previous samples was accounted for and did not affect the calculated concentration of the sample. The purity can then be evaluated using this measured sample concentration and is defined by the ratio of the measured concentration from the sample divided by the theoretical concentration of the samples. The latter is calculated from the solid added into the sample assuming that the initial solid collected from the experiment was 100 % pure.

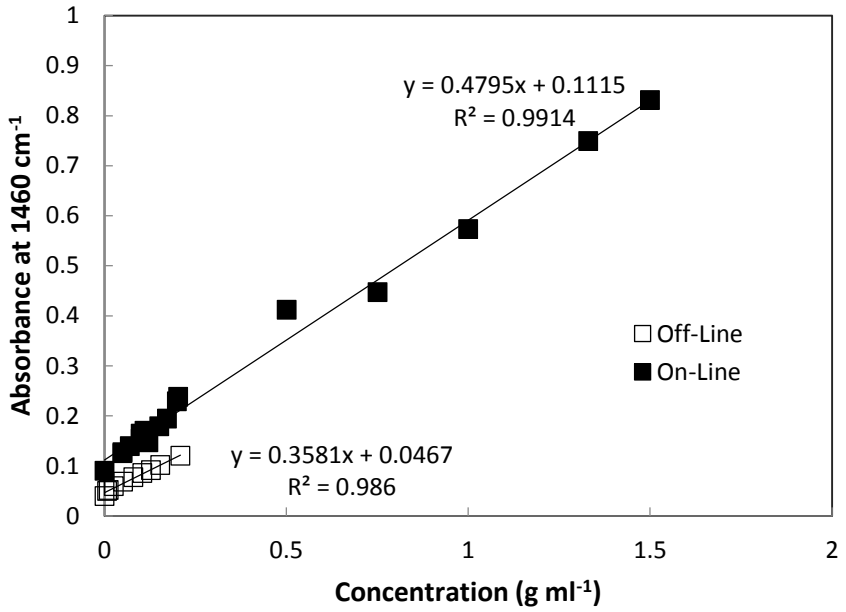

Figure 4.7 – Off-line and on-line calibration curve for absorbance vs. urea concentration

The off-line system has many advantages including minimal sample preparation and a relatively short optical path length which minimizes the loss of IR signal and consequently produces strong signals with little interference (87); however there are disadvantages, one of these is the fact that the sample plate is not temperature controlled and can only be operated at room temperature. This limits the range of concentrations which can be analysed as higher concentrations need correspondingly higher temperatures to ensure that the entire solid added

is dissolved and the reading is accurate. The other main disadvantage of the off-line system is that, in order to follow the concentration of the system during crystallization, samples would need to be constantly removed from the vessel and then analysed (2). This could cause issues with the reliability of the data as this continued removal could affect the system (89), possibly causing nucleation of the supersaturated solution (89) or producing invalid results due to the lower local room temperature as the measurement is strongly temperature dependent (90, 91). Therefore, to overcome these limitations an in-situ ATR-FTIR probe was used.

4.1.3.3 On-line IR measurement

The in-situ ATR-FTIR probe is a FlexIR™ accessory sourced from PIKE technologies and is a specially built piece of equipment which contains a metre long hollow fibre waveguide employing a diamond/ZnSe composite crystal at the end as the ATR crystal (84). The probe is placed directly into the solution and provides real time spectra of what is happening within the experimental system. Due to the longer optical path length of the probe system the IR output signal is relatively low compared to that from the off-line system, therefore an external cooled MCT (mercury cadmium telluride) detector is used which has a much higher sensitivity level than the DLaTGS (deuterated L-alanine doped triglycine sulfate) detector present within the off-line system (92).

As the system is cooled and crystallization occurs, the concentration of urea remaining within the system decreases and the corresponding peak height drops. Likewise, any biuret being incorporated into the growing crystals will also lead to a drop in biuret peak height and concentration. The probe was used in both the OBC and STC systems with spectra recorded every 30 seconds over the course of the crystallization run, with 10 spectra taken and averaged for each sample point. The Shimadzu LabSolutions IR Time Course software function was then employed to follow the peak height of the previously confirmed urea (1460 cm^{-1}) and biuret (1330 cm^{-1}) peaks as a function of time. To certify the comparisons between the vessels, the FTIR probe was kept in the same location within the vessels for every run and all due care was taken to minimise disturbance of the probe, e.g. through movement of the fibre. The background was also taken and subtracted to remove any traces left on the probe.

To fully analyse the peak traces obtained a calibration curve must be produced under the new instrumental conditions. This is done to minimise errors (93) within the system and ensure precise measurements are obtained. This second calibration curve has to account for several additional factors including the probe having a much longer optical path length, the higher concentration range used, the more sensitive detector (92), any possible solution temperature effects (94) and high temperature signal drift (95). The calibration is carried out in

a similar manner to the off-line system, with high purity urea (99.5% pure) being dissolved in distilled water to form a series of solutions with known concentrations. These were then analysed using the on-line probe at various set temperatures. The on-line calibration curve shown in Figure 4.7 (filled squares) was then produced using MATLAB® and the partial least squares (PLS) function as suggested by Pöllänen et. al (96).

It is known that the different temperatures will have an effect on the signal received from the FTIR. To ensure that this effect was understood samples of the same concentration were analysed at several temperatures during production of the calibration curve. It was noted that the absorbance did not change with varying temperature, although the location of the peak varied, i.e. urea peak moving from 1450 cm^{-1} to 1455 cm^{-1}. As the FTIR time course software measurement of peak height was to locate the maximum peak height with the range, e.g. for urea between 1445 cm^{-1} and 1460 cm^{-1}, the peak value obtained was consistently the maximum of the peak independent of the temperature. Before the range was set it was confirmed that none of the impurities had a peak within these wavenumbers.

A similar calibration curve was obtained for the biuret, as shown in Figure 4.8. Due to the poor solubility of biuret in water this was carried out separately to the urea calibration; a fixed urea concentration was added to mimic the added impurity and allow for comparisons. The biuret used was only 97 % pure, which was the highest purity commercially available and was used for all experiments in this work. As with the on-line urea calibration, MATLAB® and partial least squares was utilized.

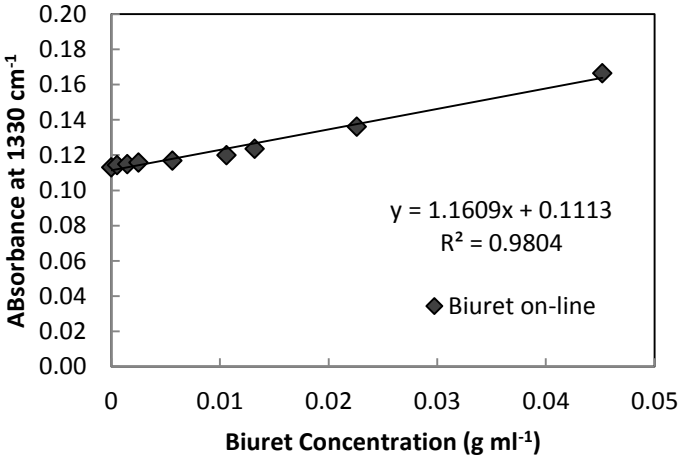

Figure 4.8 – Calibration curve for biuret concentration through on-line measurement

Note that the angle and bend-radius of the FTIR probe can also have an effect on the signal obtained (97) and a standardisation procedure was performed by taking the raw data obtained from the peak trace and plotting it onto a Microsoft Excel® spreadsheet. By analysing the graph produced, any high temperature signal drift noted was removed from the raw data. The resulting curve was then normalised to the peak height corresponding to the actual recorded solution concentration, shown in Figure 4.9. Where the original (Original) signal obtained from the FTIR is shown as the open squares and the corrected signal the filled. Once the start point relating to the initial concentration of both the urea and biuret in the solution had been fixed, any alteration in signal intensity was applied to the remaining points of the peak traces. Subsequently, the calibration correlation was used to convert the peak traces to concentrations from which the concentration of urea and biuret and supersaturation curves of urea can be constructed.

It became apparent that the mixing itself and the various intensities achieved within the systems could have an effect on the signals received from the probe. This possible issue was investigated for both the OBC and STC and it was found that when mixing was applied to the system the variation in signal reduced around a set value. It was also noted that the intensity of mixing had limited effect on the probe signal achieved, as long as the probe was not in direct contact with the mixing apparatus. Consequently care was taken to ensure the probe location was away from the mixing apparatus and was fully submerged in the solution to achieve the best results. Some of the data produced in this study is available in Appendix A.

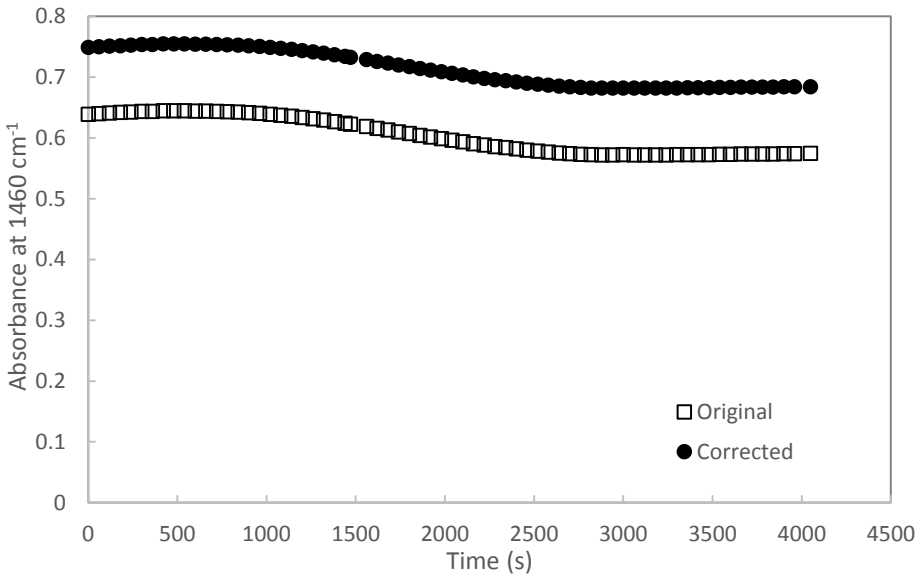

Figure 4.9 – Original and corrected On-line FTIR traces for Urea

4.1.3.4 Comparison of calibration curves

It can be seen that for urea, the on-line calibration has a similar slope to the off-line relationship while covering a much wider concentration range. With a more sensitive detector and the compensation of temperature effects, the on-line probe calibration data points are higher than the off-line ones (Figure 4.7) for the small range of similar concentrations tested. The lower parts of the two curves can be linked via equation (4.1) if required. However, it should be noted that these two calibration curves are not directly comparable as it is necessary for the calibration curve to be specific to the optical set-up of the individual instrumentation used (98).

$$\text{On-line Peak Height} = (1.3387 \times \text{off-line Peak Height}) + 0.049 \qquad (4.1)$$

4.1.4 Crystal Size Analysis and Crystal Imaging

Following crystallization at the specific conditions and analysis of the product purity, it is important to examine the actual physical properties of the crystals produced using a mastersizer for size distributions and both scanning electron microscopy and optical microscopy for crystal images and possible agglomeration. The size and shape characteristics of the crystals were analysed using the morphology G3 system. This would also give some insights into the purity results obtained.

4.1.4.1 Crystal Size Distributions

Due to the highly soluble nature of urea (74) the crystal size distribution (CSD) must be obtained on a dry basis. To complete this, a Malvern Instruments 3000 series Mastersizer was used and was fitted with an Aero dry dispersion unit which employs compressed air to disperse the solid crystals. Tests completed prior to analysis showed very little difference in results when operating at high or low pressure which suggested that the crystals were resistant to breakage at these conditions. Therefore, a standard operating procedure was established which employed a pressure of 1 bar and a 2 mm hopper gap to allow even dispersion of the crystals, complete attainment of the data took around 3 minutes. As the mastersizer only analyses a small amount of the crystals, each run was repeated for a minimum of three times to ensure both consistency and accuracy. To guarantee that the CSD was relevant to the whole product the samples taken for each run came from a different section of the product crystal bottle and were only chosen after making sure that the whole product had not settled.

The CSD results contain two sets of data; the full CSD and the diameters equivalent to certain percentages of the sample. The full CSDs allowed viewing of whether the distribution is uni- or bi-modal and to compare the distributions between vessels and conditions. An example of CSD produced between the OBC and STC are shown in Figure 4.10. These were obtained at a fixed cooling rate of 0.50 °C/min and a fixed mixing intensity of 170 W/m^3. This overall look at the crystal sizes is useful but quantitative analysis of the crystal size and statistical comparisons cannot be made from the curves alone.

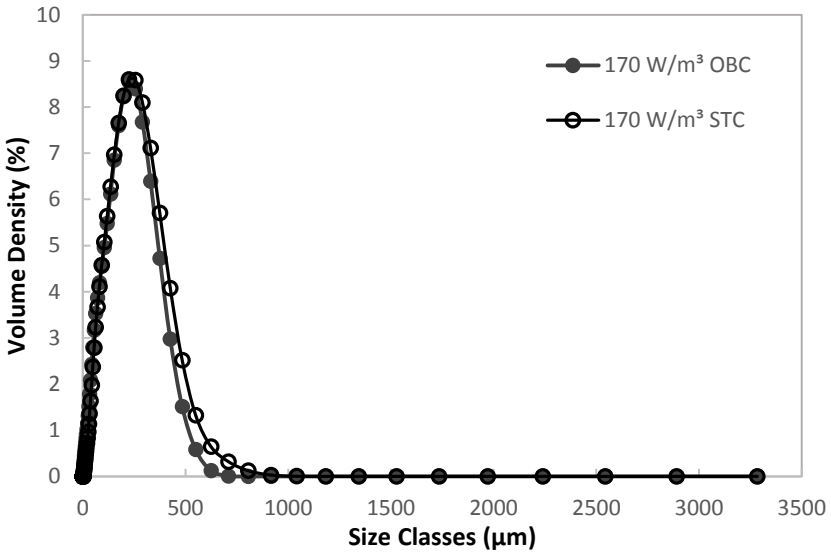

Figure 4.10 – CSD from crystals produced in the OBC and STC at a cooling rate of 0.50 °C min^{-1} with a mixing intensity of 170 W m^{-3}

The data presented in Figure 4.10 shows the volume density of each of the size classes monitored. The volume density gives an overview of the percentage of the particles analysed which were of that size. The size classes were pre-determined by the mastersizer and material testing on a small sample of the crystalline material.

As well as the CSD shown in Figure 4.10, numerical data relating to the equivalent diameter of 10 (D_{10}), 50 (D_{50}) and 90 % (D_{90}) of the sample were calculated where the equivalent diameter of 50 % of the sample is taken as the mean value. This was subsequently used for statistical analysis and direct sample comparison along with the calculated span. To obtain the span of the CSD the equivalent diameter measured at 10 % of the sample (D_{10}) was subtracted from the equivalent diameter at 90 % (D_{90}), and was then divided by the equivalent diameter of 50 % of the sample (D_{50}) shown in equation 4.2. When a small CSD span is obtained the CSD is narrow and there is not an excessive number of either fine or large agglomerates; while a larger

span implies that the CSD is possibly bi-modal and contains either a larger number of broken crystals or large agglomerated crystals.

$$\text{CSD Span} = \frac{(D_{90} - D_{10})}{D_{50}} \qquad (4.2)$$

4.1.4.2 Crystal Imaging

While the CSD data gives an idea of the size of the crystals produced it doesn't reveal much about the actual shape and formation of the crystals created. In this work three different types of crystal imaging were utilized: scanning electron microscopy (SEM), optical microscopy and Morphologi G3.

SEM

A scanning electron microscope (SEM) takes images of compounds with high resolution and greater detail than basic optical microscopy (99), because SEM uses a focused electron beam which is scanned over a surface to create an image. The SEM generally operates under a vacuum and before placing the samples in the chamber the urea crystals were spluttered with gold to stop the crystals 'charging' (99) and causing scanning faults such as unclear or 'fuzzy' images.

The experiments were carried out using high vacuum SEM with a gold coating on the crystals. Equipment was used courtesy of Heriot Watt EPS Focused Ion Beam facility.

As the crystals being analysed here were quite large, several different magnification levels were tested. An example of the three image scales obtained in this work are shown in Figure 4.11. These images are from crystals produced in the STC under high mixing intensity of 750 W/m^3 and a fast cooling rate of 0.75 °C/min. These show that while the larger scale [A] (500 µm) gives an image of a whole crystal, the closer images [B & C] (300 µm and 100 µm scales respectively) allow viewing of the crystal surface and crystal joins. It was decided to mainly use the images with a 500 µm scale for presentation.

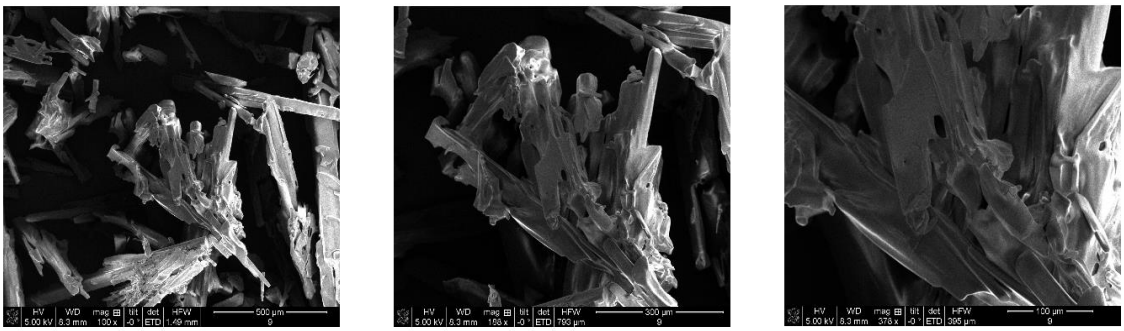

A B C

Figure 4.11 – SEM images of the same urea crystal viewed at the A) 500 µm scale; B) 300 µm scale and C) 100 µm scale

Optical Microscopy

As well as the SEM, images of the product crystals were obtained through optical microscopy. The optical microscope produces images of a larger scale than the SEM images which allows us to view more individual crystals within any given image. This is an advantage of the microscope over the SEM as viewing more crystals at once means that any trends in size or agglomeration levels can be confirmed within the same image. In order to capture the images a camera with live recording and 'snap-shot' functions was mounted above the microscope lens which was placed directly above the crystals being imaged. Due to the high birefringence (100) of the urea crystals, a polarizing lens was also used between the light source and the crystals to give clear images of crystals with minimal light interference. Birefringence is the optical property of a material having a refractive index that depends on the polarization and direction of light.

Again several magnification levels are possible depending on the size of crystals being viewed and the quality of the microscope and camera, in the end the images were all taken with a 4 times optical zoom as this allowed the maximum number of crystals to be viewed at one time. The microscope used was a Leica ATC 2000 and the camera produced by Imagingsource. An example of the images obtained are shown in Figure 4.12, these crystals were produced from the OBC and STC under the same conditions as those shown in Figure 4.11. In addition to knowing the magnification, a 200 µm scale bar is added into each image to give some sense of the size of the objects being seen.

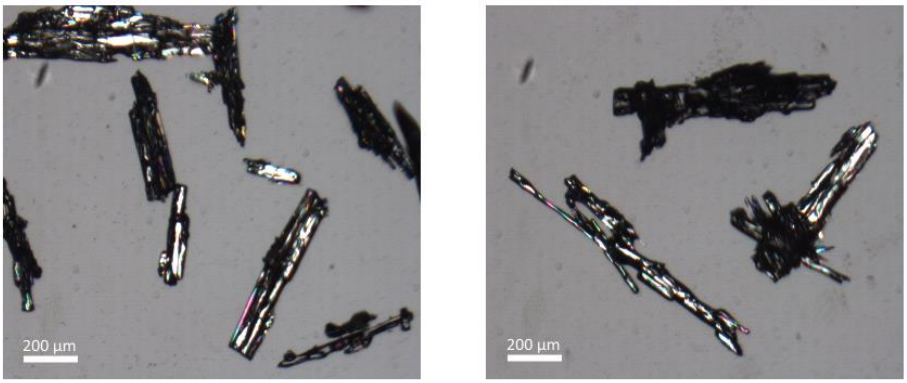

Figure 4.12 – Microscope images obtained from crystals produced by the OBC and STC using conditions of 750 W m^{-3} and 0.75 °C min^{-1}

Figure 4.12 shows that due to the high birefringence of the crystals there are sections of the crystals which appear very dark and others lighter. Without the addition of the polarizing lens all the crystals would be bright which make them very difficult to see.

Morphologi G3

Following the CSD and microscope image study of the crystals produced, further quantitative analysis of the crystals was sought. The Malvern Morphologi G3 (Courtesy of CMAC based at University of Strathclyde) examines the crystals by dispersing the dry crystals across a clear glass plate using air at 1 bar and then imaging each individual crystal automatically. One of the main advantages of this system is that it explores a wide selection of crystals (over 250 per data set), such a larger number of crystals cannot be analysed at one time by any of the previously mentioned imaging systems, complete imaging of the crystals took around 40 minutes per set. On imaging of each crystal, unique computer software investigates each image and produces specific characteristic size and shape parameters as well as the statistical standard deviations. From this analysis any rogue images, e.g. those due to dust, were removed and the results for each condition and impurity analysed. To ensure enough crystals to give reliable data per run, a specific volume of sample (7 mm^3) was dispersed in each case and the samples run were carefully selected to fully represent each individual condition. The five main characteristic size and shape parameters are given in Table 4.2. These are just a selection of the possible parameters which can be utilized and were chosen as they were the most relevant to this work.

Table 4.2 also provides a quick explanation of each term, taken from the equipment user guide (101).

Table 4.2 – Definitions of Morphologi G3 parameters used in this research

Parameter	Definition	Units
Length	Longest crystal projection on the major axis	µm
Width	Longest crystal projection on the minor axis	µm
Circularity	The ratio of the circumference of a circle equal to the objects' projected area to the perimeter of the object	-
Circle equivalent diameter	Diameter of a perfect circle with equivalent area	µm
Aspect ratio	Ratio of width values to length values	-

4.2 Statistical Analysis Methods

To ensure that any differences in the data presented in this work are actually significant and not just down to chance, statistical analysis was carried out on the raw data. This is an important step in data quality control as visible patterns in random data sets may lead to unfounded conclusions from the results. This approach is referred to as inferential statistical analysis (102), the whole point of which is to extrapolate from a limited amount of data and quantify the uncertainty from the data, to make a general conclusion. This is in contrast to descriptive statistical analysis which simply describes the data obtained.

There are many different methods for statistical analysis, with all of them requiring specific parameters to be met before any are suitable for use. It should be noted that every statistical analysis method is based on assumptions about the properties of the underlying distribution of the data. The assumption which is made in every statistical calculation is that the data is randomly sampled (102). This means that the data is representative of a larger population of values. Each method also has limitations for its specific use as well as variables which can be altered to achieve the best results.

This section identifies the possible statistical analysis methods which could be utilized in this research. Each method will then be tested against available data and a conclusion will be made as to which is the most useful one for this research.

4.2.1 Basic Statistical Parameters

4.2.1.1 Sample Distribution

The main type of distribution expected from a selection of sample data is a normal distribution. A normal distribution, as shown in Figure 4.13, is the most important and widely used distribution in statistics (103). Normal distributions can differ in both the value of their means and their standard deviations. There are several factors however which are true for all normal distributions (104); these factors are mentioned below:

- Normal distributions are always symmetrical around their mean;
- The mean, median and mode of a normal distribution are equal;
- The area under the normal curve is equal to 1;
- Normal distributions are denser in the centre than the tails;
- 68% of the area of a normal distribution is within one standard deviation of the mean and approximately 95% of the area is within two standard deviations, shown in Figure 4.13.

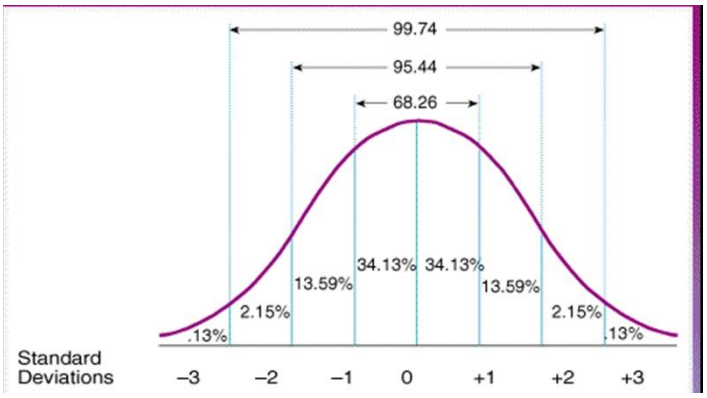

Figure 4.13 – An example of normal distribution (104) for statistical analysis

A normal distribution is required for many statistical techniques and if this cannot be confirmed, problems can occur. There are two options to deal with this problem, the first is to employ some equivalent "non-parametric" test or alternatively depending on sample size it may be possible to continue with a normal distribution-based test.

4.2.1.2 Samples Sizes

As mentioned there are several factors which can limit the suitability of certain tests; one of these factors is the sample size of the data available for analysis. If a large sample set is available

it can be assumed that the data sampling is normally distributed even if it has not been confirmed. Generally this is only true if the sample has more than 100 observations per data set (105).

As the amount of data per set to be analysed in this work is far lower than 100 the assumption of a normal distribution cannot be made automatically. Therefore the statistical tests which assume a normal distribution can only be applied if the variable can be proved to be normally distributed. However, if the sample size is small there is no way to test whether the distribution is normal and another type of test must be employed.

4.2.1.3 Parametric and Non-parametric Methods of Analysis

When the distribution is not normal, non-parametric procedures are used which rely on no, or only a few, assumptions about the shape (or parameters) of the population distribution (105, 106). Equally when a normal distribution cannot be tested because the sample size is small, non-parametric testing is also applicable.

Table 4.3 (106) shows an example of several types of analysis and the corresponding parametric and non-parametric tests which can be carried out to investigate the data.

Table 4.3 – Different statistical tests and the type of analysis they can be used for

Type of analysis	**Parametric test**	**Non-parametric test**
Comparison of means between two independent groups	Two-sample t-test	Wilcoxon rank-sum test or Kolmogorov-Smirnov two-sample test
Comparison of two quantitative measurements	Paired t-test	Wilcoxon signed-rank test
Comparison of means from three or more independent groups	Analysis of variance (ANOVA)	Kruskal-Wallis test
Estimation of the degree of association between two quantitative variables	Pearson coefficient of correlation	Spearman's rank correlation

Since non-parametric tests require few or no assumptions about the data distribution and there are many of them which test the same parameters as the parametric tests, the question arises; why are non-parametric tests not always used instead of the parametric versions? The answer is that the non-parametric tests have several drawbacks which limit their application. The first drawback is that they are generally less statistically powerful than the equivalent parametric test (106) and the second problem is that the interpretation of the results

is often harder than with parametric results. This is because many of the non-parametric tests rank the data and then use this ranking in their analysis, whereas the parametric tests use the actual data (106). Consequently while non-parametric procedures are useful and in some cases necessary, they cannot be taken as the perfect solution to statistical analysis.

As mentioned several statistical parameters are needed for the analysis to be carried out and are also used to describe the trial results. A brief discussion of some of these parameters will now be commenced before results of the statistical tests in Table 4.3 are presented.

4.2.1.4 Null Hypotheses

Every statistical analysis tool, whether a parametric or non-parametric method, uses a null hypothesis as the basis for comparison. This null hypothesis is usually the hypothesis that sample observations result purely from chance (107), i.e. assuming that the sample data are all the same and the populations of both samples are identical (102).

Once the basic null hypothesis has been decided it can then be used for hypothesis testing of the samples. Generally this is completed by asking if the null hypothesis were true, how unlikely would it be to obtain the samples randomly when the difference is as large as actually observed? This is where the P value becomes useful.

4.2.1.5 Statistical Significance (P Values)

The P value is defined as the probability of obtaining a result equal to or greater than what was actually observed, when the null hypothesis is true (102). If a large P value is obtained, the data sampled is consistent with the null hypothesis and the data are similar, if not identical. However if a small P value is obtained, there is only a small chance that the differences are due to random sampling and this suggests that the null hypothesis is false. The P value has the same general determination for all statistical tests, however its precise definition depends on the specific test being used.

For the differences between data to be statistically significant, a P value of less than 0.1 is required, often lowered to 0.05 as to ensure the statistical difference is definitely significant. There is no mathematical reason for the aforementioned limits, they are completely arbitrary but are generally well excepted as the significance level limits (102). However the actual concept of “statistical significance” is not as definitive as it seems. All it means is that the difference observed would happen by chance less than 10% or 5% of the time respectively and therefore the null hypothesis can be rejected. A large P value indicates that the data is statistically similar, however this does not necessarily mean that the null hypothesis is true (102). It is possible that the null hypothesis is false and that there is actually a difference between the populations being

tested. This can be a significant problem if the sample of data is small. On the other hand if a large data set is trialled, what may seem like a small effect or difference scientifically can be statistically significant (102), which can again be wrong and lead to incorrect conclusions about the data.

Another problem with analysing statistical results is that if several hypotheses are tested at the same time, a false result can easily be made. This means that as the number of hypotheses tested increase, the probability a statistically significant result will be obtained increases greatly, even if all of the tests are actually similar, i.e. the results gives a low P value which is false. Special methods have been designed to deal with this; however the use of these can make it more difficult to find the true results. To combat this, the minimum number of hypotheses will be tested at one time in this work, e.g. only one hypothesis will be tested in each case.

4.2.1.6 Other Important Factors (h and F values)

Depending on the statistical test, other statistical factors can be produced as well as the P value. From the tests tabulated in Table 4.3, the two other factors which will be produced and analysed here are the h value and an F ratio.

The h value relates directly to the ability to accept or reject the null hypothesis which has been put forward. The h value only has two responses which make it very simple to understand and means that it is easy to interpret as a result.

If h = 0: the statistical test has failed to reject the null hypothesis at the specified significance level;

If h = 1: the test has rejected the null hypothesis at the specified significance level.

The h value is produced as a default by the majority of the tests investigated in Table 4.3 and therefore will be of importance when deciding which test to use for the analysis of this work.

In contrast the F ratio is produced by the ANOVA test (108), and is more open to interpretation than the h value. This ratio will be discussed in detail during description of the relevant test in Section 4.2.2.1.

4.2.1.7 System Errors

As there are inbuilt errors associated with all experimental monitoring techniques these can then affect the accuracy of the statistical analysis. It has been shown that by increasing the measurement error of dependent variables the chance of getting an incorrect result, i.e. a non-

significant result when a significant result is the correct outcome (102), increases. It is therefore important to minimise these errors by using calibrated equipment with known low error values and by keeping the monitoring tools and location constant, e.g. thermocouple and FTIR probe. The experimental runs were also all carried out in triplicate to minimise the system errors and help the accuracy of the results.

4.2.2 General Tests

Following the brief explanation of the statistical parameters, a selection of the possible tests, mentioned in Table 4.3 will now be reviewed. This will be completed with an appraisal of the assumptions required and a brief summary of the advantages for each one. Section 4.2.2.1 discusses parametric tests, while section 4.2.2.2 looks at the equivalent non-parametric tests.

4.2.2.1 Parametric Tests

Student's t-Test

The first statistical test to be trialled is the students' t-test, which is one of the most commonly used statistical tests available (109) to test whether two sets of data are really different. This is completed by testing hypotheses about a mean value (110). An advantage of this test is that it only requires a small data sample which is drawn from a normally distributed population where the standard deviation is unknown.

As mentioned previously a null hypothesis is formulated before any analysis occurs. This hypothesis generally states that there is no effective difference between the observed sample mean and the hypothesized population mean. The t-test is commonly carried out as either a two-sided test that simply shows whether the means are equivalent or not, or as a one-sided test which specifies whether the observed mean is larger or smaller than the hypothesized mean. Once the test statistic has been calculated it is compared to a critical value determined by a reference distribution (109). If this test factor is more extreme than the critical value the null hypothesis can be rejected (i.e. small P value). As mentioned previously the critical value depends on the significance level of the test. This test statistic (t) is calculated from equation 4.3.

$$t = \frac{\bar{x} - \bar{y}}{\sqrt{\frac{s_x^2}{n} + \frac{s_y^2}{m}}} \qquad (4.3)$$

Where $\bar{x}$ and ȳ are the sample means, S_x and S_y are the sample standard deviations and n and m are the sample sizes for each data set.

Example:

To analyse whether this test would be appropriate for use in this work, a test run is carried out using the data from Table 4.4. Table 4.4 presents an example of purity results from three experimental trials in two different vessels carried out in this research. As can be seen the sample size is small but this is not a problem with this type of test.

Table 4.4 – Example of initial purity results obtained

Experimental run	OBC	STC (S1)
1	96.4	94.7
2	96.5	95.4
3	96.3	95.3

After running a two sample t-test, *ttest2*, on this data using MATLAB®, an h and a P value can be obtained, as discussed previously and shown in Table 4.5. The results in Table 4.5 suggest that the null hypothesis can be rejected at the 5 % significance level, with the P showing that the probability of this result being down to chance is only 2 %.

Table 4.5 – Results of Students' two-sample t-test

Students' two-sample t-test	Results
h	1
P	0.02

This is a positive result as the sample means do appear to be different when looking at the actual numbers and both means have small standard error values.

One-Way ANOVA

Often it is required to compare data from more than two data sets, the ANOVA test could be used for such a comparison. ANOVA stands for analysis of variance and the purpose of a one-way ANOVA is to determine whether the data presented from several groups have a common mean (108). This test determines whether the groups being compared are actually different in

the measured characteristics. The underlying model used by ANOVA analysis assumes a random distribution with a Gaussian population; other assumptions used by this test are that the samples are independent, with equal variances and all sample groups must have the same size.

The ANOVA test is very similar to the Student's t-test, except that it tests three or more sample sets at the same time. The ANOVA analysis consists of a series of calculations and treatments carried out on a data table. As with the t-test results, a P value, the statistical probability, is returned and in this case so is an F ratio value.

The ANOVA model is based on a special case of a linear model. The one way ANOVA version of this model is shown in equation 4.4.

$$y_{ij} = \alpha_j + \varepsilon_{ij} \quad (4.4)$$

Where y_{ij} is an observation*; i* is the observation number and *j* is indicative of the different group of indicator variable *y,* α_j is the population mean for the *j*th group and ε_{ij} is the random error which is independent and normally distributed.

The F ratio is simply a ratio of differences obtained by dividing the variance between the sample groups by the variance within the sample groups, shown in equation 4.5.

$$F = {}^{variation\ between\ sample\ means}/_{variation\ within\ the\ sample} \quad (4.5)$$

If the null hypothesis is true and the sample groups are similar, an F value close to 1 would be expected most of the time. If a large F ratio is obtained this means that the variation noted between the groups being tested is more than expected to be seen by chance. However this does not necessarily mean that the null hypothesis is wrong. While a large F ratio is obtained when the null hypothesis is wrong, one can also be found when random sampling happens to end up with large values in some groups and small ones in others.

The ANOVA test can also be carried out in using the *ANOVA: Single Factor* function found under the Data Analysis tab in Excel. Similar to the MATLAB function this returns an *F* value, an F_{crit} value and a P value to allow you characterise the data.

Example:

As this test requires at least three sample sets, another column must be added to the data presented in Table 4.4, this is shown in Table 4.6. Again the null hypothesis suggests that all three sample means are similar.

Table 4.6 – Example of purity results for one experimental condition

Experimental run	OBC	STC (S1)	STC (S2)
1	96.4	94.7	95.4
2	96.5	95.4	95.7
3	96.3	95.3	95.2

Again using the MATLAB® statistics package, this test was completed using the *anova1* function and the results given in Table 4.7, along with the resulting box-plot (Figure 4.13). From Table 4.7, it can be seen that a large F ratio has been obtained along with a small P value. This suggests that the null hypothesis can be rejected with confidence, as the probability that the results occurred by change are small.

Table 4.7 – One-way ANOVA results

One-Way ANOVA	Results
P	0.003
F	18.2

However, the results in Table 4.7 cannot directly tell us which groups are significantly different from each other, only that at least two groups are different, for example from Table 4.6, it would seem that the OBC results are different from the two STC results; however this cannot directly be inferred from Table 4.7. If the box-plot shown in Figure 4.14 is also analysed, it confirms that the difference is indeed between the OBC and the two STC results, demonstrating that for this test to be useful both the numerical and graphical results must be analysed together.

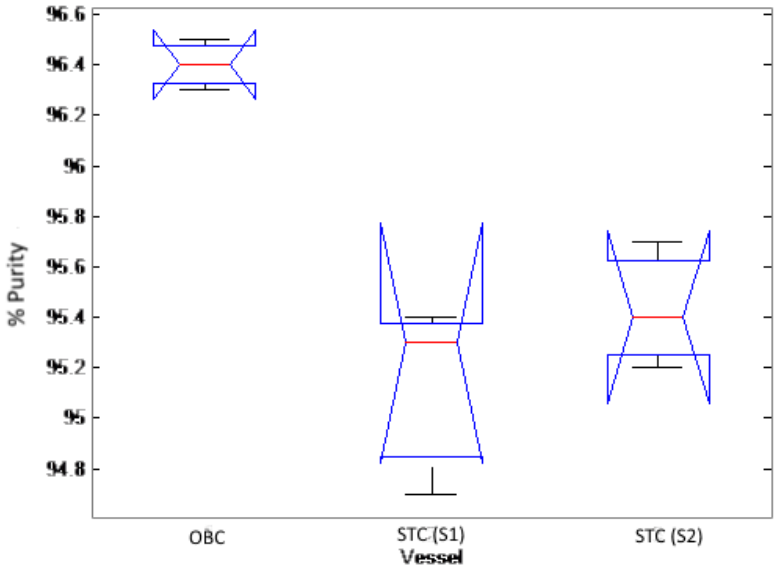

Figure 4.14 – One-way ANOVA box-plot result

A quick explanation of the box-plot must be given, the top and bottom lines of each box represent the 25th and 75th percentiles of the samples respectively (108). These are the limit of the mid-spread, which describe the middle section of the distribution and give an indication of whether a normal distribution is present. They are not equal in this case suggesting the distribution is not normal, possibly due to the small sample size. The line in the middle of the box is the sample median and if this line is not centred it shows the unevenness of the sample distribution. Any lines outwith the box show the total spread of data.

If the assumptions required to carry out both the previous statistical tests are looked at, it is apparent that a normal distribution was assumed. While the results suggest that this may be true, as a low P value and clear difference in the box-plot, there is no way of confirming this distribution due to the small sample size. Consequently further tests must be carried out using non-parametric tests to ensure that false results are not being obtained due to poor assumptions.

4.2.2.2 Non-parametric Tests

Following the discussion of parametric tests, equivalent non-parametric tests will now be considered (Table 4.3). For the comparison of two sample data sets, the Wilcoxon rank sum test and the Kolmogorov-Smirnov test will be tried and compared to the Student's t-test. While the Kruskal-Wallis test will be used to compare data for three or more sample data sets.

Wilcoxon Rank Sum Test

The Wilcoxon rank sum test is one of the non-parametric tests which are equivalent to the two-sample Students' T-test analysed previously. It differs from the previous test in that the result is based solely on the order in which the observations fall from the two samples, not the actual data values (111). Every observation has a rank, with the smallest being ranked 1, the next 2 and so on until the largest value is reached. The Wilcoxon rank-sum test statistic, *W,* is based on the sum of these ranks from each of the sample sets, which is compared to the sum from the second set. To confirm whether a sample is different the value *W* is taken as the smaller of the two rank-sums, this is then compared to the critical value, W_{crit}, from Wilcoxon rank sum table. The value used is taken at the required confidence (e.g. 0.05) and for the relevant sample size data points. If the *W* value is lower than the critical value the null hypothesis can be said to be true. When using MATLAB the software calculates a probability level when the null hypothesis is true and returns this as the P value.

When using this test a normal distribution is not assumed and the test can be completed assuming that the two independent samples are drawn from populations with an ordinal distribution (111). A set of data can be said to be ordinal if the values can be ranked or put in some order (112).

The null hypothesis is slightly different from that of the t-test, in this case we assume that 'the observations come from the same population' (111). From a practical point of view this suggests that the populations for each sample have the same median. A P value will be produced, with a small P value again suggesting the null hypothesis can be rejected.

Example:

Taking the data from Table 4.4, this can easily be ranked from the smallest to the largest in terms of its numerical value, shown in Table 4.8. From this it can be seen that the rank total in the OBC is higher than that in the STC.

Table 4.8 – Example results with added ranking

Experimental run	OBC	Rank	STC (S1)	Rank
1	96.4	5	94.7	1
2	96.5	6	95.4	3
3	96.3	4	95.3	2
Rank sum		12	Rank sum	6

If these results are then analysed again using the in-built *ranksum* statistics function in MATLAB® the results are shown in Table 4.9, where the P value is higher than the standard limit for statistical significance (i.e. P > 0.1) and subsequently this leads to an h value of 0, meaning that the null hypothesis cannot be rejected.

Table 4.9 – Wilcoxon rank-sum test results

Wilcoxon rank-sum test	Results
P	0.11
h	0

This result is contrary to what has been suggested by the t-test and the ANOVA method. There are two possible reasons: either (1) the distribution of results is not normal in this case and therefore the parametric tests were giving incorrect answers; or (2) the data sets are too small for the analysis and thus this test cannot be used for these results. At this stage the exact reason cannot be established as we cannot confirm either case. Therefore another non-parametric test, the Kolmogorov-Smirnov test, which is again equivalent to the Student's t-test, will be analysed.

Kolmogorov-Smirnov Test

The Kolmogorov-Smirnov test also determines whether two data sets differ significantly and has the advantage of making no assumptions about the distribution of the data (113). It is similar to the two-sample t-test in that it can compare two different data sets and is able to cope with small sample sets as there is no specific limit on the size of the sample, unlike the Wilcoxon rank-sum test.

The statistical test itself measures the greatest distance between the empirical distribution function (EDF) of a data set and the comparison step function of the second data set (113). This is shown as an equation in Equation 4.6; where the EDF test statistic, D, is produced from the maximum distance (max) between two steps, *F*1(x) and *F*2(x). An example of an EDF plot is given in Figure 4.15 and gives a graphical representation of the two data sets. These are shown as an unbroken line and a dashed line and clearly show that there is a large difference between the data sets, which is the test statistic, D

$$D = max(|F1(x) - F2(x)|) \quad (4.6)$$

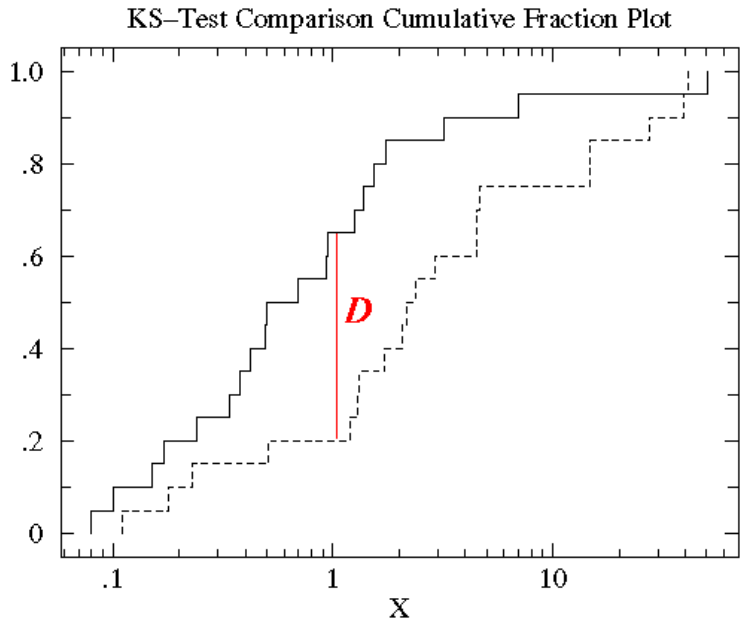

Figure 4.15 – EDF example plot for Kolmogorov-Smirnov test (113)

In this case the null hypothesis suggests that a chosen data set is drawn from the same population as a second data set, i.e. they are the same data. As before the results obtained here are in the form of a P value to give an indication of the probability and an h value showing whether or not the null hypothesis can be rejected.

Example:

Again, the data being tested is that shown in Table 4.4. Using the two-sample Kolmogorov-Smirnov function, *kstest2*, to analyse the data in MATLAB® the following results are produced (Table 4.10).

Table 4.10 – Two-sample Kolmogorov-Smirnov test results

Kolmogorov-Smirnov test	Results
P	0.06
h	0

The results in Table 4.10 are interesting with the h value being 0, suggesting that we cannot reject the null hypothesis, even though the P value is small. This is because the significance level is automatically set at 5 % (or a P value of 0.05) in the MATLAB function, the P value in Table 4.10 is just above that. As this significance level is completely arbitrary, it can be

varied within reason and in fact if it is raised to 10 % we get an h value of 1. As previously mentioned a significance level of 10 % is acceptable and will be used in this work due to the small sample size available.

These results appear to be similar to the two-sample t-test results, although the P value is slightly higher. This is likely to be due to the reduced sensitivity previously noted (106) when comparing non-parametric tests to the equivalent parametric ones. This Kolmogorov-Smirnov test suggests that the results obtained using the Wilcoxon rank-sum were due to the sample size being below an in-built limit within the test.

Kruskal-Wallis Test

For more than two data sets, the Kruskal-Wallis test will be trialled for non-parametric analysis.

As with the Wilcoxon rank-sum test, the Kruskal-Wallis test ranks the data from the lowest to the highest and then uses these ranks in the statistical test (114). The ranking step takes no account of the location of each data point, i.e. no attention is paid to which sample set the data is in. If any data points have the same value, these are treated as tied values and are given an average of the two (or more) ranks over which they are tied. The ranks are then summed and the differences between the rank sums of each sample set are used to form a Kruskal-Wallis statistic. A large value in the Kruskal-Wallis statistic corresponds to a large discrepancy between the groups (114). The test statistic (H) is calculated from equation (4.7), where *n* is the number of entries and SS_B' is the sum of squares between groups using the ranks instead of raw data. The sum of squares between groups represents the degree of variation from the mean between the groups. It is calculated through the initially determining the squared differences between the mean rank values of the individual sets and the overall mean of the sample ranks. Each difference is then multiplied by the number of ranks within each set before all squared rank values are added together.

$$H = \frac{12}{n(n+1)} SS_B' \qquad (4.7)$$

This test statistic is similar to a chi-square distribution, if this statistic is less than the critical chi-square value the null hypothesis cannot be rejected. If on the other hand the test statistic is greater than this chi-square values, the null hypothesis can be rejected and the samples can be said to come from a different population. The P value is calculated from the chi-square distribution.

The null hypothesis assumed here is similar to those above in that it suggests that the groups are sampled from identical distributions. Again the P value is the resultant outcome, with a small P value suggesting that the populations have different distributions while a large P value does not give any reason to conclude the distributions are different, i.e. the null hypothesis cannot be rejected.

It is important to note that as with the ANOVA test, the result of the Kruskal-Wallis test is an overall value which only tells you if at least two groups are different (114). Consequently a box-plot is also needed.

Example:

Similar to the Wilcoxon rank-sum test, the data is ranked and the resulting set is shown in Table 4.11.

Table 4.11 – Experimental purity values with added ranking

Experimental run	OBC	Rank	STC (S1)	Rank	STC (S2)	Rank
1	96.4	8	94.7	1	95.4	4.5
2	96.5	9	95.4	4.5	95.7	6
3	96.3	7	95.3	3	95.2	2
Rank Sum		24		8.5		12.5

These total rank values are then analysed using the in-built *kruskalwallis* function in MATLAB® to give the P value (Table 4.12), as well as a box-plot of the data shown in Figure 4.16.

Table 4.12 – Results of Kruskal-Wallis test

Kruskal-Wallis test	Results
P	0.06

From Table 4.12 it can be seen that only a P value of 0.06 has been produced suggesting that while there are some differences within the data groups it is not statistically significant at the 5 % significance level. This is a different outcome to that indicated by the ANOVA over the same data and is likely due to the fact that the ranking values between the STCs are fairly similar overall. This is confirmed by the box-plot produced from the Kruskal-Wallis test, which as the

data used is the same as for the ANOVA test is identical to Figure 4.14. This implies that the similarity between the two STC values may be having a bigger effect on the overall P value in the Kruskal-Wallis test than that in the ANOVA test. This supports the need to have another test result, like a box-plot, with this type of analysis to ensure that any conclusions drawn are valid.

4.2.3 Conclusions

The above sections have given a brief overview of the basis for several statistical tests as well as an example of each test. It has been noted that the most important factor, to ensure the suitability of the test, is whether the data is normally distributed. If it is, a parametric test can be employed for the analysis; however if not, a non-parametric test must be used.

It is also important to know how many groups of data to analyse. If the wrong type of test is trialled the results obtained may be inaccurate and lead to false conclusions about statistical significance.

Consequently, as the sample sizes analysed in this research are rather small, the Kolmogorov-Smirnov test will be used for the comparisons of two data groups with a significance level of 10 % since the data cannot be confirmed as normally distributed. The 10 % significance level allows the user to be confident of the results even with these small data sets. When three or more data sets are compared the Kruskal-Wallis test and the corresponding box-plots will be used to ensure any results are accurate. These tests are being used to ensure the highest confidence in the similarities and differences presented within the data are obtained given the small sample size.

Chapter 5 Verification and Explanation of Previous Results

5.1 Introduction

As previously mentioned, unpublished confidential industrial trials (11) have shown that the oscillatory baffled crystallizer (OBC) produces crystals having a higher purity than that in the stirred tank (STC) under comparable conditions. The initial aim of this research project was to verify these unpublished results and then find reasons for any differences and trends noted.

This was completed using the procedure aforementioned in Section 3.4.1, with the specific components added into the system to obtain the required supersaturation of 1.05 for a saturation temperature of 30 °C shown in Table 3.2. Both the moving baffle OBC and a STC with a two blade flat-paddle impeller were used for this work, the set up are described in Section 3.1. Five separate conditions, suggested by previous unpublished work, were investigated in both vessels, including two different linear cooling rates (0.50 and 0.75 °C/min) and three target mixing intensities (20, 170 and 750 W/m^3) as shown in Table 3.1. The number of results used for statistical analysis is 3 for each experiment unless stated otherwise.

5.2 Purity Results

The purity results obtained from the off-line IR analysis are shown in Table 5.1 for the five investigated conditions. These results are the average values achieved from a minimum of three experiments at each condition and are presented in Table 5.1 and Figure 5.1. The standard deviation ($\pm$ SD) is given to give an indication of the spread of results as well as the statistical probability factor (P) calculated from the Kolmogorov-Smirnov non-parametric statistical test. As previously described in Section 4.2, for the results to be statistically different a P value of less than 0.10 must be obtained.

Table 5.1 – Average purity results obtained for urea with standard deviations and statistical probability

Average % purity $\pm$ SD		Cooling rate (°C min^{-1})					
		0.50			0.75		
		OBC	STC	P	OBC	STC	P
Mixing intensity (W m^{-3})	20				96.1 $\pm$ 0.36	95.8 $\pm$ 0.21	0.32
	170	96.4 $\pm$ 0.21	95.9 $\pm$ 0.21	0.06	96.2 $\pm$ 0.15	95.5 $\pm$ 0.42	0.06
	750	96.4 $\pm$ 0.21	95.1 $\pm$ 0.36	0.06	97.3 $\pm$ 0.12	96.5 $\pm$ 0.12	0.03

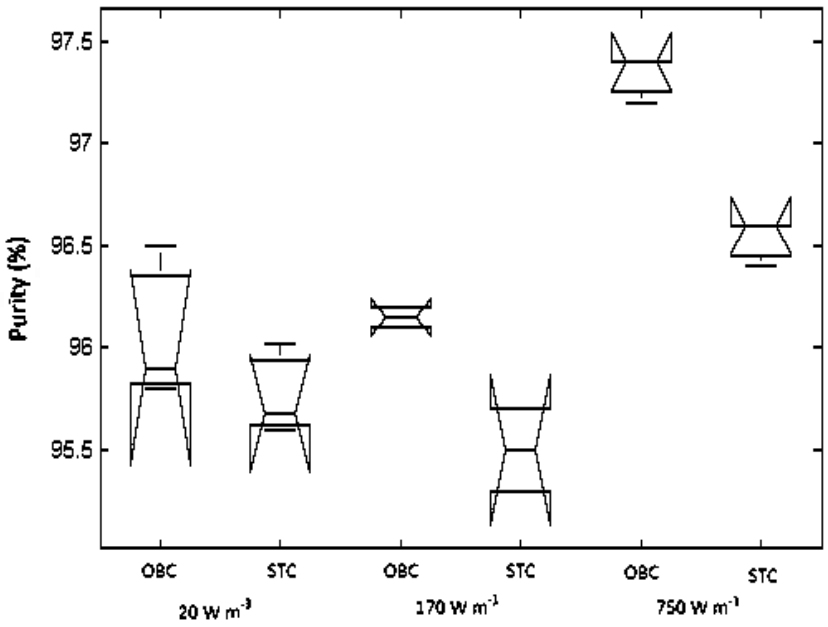

Figure 5.1 – Kruskal-Wallis Box-plot for purity values at fixed cooling rate (0.75 °C min^{-1}) from both OBC and STC at three mixing intensities

The box-plot shown in Figure 5.1 was produced using the Kruskal-Wallis statistical function and shows graphically the difference between the OBC and STC purity results at fixed cooling rate of 0.75 °C/min. This emphasises the purity result differences between the OBC and STC at each of the three mixing intensity shown in Table 5.1. At the lowest mixing intensity (20 W/m^3) it becomes apparent that the OBC and STC results overlap and are therefore similar. The other two conditions shown, indicate that the OBC purity is higher than the STC values and there is no overlap between the two result sets. This supports the previously tabulated results which indicate that the OBC produces higher purity crystals than the STC.

The purity results given in Table 5.1 verify the previous data from industrial trials with the OBC crystals of a higher purity than the STC counterpart at comparable conditions. This difference is statistically significant for four of the five conditions investigated in this work.

5.3 Discussion of Results

Following confirmation of the purity results the next step is to discover what has influenced this purity in the two crystallization systems. To investigate the possible reasons, several parameters will be compared and discussed in detail including concentration profile, supersaturation profile, nucleation temperature and crystal size and shape.

5.3.1 Concentration Profiles

Using the FTIR probe and the calibration method described in Section 4.1, the concentration profile of the crystallizing solution can be obtained and plotted as a function of either temperature (Figure 5.2) or time (Figure 5.3) for both crystallization systems.

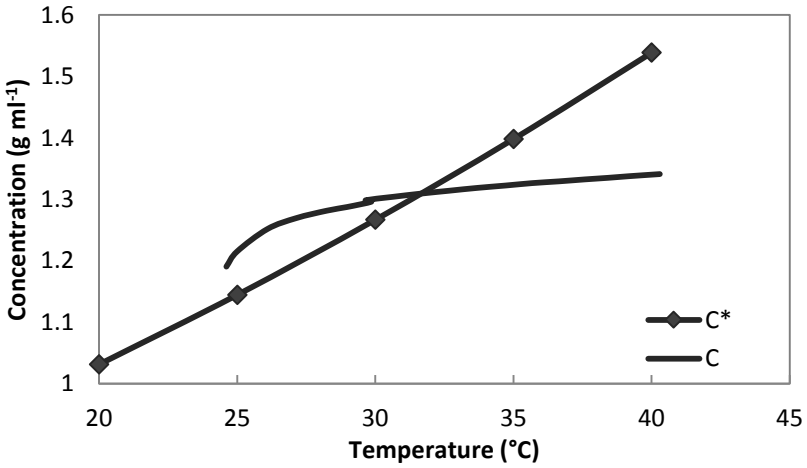

Figure 5.2 – Example of solute concentration (C) and saturation concentration (C*) vs. temperature obtained for a crystallization in OBC (mixing intensity = 750 W m^{-3}, cooling rate = 0.75 °C min^{-1})

To compare the two vessels at each condition, the concentration as a function of time is used (Figure 5.3) for both the medium (170 W/m^3) and high (750 W/m^3) mixing intensities in the OBC and STC at a fixed cooling rate of 0.50 °C/min. From Figure 5.3 it can be observed that the concentration within the solution is constant until the cooling is started at around 600 seconds. After this it increases up to a peak around its saturation temperature before decreasing. This increase is small and is likely due to movement within fibre and variation in refractive index as the cooling began and the solution moved into the supersaturated region of the crystallization, as shown in Figure 2.6.

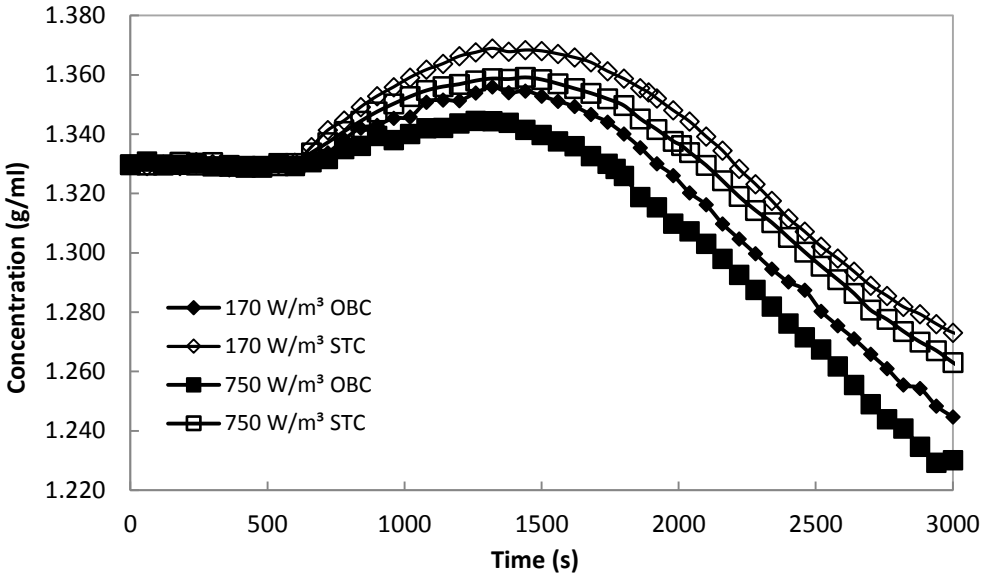

Figure 5.3 – Profiles of concentration vs. time at a fixed cooling rate of 0.50 °C min^{-1}

It can be seen that the curves for the STC (open squares) were higher than those for the OBC (filled squares). This difference is intriguing, as the same solute concentration was made up in the two systems at the start of each experiment and the same cooling rate was applied to both vessels. These measurements were repeated and the same trends were visible in all cases. Thus the trends cannot be due to any error within the IR probe. Recent work (115) revealed that the way in which mixing was generated in crystallizers (e.g. stirring vs. oscillation), when operated at the same mixing intensities, can affect nucleation mechanism, concentration and the supersaturation achieved within vessels. Could the data in Figure 5.3 indicate that the mixing in the OBC is somewhat stronger or more uniform than that in the STC at equivalent conditions? The uniform mixing present in the OBC could disperse the solute more evenly than the STC producing a lower curve than the STC. The question is then: could local high solute concentration be noted in the STC? If this hypothesis is correct, higher supersaturation results in the STC would be expected.

5.3.2 Supersaturation Profiles

To calculate the supersaturation, the solute concentration (C) is divided by the saturation concentration (C*) at each temperature, as discussed earlier in Section 2.1.1; the resulting data can then be plotted against time; an example from the OBC is shown in Figure 5.4 along with the corresponding temperature profile. This plot is a typical example of those obtained at all conditions in both vessels. It can be seen in Figure 5.4 that the profile of the supersaturation is a mirror image of the temperature. When cooling was initiated the supersaturation began to

rise and continued to do so as the cooling continued. There was a decrease in the supersaturation, denoted by arrow (2), when nucleation took place. This was then followed by a further increase as the cooling continued post-nucleation. Note that the saturation concentration (C*) decreases faster than the concentration of the solution (C) at temperatures less than *ca.* 30 °C (an example of this difference is given in Figure 5.2). Once the final temperature has been reached, the supersaturation can be seen to level off until the system was stopped. The rising slope of the supersaturation profile, illustrated by arrow (1) on Figure 5.4, effectively relates to the rate of supersaturation generation. Similarly, the decreasing slope, arrow (2), would denote the depletion rate. Both rates are calculated from the difference in the supersaturation values over the relevant time.

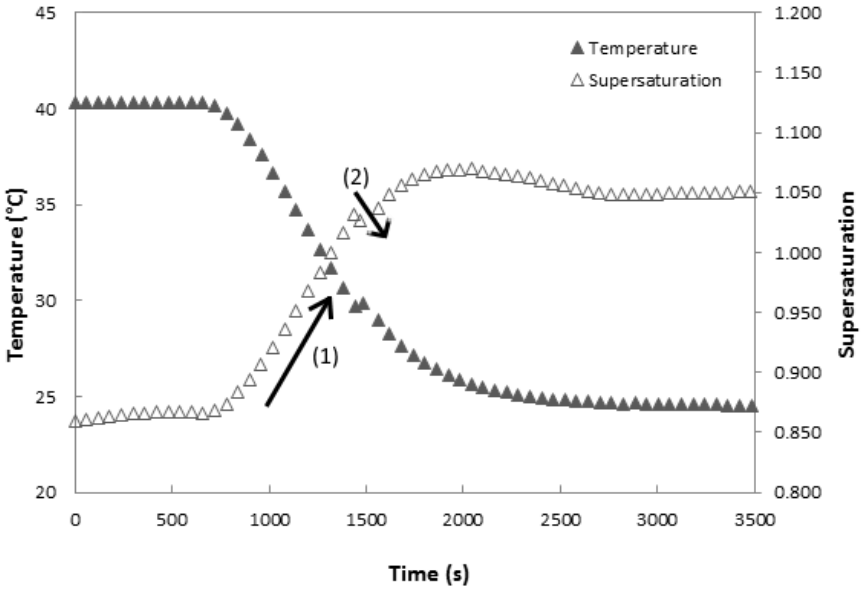

Figure 5.4 – Profiles of supersaturation and temperature against time obtained from the OBC (mixing intensity = 750 W m^{-3}, cooling rate = 0.75 °C min^{-1})

The rate of supersaturation generation was calculated as an average value and is presented in Table 5.2, along with the Kolmogorov-Smirnov statistical factor. Visually, the STC appears to have a faster generation rate than the OBC at each condition, although this difference is not statistically significant under these conditions.

Table 5.2 – Rates of supersaturation generation [s^{-1}]

Average supersaturation generation rate ± SD (all x10^{-4}) [s^{-1}]		Cooling rate (°C min^{-1})					
		0.50			0.75		
		OBC	STC	P	OBC	STC	P
Mixing intensity (W m^{-3})	20				1.60 ± 0.51	1.98 ± 0.39	0.32
	170	1.48 ± 0.18	1.72 ± 0.15	0.32	1.94 ± 0.30	2.07 ± 0.60	0.98
	750	1.40 ± 0.45	1.64 ± 0.06	0.32	2.23 ± 0.08	2.24 ± 0.60	0.98

Similarly, the rate of supersaturation depletion shown in Table 5.3 also infers that the STC generally has faster depletion rates than the OBC but again these differences are not always statistically different.

Table 5.3 – Rates of supersaturation depletion [s^{-1}]

Average supersaturation depletion rate ± SD (all x10^{-4}) [s^{-1}]		Cooling rate (°C min^{-1})					
		0.50			0.75		
		OBC	STC	P	OBC	STC	P
Mixing intensity (W m^{-3})	20				-1.76 ± 1.02	-4.20 ± 1.47	0.03
	170	-2.88 ± 1.56	-4.65 ± 1.53	0.32	-3.20 ± 0.78	-2.27 ± 1.32	0.32
	750	-1.34 ± 1.08	-1.36 ± 0.63	0.98	-1.32 ± 0.93	-2.36 ± 0.21	0.32

If the point at which the supersaturation started to drop coincided with when nucleation occurred (90, 96), then the supersaturation value at the onset of nucleation can then be compared for the OBC and STC, as shown in Table 5.4, where the STC gave higher and statistically different supersaturation values than the OBC for almost every condition.

Table 5.4 – Supersaturation values at nucleation

Average supersaturation value ± SD		Cooling rate (°C min^{-1})					
		0.50			0.75		
		OBC	STC	P	OBC	STC	P
Mixing intensity (W m^{-3})	20				1.059 ± 0.015	1.100 ± 0.009	0.03
	170	1.074 ± 0.009	1.103 ± 0.003	0.03	1.035 ± 0.042	1.040 ± 0.012	0.32
	750	1.056 ± 0.012	1.078 ± 0.003	0.03	1.037 ± 0.012	1.062 ± 0.018	0.03

This higher level of supersaturation in the STC could offer some explanation for the lower purity results observed in comparison with the OBC. Previous work (23, 25, 45) suggests that a higher purity can be obtained from nucleation and growth carried out at low levels of supersaturation. This was due to the production of more small crystals at the high supersaturation levels, because a higher supersaturation led to a higher nucleation rate.

The averaged nucleation temperatures were obtained and shown in Table 5.5 and for almost every condition the OBC nucleated at a higher temperature than the STC. This agrees with work by Ni and Liao (70), who suggested that the OBC was more effective in promoting nucleation than the STC under similar conditions.

Table 5.5 – Corresponding temperatures at which nucleation took place

Nucleation temperature ± SD [°C]		Cooling rate (°C min^{-1})					
		0.50			0.75		
		OBC	STC	P	OBC	STC	P
Mixing intensity (W m^{-3})	20				28.44 ± 0.72	28.20 ± 0.27	0.98
	170	29.55 ± 0.78	29.31 ± 0.87	0.98	28.59 ± 0.24	29.30 ± 0.36	0.03
	750	30.45 ± 0.48	30.18 ± 0.36	0.98	29.83 ± 0.15	29.48 ± 0.42	0.32

The lower nucleation temperature in the STC accompanied by a higher supersaturation level would mean that there was less time for crystal growth which would therefore be associated with the increased production of small single crystals (45). It has been proposed that a larger amount of small single crystals are more likely to agglomerate in the poor mixing and high supersaturation environment observed in an STC post-nucleation (51) as the solid content increases. As previously mentioned it has recently been suggested that how the mixing is generated in crystallizers, e.g. stirring vs. oscillation, can affect the nucleation mechanism, concentration and the supersaturation achieved within vessels when operating under similar conditions. The data presented above support this suggestion. It also leads us to question whether this difference in how mixing was generated at the same intensity could also affect the crystal size, the amount of agglomeration and in turn, the purity obtained?

5.3.3 Crystal Size Distributions

Subsequently, crystal size distributions (CSD) of these samples were examined along with SEM and microscope images. This was completed in accordance with the method discussed in Section 4.1.4. The results presented here (Table 5.6) are the D_{50} and span values for all conditions along with the standard deviation and statistical comparison values. Examples of the full CSD are shown in Figure 5.5 for both the OBC and STC at a fixed cooling rate of 0.50 °C/min and two mixing intensities.

Table 5.6 – Mean crystal size and span values for CSD

0.50 °C min^{-1}	OBC		STC		P (D_{50})
	D_{50} [μm]	Span	D_{50} [μm]	Span	
Medium mixing	157.8 ± 45.0	1.91	172.1 ± 37.8	1.92	0.84
High mixing	184.3 ± 12.5	2.08	210.7 ± 70.2	1.90	0.56
0.75 °C min^{-1}	D_{50} [μm]	Span	D_{50} [μm]	Span	P (D_{50})
Low mixing	137.9 ± 6.09	2.32	164.5 ± 10.6	2.03	0.03
Medium mixing	194.1 ± 8.43	2.03	188.7 ± 6.96	2.11	0.84
High mixing	151.3 ± 3.15	2.00	186.2 ± 7.32	2.65	0.06

From the results in Table 5.6, it can be seen that the crystals produced in the STC generally have a larger mean crystal size (D_{50}) and CSD span than the OBC at comparable conditions although the differences are not always statistically significant. This difference is also confirmed by the CSD in Figure 5.5, showing the STC with a wider size distribution at both mixing intensities. It would be expected that as the mixing intensity was increased at each fixed cooling rate, the mean crystal size would decrease due to enhanced attrition (25). However, this is not always apparent from the data presented above. For this reason, crystal imaging has also been carried out.

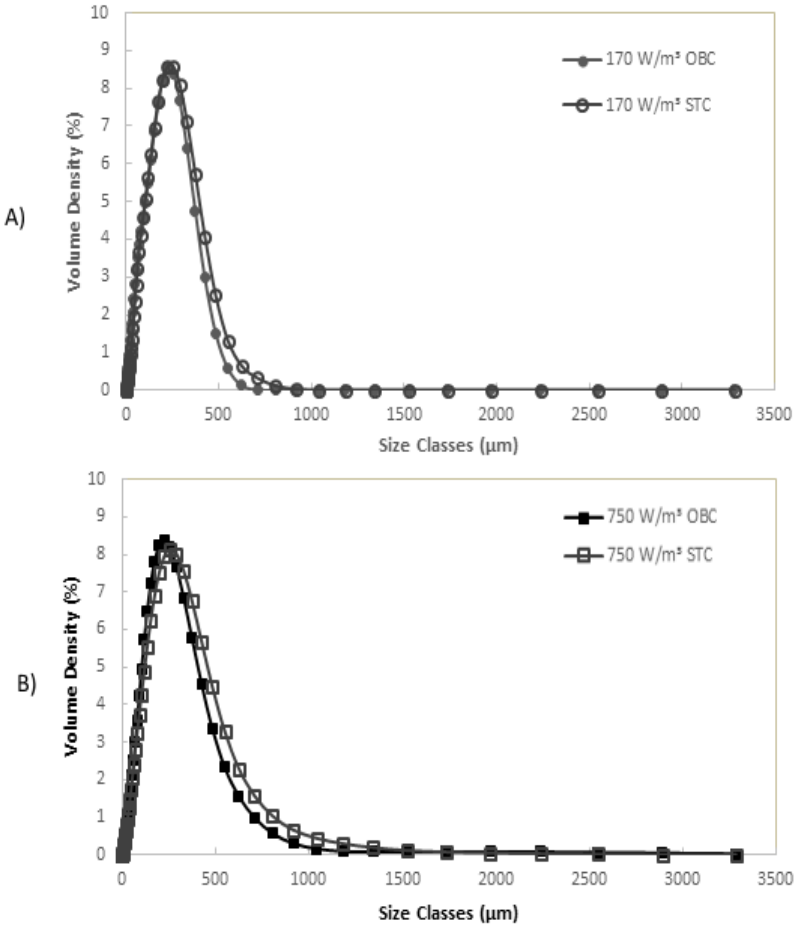

Figure 5.5: CSD of crystals from the OBC and STC at a fixed cooling rate of 0.50 °C min^{-1} with A) medium mixing intensity of 170 W m^{-3} and B) high mixing intensity of 750 W m^{-3}

5.3.4 Crystal Imaging

The first type of imaging utilized was scanning electron microscopy (SEM), which gives views of the crystal surfaces or connections. As previously mentioned, if impurity is being incorporated into the growing crystals a cubic habit would be expected and if the crystals are 'pure', needle-like crystals would be expected. Figure 5.6 provides images of some of the crystals on a 500 µm scale. Note that the crystals chosen for the imaging were randomly selected from samples which gave purity results close to the average values of each condition. Care was taken to ensure that no damage occurred to the crystals before or during the imaging itself.

The crystal images shown in Figure 5.6 indicate that the STC has larger agglomerates than the OBC at each of the conditions. Both vessels have needle-like crystals, suggesting that impurity is not being directly incorporated into the growing crystals, instead the purity differences noted in Table 5.1 are due to variations in the agglomeration level between the two vessels.

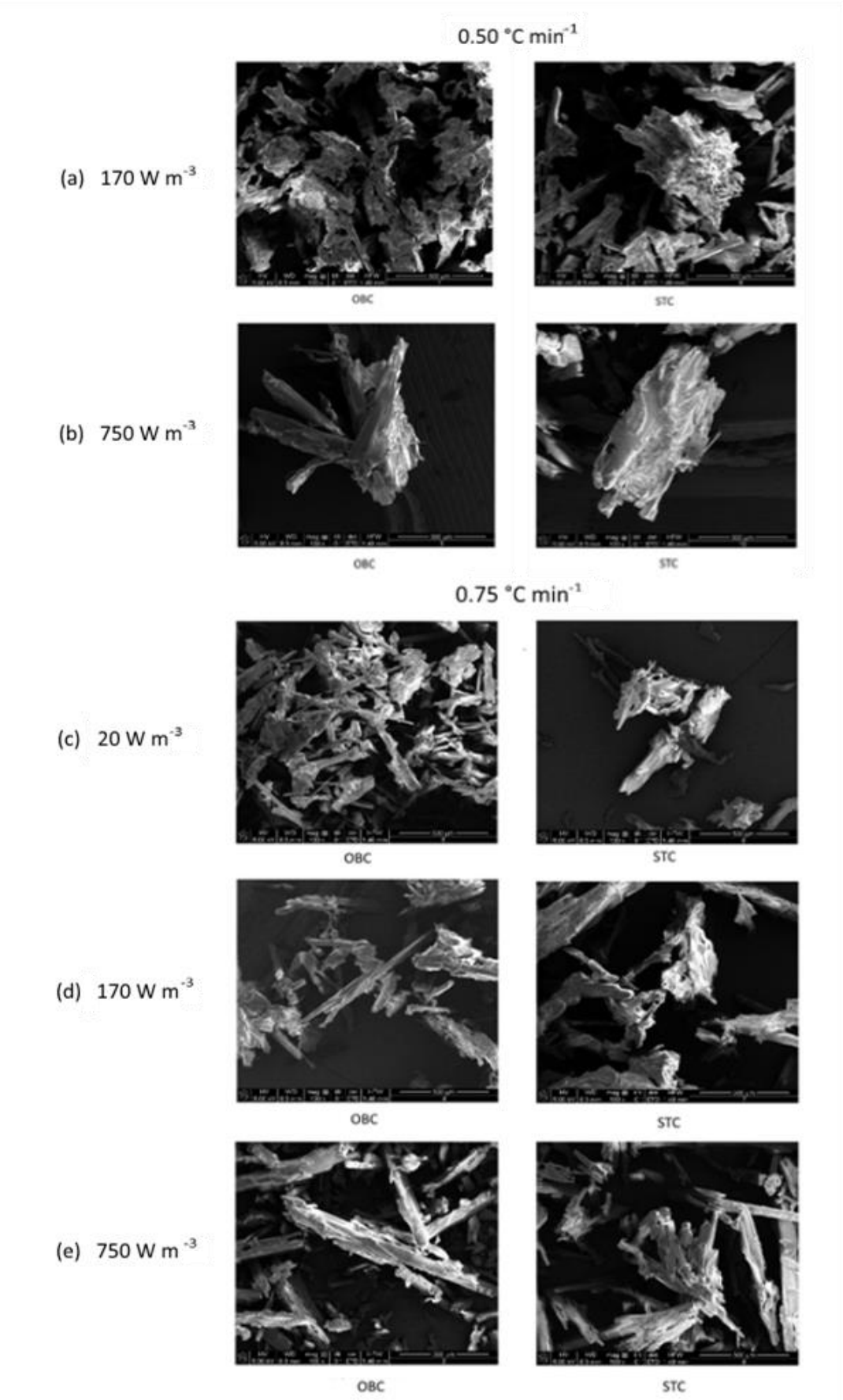

Figure 5.6: SEM images of crystals produced in both OBC and STC at all conditions; all images shown are on a 500 µm scale

While the SEM images in Figure 5.6 provide clear information about the individual agglomerates formed, they do not give an overall view of the other crystals surrounding it. To help overcome this problem optical microscopy was also used to view a greater number of crystals per image, as presented in Figure 5.7. A 200 µm scale bar is added to each image in Figure 5.6 to indicate the crystal size. The crystals imaged were from the same samples as those used for the SEM in Figure 5.5 and were, again, randomly selected.

Crystal images presented here in Figure 5.7 again propose that the STC has larger agglomerates than the OBC. This is in line with the larger mean crystal size shown by the CSD data in Table 5.6. These agglomerates are therefore the likely cause of the lower STC purity in Table 5.1 and may also explain why the mean diameters in Table 5.6 are increased with higher mixing in both systems, which is the opposite of what would be expected.

In addition, the crystals produced from the higher supersaturation levels, at low and medium mixing in both systems, are shown to be poorly defined with rough edges and a wider range of crystal sizes (Fig. 5.7 (a, c &d)). This is probably related to the increased nucleation rate and likely poorer mixing due to increased solids concentration. As the mixing intensity increased the supersaturation level was more uniform in the OBC and STC (116) and the crystal edges became more clearly defined in both vessels. However, more agglomerates are still visible in the STC, even with higher mixing.

Previous work (45) noted that as the mixing intensity was increased in the STC, the purity of crystals decreased. This is not shown in the results presented in this work where the purity increases with the increasing mixing (Table 5.1) in both vessels. The work by Charmolue & Rousseau (25) suggested that there was some mixing threshold in the STC which, if crossed, led to a decrease in purity with any further increase in mixing intensity. Under this threshold, when the mixing was low, agglomerated crystals were obtained, as noted in Figure 5.6 (c), and as the mixing was intensified the number of single crystals produced rose (Fig. 5.6 (d & e)). This increase in single crystal production would lead to the amount of impurity trapped between the agglomerated crystals decreasing, leading to a higher purity. Charmolue (25) then observed that a further increase in mixing enhanced crystal breakage and the crystal shape became irregular and agglomerates were reformed. Long needle-like crystals with some agglomeration, rather than irregularly shaped small crystals, are seen at the highest mixing in both vessels in this work (Fig. 5.6 b & e). It is likely that the mixing conditions used here were under the aforementioned threshold, while the results from the previous work (25, 45) would be associated with conditions which were above this threshold.

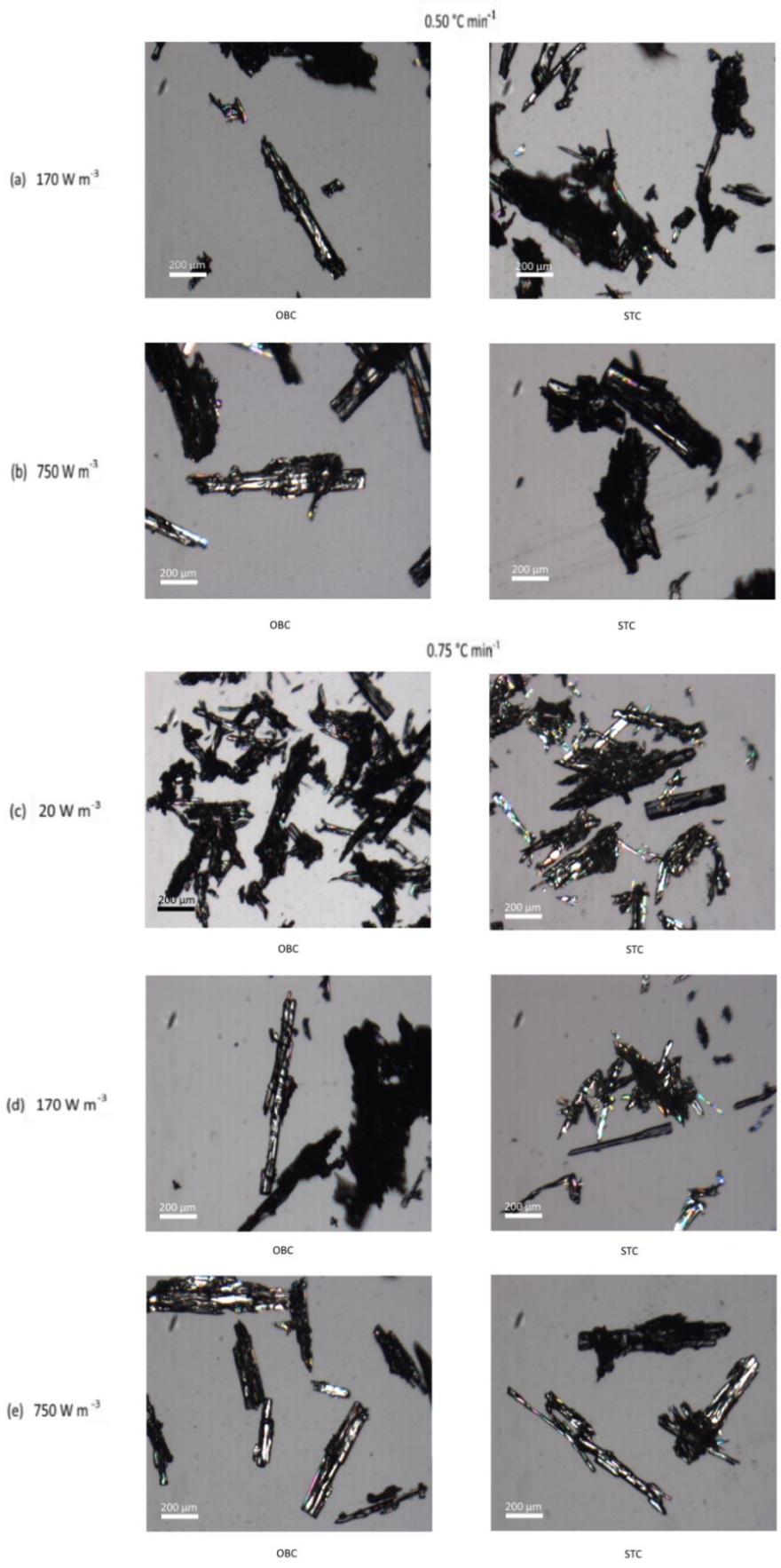

Figure 5.7: Microscopy images of urea crystals produced by the OBC and STC at all conditions.

The microscopy images of crystals in Figure 5.7 also show that while more agglomerates are formed in the STC, more single crystals are evident in the OBC. A possible reason for more single crystals in the OBC could be the increased surface area of the agitating baffles (baffles and connecting rods – 13320 mm^2) in comparison with that of the rotational impeller in the STC (3070 mm^2). This may induce more nucleation and cause more collisions that break up any agglomerates particularly early in the crystallization, leading to increased production of single crystals (25, 117). The increased surface area could also offer some possible explanation of the higher nucleation temperature noted in Table 5.5.

In terms of agglomeration, Brunsteiner et al. (51) explained that slower mixing can lead to more agglomerates being formed, in turn leading to a lower purity product. Ineffective mixing was particularly evident at the low mixing in both vessels, as well as the medium mixing intensity in the STC, where there was more agglomeration (Figure 5.6 a, c & d) with lower purities (Table 5.1). In previous work (5, 118), the entrapment of mother liquor and impurities was shown to increase with presence of agglomeration, lowering the purity. Unfortunately currently there are no practical methods available to fully quantify the exact degree of agglomeration in each vessel. Nevertheless, the images and numbers presented here support our hypothesis that the lower crystal purity in the STC was due to a higher level of agglomeration than that in the OBC.

5.4 Conclusions

The initial aim of this Chapter was to verify the confidential findings that crystals with a higher purity were produced in the OBC than in the STC under similar experimental conditions. This has been achieved with all data comparisons, except one, being statistically significant.

The next step of this study was to investigate possible reasons for the purity results obtained. The results have indicated that a higher level of supersaturation was measured in the STC than the OBC which would have led to a higher nucleation rate. This would suggest a smaller mean crystal size in the STC. The CSD results presented here show the opposite effect, i.e. the STC with a larger mean crystal size. By analysing the images of crystals, increased agglomeration in the STC appears to be the reason for the larger mean size when compared to the OBC. This could also imply that the way in which mixing is generated in a crystallizer affects the uniformity of mixing even though the mixing intensities are the same. The lower purity in the STC seems to be the direct result of larger agglomerates entrapping more mother liquor as impurity than single crystals.

Chapter 6 Effect of Impeller

Within the STC different types of impeller can be used to mix the contents. As mentioned the flat-paddle impeller (S1) is employed during the majority of the tests in this work, this type of impeller has however been shown to lead to poor mixing due to the production of dead zones within the vessel and poor heat transfer (7). The mixing within the system is an important parameter for crystallization; hence a four pitch-blade impeller (S2) was used in accordance with the procedure described in Section 3.4, while keeping the same mixing intensities as the first impeller (S1) given in Table 6.1. Operation at the same mixing intensity allows direct comparison of all results and gives an insight into whether the different type of stirrer could affect the results. Figure 6.1 shows the two different impellers utilized within this chapter, due to imaging limitations only two of the four pitched blade can be seen for impeller S2.

Table 6.1 – Mixing Intensities and Stirrer Rates for STC Impellers S1 and S2

Mixing Intensity ($W\ m^{-3}$)	Stirrer Rate S1 (RPM)	Stirrer Rate S2 (RPM)
20	104	154
170	201	318
750	351	450

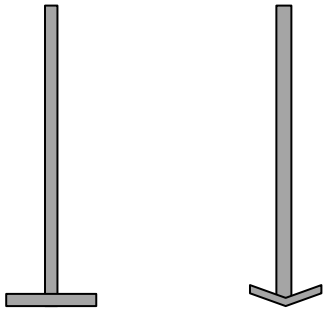

Figure 6.1 – Pictorial image of two impellers use; Impeller S1 (left image) and Impeller S2 (right image)

6.1 Comparison of Impeller Type within the STC

Following completion of the experimental trials, the supersaturation generation and depletion rates are compared in Tables 6.2 and 6.3 respectively and both rates are calculated from the supersaturation traces of the systems, as described in Section 5.3.2. As before all values given

are an average of three experiments, which are presented with the standard deviation and Kolmogorov-Smirnov statistical probability factor.

Table 6.2 – Rate of supersaturation generation [s^{-1}] from Impeller (S1 and S2) in the STC

Supersaturation generation rate ± SD [All rates x10^{-4}]		Cooling rate [°C min^{-1}]					
		0.50			0.75		
		S1	S2	P	S1	S2	P
Mixing intensity [W m^{-3}]	20				1.98 ± 0.39	2.51 ± 0.24	0.32
	170	1.72 ± 0.15	1.51 ± 0.24	0.42	2.07 ± 0.60	1.90 ± 0.60	0.78
	750	1.64 ± 0.06	1.67 ± 0.09	0.99	2.24 ± 0.63	2.25 ± 0.12	0.98

Table 6.3 – Supersaturation depletion rates with varying impeller [s^{-1}]

Supersaturation depletion rate ± SD [All values x10^{-4}]		Cooling rate [°C min^{-1}]					
		0.50			0.75		
		S1	S2	P	S1	S2	P
Mixing intensity [W m^{-3}]	20				-4.20 ± 1.47	-2.48 ± 0.30	0.03
	170	-2.54 ± 1.96	-1.88 ± 0.66	0.98	-2.27 ± 1.32	-2.07 ± 1.53	0.78
	750	-1.36 ± 0.63	-2.41 ± 0.06	0.06	-2.36 ± 0.21	-2.11 ± 0.93	0.98

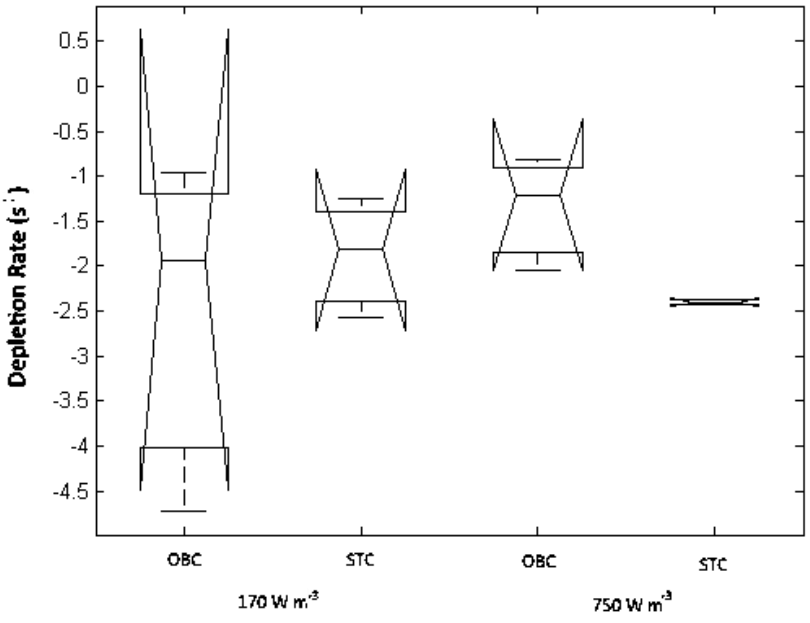

Figure 6.2 – Supersaturation depletion rates calculated from the OBC and STC results for fixed cooling are of 0.50 °C min^{-1}

From both Tables 6.2 and 6.3 and Figure 6.2, all calculated values are similar between the two impeller systems. To further investigate this similarity, the crystallization rates for urea are compared between the two impellers and tabulated in Table 6.4. These are calculated as the slope from the concentration profile, an example of which was given in Figure 5.3. At every condition trialled the two impellers are producing similar crystallization rates.

Table 6.4 – Urea crystallization rates from the STC systems (S1 and S2) [g ml.s^{-1}]

Urea crystallization rate ± SD [All Values x10^{-5}]		Cooling rate [°C min^{-1}]					
		0.50			0.75		
		S1	S2	P	S1	S2	P
Mixing intensity [W m^{-3}]	20				4.17 ± 0.48	2.69 ± 0.87	0.06
	170	4.89 ± 1.32	5.13 ± 0.81	0.98	4.67 ± 0.60	2.77 ± 1.56	0.43
	750	5.87 ± 0.81	5.73 ± 0.51	0.99	6.12 ± 0.00	6.14 ± 0.93	0.98

If the mixing is improved with the second impeller the level of supersaturation required for crystallization to occur would be expected to be lower than for the first impeller. This is due to higher shear rates, improved material transfer and promoted nucleation in the system (25). The effect of supersaturation upon nucleation and nucleation temperatures for both impellers (S1 and S2) are shown in Tables 6.5 and 6.6 respectively.

Table 6.5 – Average supersaturation level upon crystallization for S1 and S2

Supersaturation level at crystallization ± SD		Cooling rate [°C min^{-1}]					
		0.50			0.75		
		S1	S2	P	S1	S2	P
Mixing intensity [W m^{-3}]	20				1.100 ± 0.009	1.089 ± 0.003	0.32
	170	1.103 ± 0.003	1.087 ± 0.039	0.32	1.040 ± 0.008	1.069 ± 0.039	0.43
	750	1.078 ± 0.003	1.063 ± 0.018	0.06	1.062 ± 0.018	1.039 ± 0.021	0.32

From Table 6.5 there is some evidence of supersaturation improvement with the second impeller (S2), as a lower supersaturation value at nucleation is observed for almost every condition when using the second impeller. This indicates that any improvement in mixing is

having limited effect on the supersaturation required for nucleation under these conditions. Lower nucleation temperatures for the second impeller are also seen in Table 6.6, albeit not all are statistically significant.

Table 6.6 – Average nucleation temperatures for S1 and S2 systems

Nucleation temperature ± SD [°C]		Cooling rate [°C min^{-1}]					
		0.50			0.75		
		S1	S2	P	S1	S2	P
Mixing intensity [W m^{-3}]	20				28.20 ± 0.27	27.92 ± 1.20	0.32
	170	29.31 ± 0.87	28.61 ± 1.29	0.98	29.34 ± 0.36	28.64 ± 0.96	0.32
	750	30.18 ± 0.36	29.71 ± 0.12	0.03	29.48 ± 1.44	29.71 ± 0.24	0.32

Following comparison of the supersaturation values and crystallization rates, the purity values obtained for both impellers are analysed and tabulated in Table 6.7.

Table 6.7 – Average % purity results for crystals from both impeller systems in the STC

% Purity ± SD		Cooling rate [°C min^{-1}]					
		0.50			0.75		
		S1	S2	P	S1	S2	P
Mixing intensity [W m^{-3}]	20				95.8 ± 0.21	95.9 ± 0.51	0.98
	170	95.9 ± 0.30	96.2 ± 0.36	0.32	95.5 ± 0.42	95.8 ± 0.18	0.42
	750	95.1 ± 0.39	95.4 ± 0.24	0.98	96.5 ± 0.12	97.0 ± 0.24	0.32

From Table 6.7 although the second stirrer appears to be producing crystals of a higher purity than the first stirrer, which is in line with the supersaturation level results presented in Table 6.5, the data are statistically similar.

Previous work indicated that the higher supersaturation in the STC produced smaller single crystals due to a higher nucleation rate, which were more likely to form agglomerates as the solids concentration increased in the poor mixing environment of the STC with impeller S1. If the mixing is improved with the second impeller (S2), could the size of agglomerates noted in

this work be smaller than those produced at the same conditions as impeller S1? To analyse this trend, CSD and microscope imaging are presented below. Table 6.8 shows the average values of the mean crystal size (D_{50}) and span, with the standard deviations calculated for every condition. Also given is the Kolmogorov-Smirnov probability value for the mean crystal size results, which show that the mean crystal sizes are generally similar from the two impeller systems.

Table 6.8 – Average equivalent diameter and span values for crystals from STC (S1) and STC (S2)

		STC (S1)		STC (S2)		
Fixed cooling rate (0.50 °C min^{-1})	Fixed mixing intensity	D_{50} [µm]	Span	D_{50} [µm]	Span	P (D_{50})
	170 W m^{-3}	172.05 ± 37.8	1.92	214.86 ± 12.8	1.94	0.06
	750 W m^{-3}	210.74 ± 70.2	1.90	191.03 ± 13.6	2.18	0.32
Fixed cooling rate (0.75 °C min^{-1})	Fixed mixing intensity	D_{50} [µm]	Span	D_{50} [µm]	Span	P (D_{50})
	20 W m^{-3}	164.45 ± 10.6	2.03	175.85 ± 27.7	2.49	0.32
	170 W m^{-3}	188.87 ± 6.96	2.09	202.02 ± 12.9	2.27	0.43
	750 W m^{-3}	186.18 ± 7.32	2.65	187.97 ± 16.6	2.06	0.32

The data in Table 6.7 illustrates that the equivalent diameters for the STC (S2) are generally larger than those of the STC (S1) at similar conditions, although almost all pairs give statistically similar values. This has been confirmed by the full CSD curves (Figure 6.3) which appear similar. It can be noted from Figure 6.1, that the difference between CSD for the impellers is more apparent at the lower mixing intensity (170 W/m^3), than the higher value, which correlates with the statistical differences in mean crystal size in Table 6.7. The similarity between CSD is possibly due to the similar surface area of the two impellers (S1 = 3070 mm^2 and S2 = 2950 mm^2), affecting the crystals in a similar manner and giving corresponding mean crystal sizes.

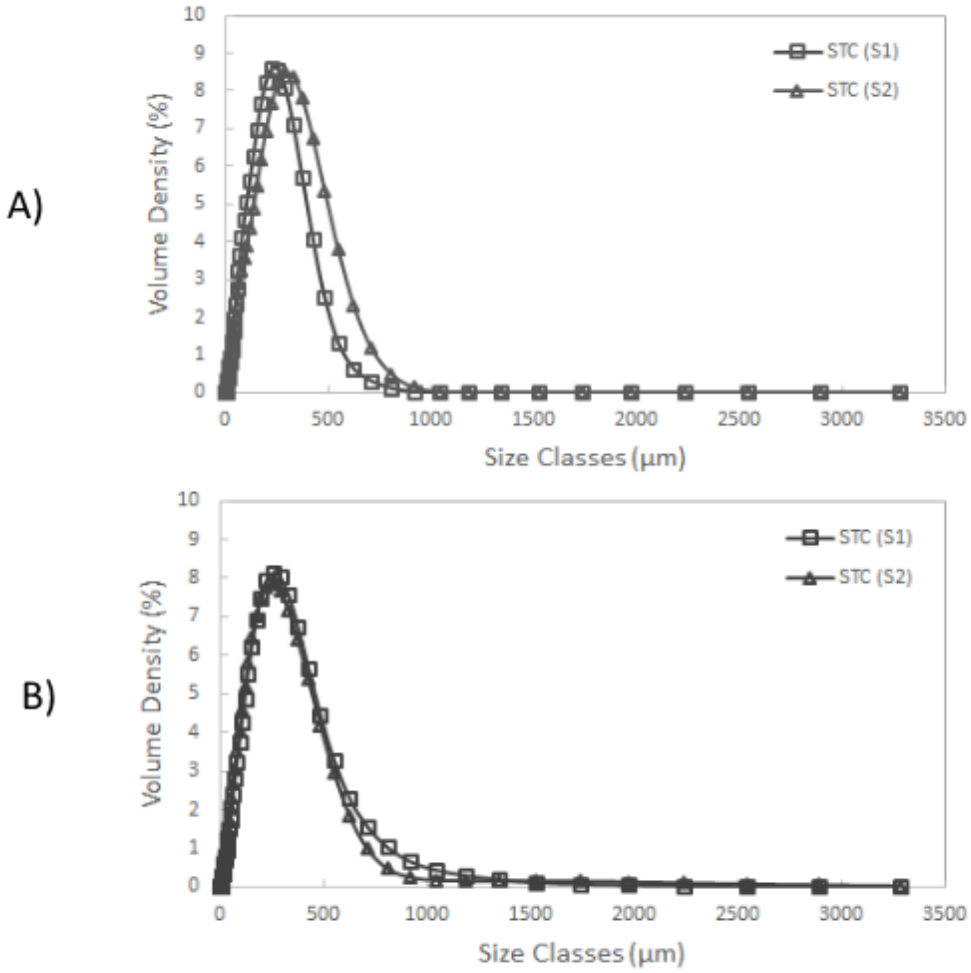

Figure 6.3 – CSD from the STC (S1) and (S2) crystals at a cooling rate of 0.50 °C min^{-1} and mixing intensities of A) 170 W m^{-3} and B) 750 W m^{-3}

Figure 6.4 shows microscopy images from both impellers which were taken for the same conditions as the CSD in Figure 6.3, and were produced using a 4 times optical zoom and are presented with an added 200 µm scale bar.

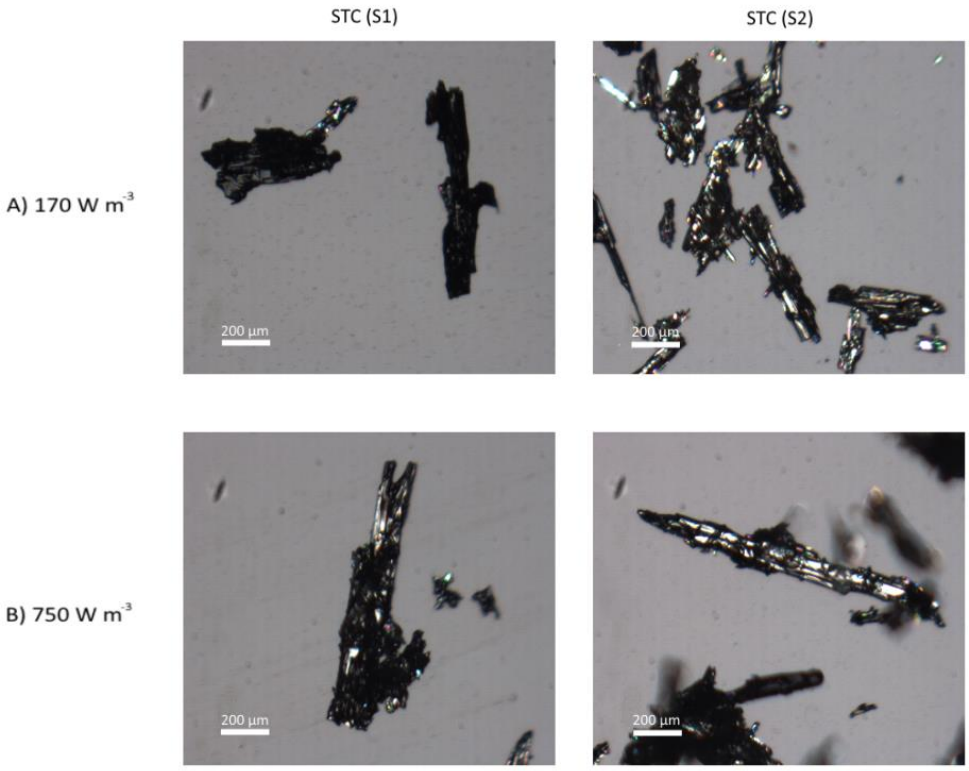

Figure 6.4 - Microscope images from the crystals produced from S1 and S2 systems at the cooling rate of 0.50 °C min^{-1} at A) mixing intensity of 170 W m^{-3} and B) mixing intensity of 750 W m^{-3}

The crystal images in Figure 6.4 show that for both mixing intensities the crystals produced with impeller S2 appear to have a wider variation in crystal size than the STC (S1) crystals, this gives a possible explanation to the larger CSD results from impeller S2.

6.2 Conclusions

In conclusion, although a different type of impeller in the STC has shown improvements in the mixing visually due to the higher impeller rates using S2, little statistical difference was made to the crystal properties. This would be somewhat expected as the mixing dissipation rates were kept the same.

Chapter 7 Effect of Impurity

7.1 Introduction

Following the verification of the higher purity crystals produced in the OBC from a 'pure' starting environment, it is important to investigate whether this trend is still apparent in an impure starting environment, as industrial processes often involve an 'impure' environment (15, 119). To do this, both crystallization vessels and experimental conditions must be kept constant (as shown in Section 3.2), with the only variable being the addition of known impurity at 1 wt. % and 5 wt. %. The specific impurity added in the system is biuret and more detail on biuret can be found in Section 3.4.

7.2 'Pure' System Results

It is important to recap the results which have been obtained from the pure system as the base, before the results from the impure system are presented and discussed. Table 7.1 presents the averaged purity data from Chapter 5, along with new data contained at the cooling rate of 0.25 °C/min.

Table 7.1 – Initial purity results for the 'Pure' (0 % AI) system crystals

0 % AI		Cooling rate [°C min^{-1}]								
% Average purity ± SD		0.25			0.50			0.75		
		OBC	STC	P	OBC	STC	P	OBC	STC	P
Mixing intensity [W m^{-3}]	20							96.1 ± 0.39	95.8 ± 0.21	0.32
	170	96.8 ± 0.09	96.3 ± 0.24	0.03	96.4 ± 0.21	95.9 ± 0.21	0.06	96.1 ± 0.15	95.5 ± 0.42	0.06
	750							97.3 ± 0.12	96.5 ± 0.12	0.03

As previously stated, the OBC has a statistically higher purity than the STC at almost every condition investigated (102). This includes the data from the new condition of 0.25 °C/min and 170 W/m^3. The results also show that as the cooling rate increases the purity obtained from crystals in both systems decreases. This is in-line with work carried out by Givand et al (45) who previously showed similar trends in the STC.

Likewise Tables 7.2 to 7.4 show the averaged supersaturation at nucleation, the nucleation temperature and the mean size plus span for the pure (0 % AI) condition, including

the new extra condition. The purity and supersaturation values at nucleation for 0 % AS are shown in Figure 7.1, this shows that as the power density increases the supersaturation upon nucleation decreases and the purity increases.

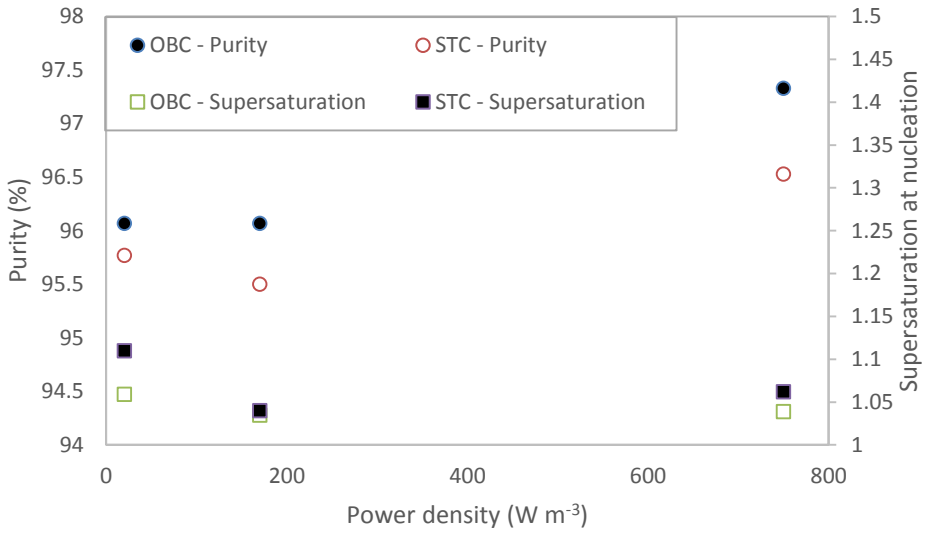

Figure 7.1 – Diagram showing overall purity and supersaturation trends with power density at fixed cooling rate of 0.75 °C min^{-1} for both OBC and STC

Table 7.2 – Average supersaturation values at nucleation for 0 % AI

Average supersaturation level ± SD		Cooling rate (°C min^{-1})								
		0.25			0.50			0.75		
		OBC	STC	P	OBC	STC	P	OBC	STC	P
Mixing intensity (W m^{-3})	20							1.059 ± 0.015	1.100 ± 0.009	0.03
	170	1.080 ± 0.012	1.153 ± 0.051	0.06	1.074 ± 0.009	1.103 ± 0.003	0.03	1.035 ± 0.042	1.040 ± 0.012	0.32
	750							1.037 ± 0.012	1.062 ± 0.018	0.03

Table 7.3 – Average nucleation temperatures for 0 % AI system

Average nucleation temperature ± SD [°C]		Cooling rate (°C min^{-1})					
		0.25		0.50		0.75	
		OBC	STC	OBC	STC	OBC	STC
Mixing intensity (W m^{-3})	20					28.44 ± 0.78	28.20 ± 0.27
	170	30.39 ± 0.39	29.77 ± 0.3*	29.55 ± 0.78	29.31 ± 0.87	28.59 ± 0.27	29.34 ± 0.36
	750					29.84 ± 0.15	29.48 ± 0.42

Table 7.4 – Average D_{50} and CSD span results for crystals from the 'Pure' OBC and STC systems

Cooling rate (°C min^{-1})	Mixing intensity (W m^{-3})	OBC		STC		P(D_{50})
		D_{50} (µm)	Span	D_{50} (µm)	Span	
0.25	170	279.84 ± 32.4	2.50	303.30 ± 80.7	3.91	0.78
0.50	170	157.76 ± 45.0	1.91	172.05 ± 37.8	1.95	0.84
0.75	20	137.94 ± 6.09	2.32	164.45 ± 10.6	2.03	0.03
0.75	170	194.06 ± 6.84	2.03	188.74 ± 6.96	2.11	0.84
0.75	750	151.29 ± 3.15	2.00	186.18 ± 7.32	2.65	0.06

7.3 1 wt. % Added impurity

The corresponding tables with 1 wt. % added impurity (1 % AI) in short are given below. As with the results above all experimental results are shown as an average of 3 trials unless otherwise stated.

Table 7.5 – Initial purity results for the crystals produced by the 1 % AI system

1 % AI		Cooling rate [°C min^{-1}]								
% Average purity ± SD		0.25			0.50			0.75		
		OBC	STC	P	OBC	STC	P	OBC	STC	P
Mixing intensity [W m^{-3}]	20							94.67 ± 0.57	94.86 ± 0.60	0.98
	170	94.34 ± 0.30	94.17 ± 0.48	0.98	95.42 ± 0.30	94.43 ± 0.27	0.03	95.40 ± 0.30	94.60 ± 0.24	0.03
	750							96.21 ± 0.48	95.23 ± 0.24	0.03

The results in Table 7.5 show that the purity obtained from the OBC is still higher than that from the STC at most conditions investigated. This is positive as it indicates that the trend from a 'pure' environment still stands for an impure starting environment. However, the number of statistically similar purity results has increased compared to that of 0 % AI (Table 7.1), e.g. in the 0 % AI results only the lowest mixing intensity produced crystals with a similar purity, while in the 1 % AI data the crystals from the lowest cooling rate also gave statistically similar purity results.

Table 7.6 – Average supersaturation values at nucleation for 1 % AI systems

Average supersaturation ± SD		Cooling rate (°C min^{-1})								
		0.25			0.50			0.75		
		OBC	STC	P	OBC	STC	P	OBC	STC	P
Mixing intensity (W m^{-3})	20							1.099 ± 0.015	1.115 ± 0.021	0.32
	170	1.101 ± 0.012	1.115 ± 0.012	0.32	1.097 ± 0.033	1.125 ± 0.024	0.10	1.084 ± 0.027	1.099 ± 0.024	0.98
	750							1.067 ± 0.033	1.078 ± 0.018	0.98

From the supersaturation values in Table 7.6 the OBC still appears to crystallize at a lower level than the STC under comparable conditions, similar to the 'pure' work. However, none of these comparison pairs are statistically different.

Table 7.7 – Average nucleation temperatures for 1 % AI systems

Nucleation Temperature ± SD		Cooling Rate (°C min^{-1})								
		0.25			0.50			0.75		
		OBC	STC	P	OBC	STC	P	OBC	STC	P
Mixing Intensity (W m^{-3})	20							24.41 ± 0.60	24.38 ± 1.11	0.32
	170	27.77 ± 0.39	27.50 ± 0.39	0.32	26.53 ± 0.06	26.68 ± 0.27	0.98	26.63 ± 1.17	25.57± 0.33	0.32
	750							27.15 ± 0.63	26.90 ± 0.15	0.32

From Table 7.7 the OBC nucleates at a higher temperature than the STC at all experimental conditions and similar to the 0 % AI results, all comparison pairs are similar. When the impurity biuret added into the system is followed using the in-situ IR probe, the concentration profile of the biuret can be obtained. This profile can be analysed to offer an insight into what is causing the purity results shown in Table 7.5.

Similar to the urea concentration profile shown in Figure 5.2, the biuret profile increases when the cooling is initially applied and then decreases as the system begins to crystallize. An example of a biuret and urea curve is shown in Figure 7.2. It can be noted that the biuret curve follows a similar trend to the data obtained from urea, although at a much lower absorbance value. If crystals are rejecting the impurity then the concentration of biuret in solution should stay high and consequently the rate of crystallization (nucleation and growth) of biuret will be comparatively low. Conversely, if the impurity is being incorporated, the concentration will

show a larger reduction and a higher rate should be observed. The average rates of biuret are tabulated in Table 7.8 with the standard deviations and statistical probability values.

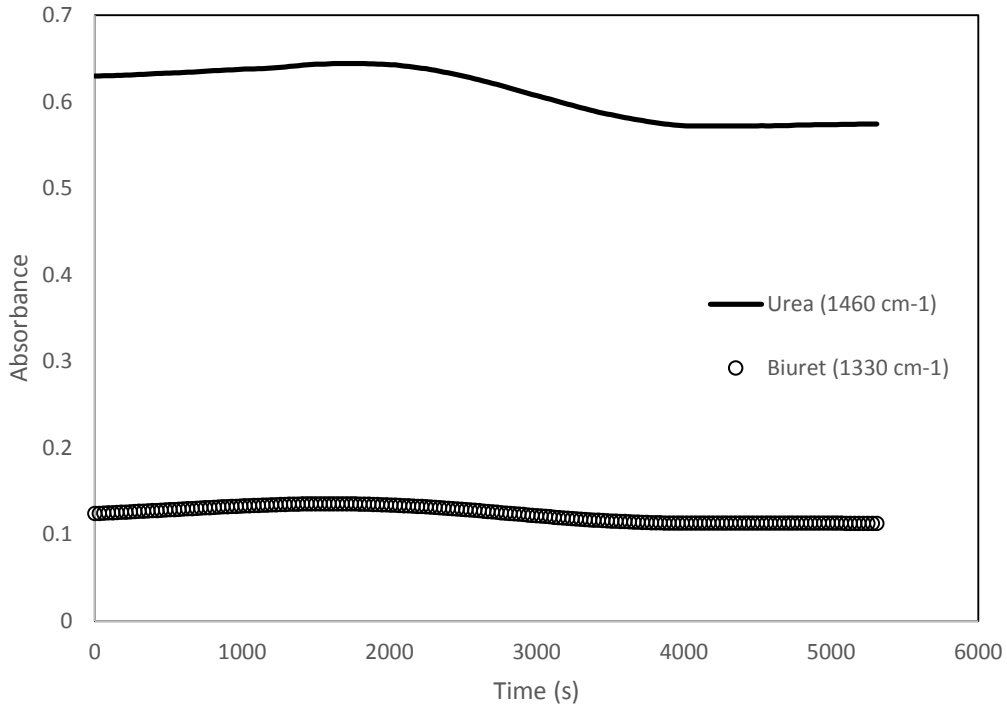

Figure 7.2 – Example FTIR traces for Urea (1460 cm^{-1}) and Biuret (1330 cm^{-1}) obtained at 1 % added impurity in the OBC

Table 7.8 – Average biuret crystallization rate for 1 % AI system, all values $x10^{-6}$

Average biuret crystallization rate ± SD (all x 10^{-6}) [g $ml.s^{-1}$]		Cooling rate (°C min^{-1})								
		0.25			0.50			0.75		
		OBC	STC	P	OBC	STC	P	OBC	STC	P
Mixing intensity (W m^{-3})	20							5.73 ± 2.61	4.56 ± 1.11	0.84
	170	2.63 ± 1.26	2.15 ± 0.39	0.32	2.58 ± 1.71	5.97 ± 0.00	0.09	5.06 ± 1.71	7.64 ± 1.83	0.06
	750							5.79 ± 1.59	10.53 ± 0.39	0.03

The biuret crystallization rates presented in Table 7.8 show that three pairs have statistically different data, coinciding with the purity data in Table 7.5. This implies that the purity differences noted are partly due to a higher rate of impurity incorporation in the STC at

these conditions, which is likely leading to a lower crystal purity. This higher rate of impurity incorporation could lead to the production of more rod-like or 'cubic' crystals.

Table 7.9 gives the mean crystal size (D_{50}) and span for the 1 % AI crystals with the Kolmogorov-Smirnov statistical factor.

Table 7.9 – Average D_{50} and CSD span results for crystals from 1 % AI systems from both OBC and STC

Cooling rate (°C min^{-1})	Mixing intensity (W m^{-3})	OBC		STC		P(D_{50})
		D_{50} (µm)	Span	D_{50} (µm)	Span	
0.25	170	195.05 ± 19.8	2.40	367.66 ± 212.1	2.45	0.06
0.50	170	229.78 ± 6.09	2.60	345.51 ± 24.3	2.72	0.06
0.75	20	195.43 ± 3.06	2.38	371.58 ± 40.8	2.68	0.03
0.75	170	188.70 ± 64.2	2.40	332.28 ± 9.12	2.64	0.03
0.75	750	182.19 ± 28.1	2.20	366.88 ± 75.0	2.53	0.03

Once again the STC produced crystals with a statistically larger mean crystal size and larger span at every condition. The CSD in Figure 7.3 for one of the conditions (cooling rate of 0.75°C/min and mixing intensity of 750 W/m^3) support the data in Table 7.9 that the STC curve has a much longer 'tail', the likely fingerprint of more agglomerates of a larger size in the STC. The presence of these agglomerates in the STC is confirmed by the microscope imaging in Figure 7.3 which gives an example of the crystals produced at each condition. These images were taken using a 4 times optical zoom and are shown with an added 200 µm scale.

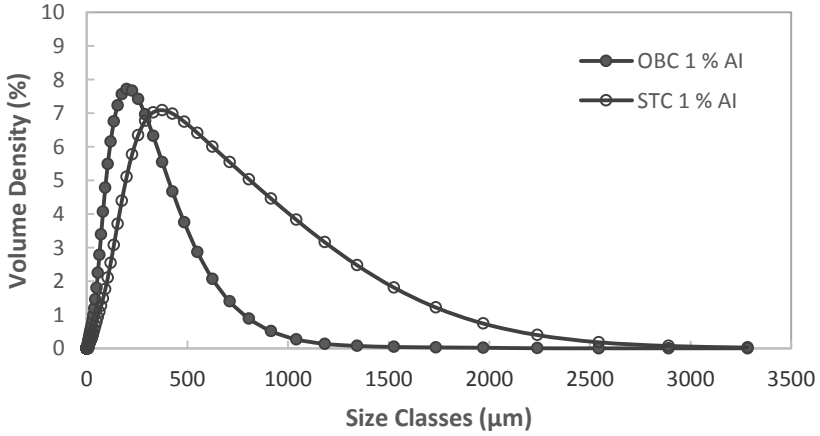

Figure 7.3 – Full CSD from crystals produced by both OBC and STC at 750 W m^{-3} and 0.75 °C min^{-1}

From the crystal images in Figure 7.4, there is evidence of agglomeration at all conditions and in both vessels, however the STC still appears to have a higher incidence of agglomeration than the OBC at comparable conditions. As discussed for the 0 % AI system, the higher supersaturation level upon nucleation (51) and the poorer mixing environment noted in the STC are the likely causes of this lower STC purity due to increased agglomeration. While the evidence of this is not as clear for the 1 % system, the supersaturation level in the STC is still higher (Table 7.6).

One of the possible causes for this apparent size difference is the increased evidence of smaller broken crystals in the OBC (Fig. 7.3 (c)), due to the increased baffle surface area.

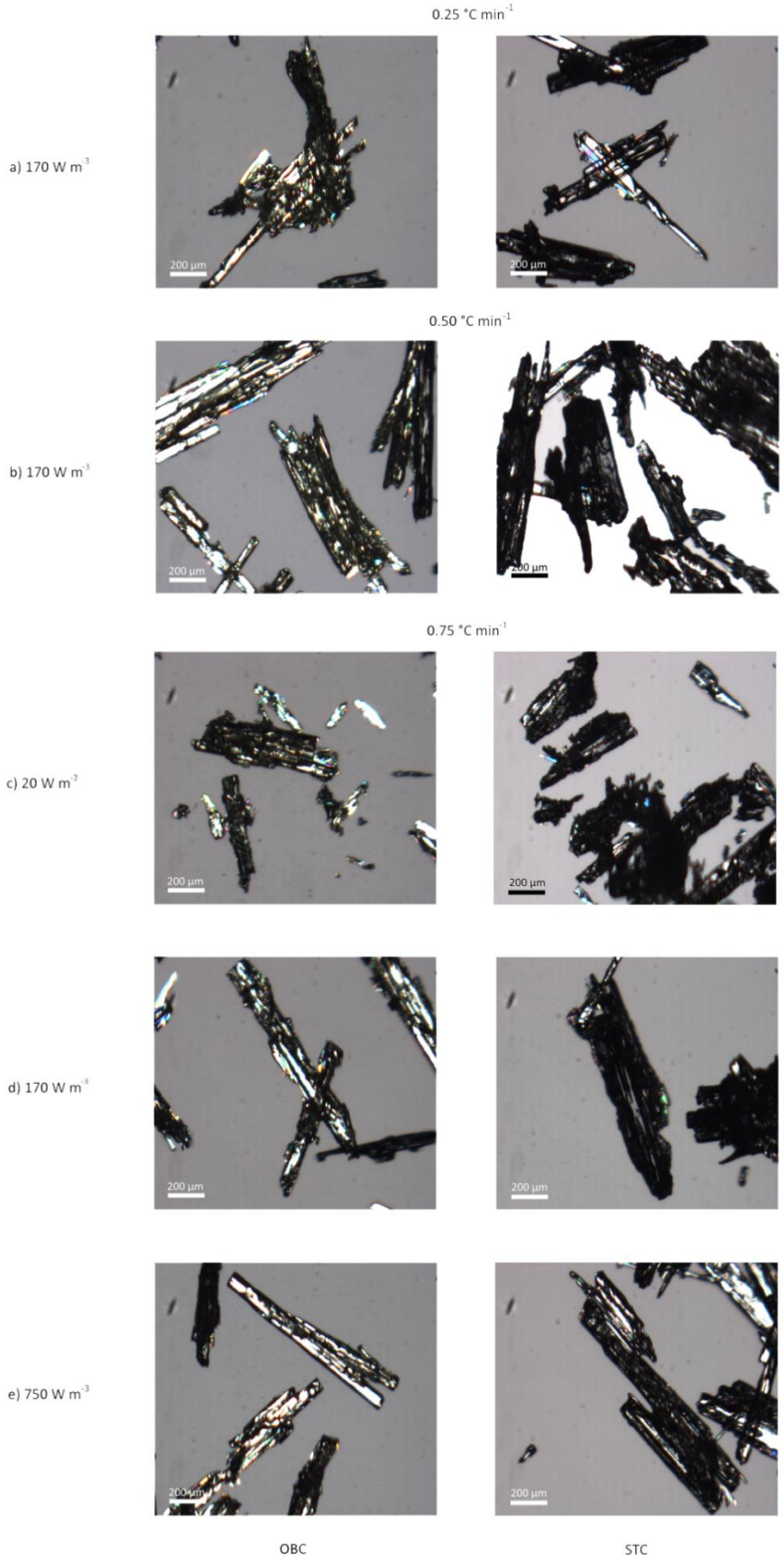

Figure 7.4 – Crystals produced when 1 wt. % Impurity is Added in OBC and STC

Looking at the images in the STC in Figure 7.4 (b, d & e in particular), agglomeration is noted at all three conditions and crystals become thicker. When biuret is incorporated into growing urea crystals (76), it has been noted that the impurity inhibits growth in the [001] direction leading to the production of much squatter and 'fatter' crystals. When the amount of impurity incorporated reaches 5 wt. % the crystals appear cubic in nature. For 1 wt. % biuret it would be expected to produce wider crystals with flatter edges than those in the 'pure' environment but not the production of fully cubic crystals. This impurity incorporation is supported by the CSD which shows a significant physical shift to a larger size class in the STC compared to the OBC (Figure 7.3) which is not shown by the agglomeration differences in the 'pure' system. Therefore, from both the CSD data and the crystal imaging, the STC has both agglomeration of mother liquor and impurity incorporation at these conditions.

Table 7.10 shows the aspect ratio of the crystals, which was analysed by the Malvern Morphologi G3, for the experimental conditions trialled above. As previously mentioned, the aspect ratio is defined as the width of a specific crystal divided by the length of that crystal and gives an indication of crystal shape. It is noted that at the lowest cooling rate and the lowest mixing intensity, both vessels have similar aspect ratios due to the similar level of agglomeration (Figure 7.4 (a)). In contrast, the STC has a much larger aspect ratios than the OBC at the other three conditions indicating that the needle thickness has increased when compared to the length. These three conditions also had higher biuret crystallization rates in the STC (Table 7.8) and statistically different purity values in Table 7.6. This aspect ratio presents another way of clarifying one of the main indicators of impurity incorporation in the 'doped' systems.

Table 7.10 – Aspect ratio (W/L) results for crystals from OBC and STC at all conditions

Cooling rate (°C min^{-1})	Mixing intensity (W $m^{-3)}$	OBC		STC	
		Number of crystals imaged	Aspect ratio	Number of crystals imaged	Aspect ratio
0.25	170	577	0.556 $\pm$ 0.15	725	0.570 $\pm$ 0.15
0.50	170	364	0.582 $\pm$ 0.16	506	0.609 $\pm$ 0.16
0.75	20	1061	0.578 $\pm$ 0.15	246	0.598 $\pm$ 0.16
0.75	170	828	0.583 $\pm$ 0.15	557	0.638 $\pm$ 0.17
0.75	750	693	0.561 $\pm$ 0.15	346	0.602 $\pm$ 0.16

At the fixed mixing intensity in Table 7.10 it is also apparent that when the cooling rate increases the aspect ratio also increases, more so in the STC than the OBC. This is due probably

to the increasing rate of supersaturation generation with increasing cooling rate (45). Similarly, the higher mixing intensity produces smaller aspect ratio values in both vessels than the lower mixing intensity at this fixed cooling rate. The reason for this is likely the increased probability of crystal collisions at the higher mixing intensity.

The crystal images suggest that in the OBC at all conditions it is the level of agglomeration that led to the purity results obtained, similar to the 'pure' system. The incorporation of some impurity into the growing crystals has caused the statistically lower purity in the STC despite the similar supersaturation levels. The degree of this incorporation in the STC depends on the mixing and cooling conditions.

At the lowest mixing intensity large agglomerates with the largest D_{50} size can be seen in Table 7.9, probably due to the relatively poorer mixing in the STC post-crystallization. So why, at this mixing intensity, is there little evidence of impurity incorporation in the STC, especially as we would have expected that the impurity incorporation would be at its highest? One possible reason is that at this mixing intensity the biuret may have not been fully dispersed within the solution and therefore has limited impact on the growing crystals post-nucleation. However, comparing the nucleation temperatures at this condition for 0 % AI (Table 7.3) and 1 % AI (Table 7.7), the lower nucleation temperature with the presence of impurity suggests that impurity affected nucleation more than crystal growth (15, 23). When the mixing intensity was increased the added impurity had a greater effect on the crystals produced in terms of crystal size, habit and final purity as shown previously. This implies that at these higher mixing intensities the mixing was sufficient to fully disperse the impurity allowing it to become incorporated, hence affecting the final purity.

So, why has the lowest cooling rate rejected the impurity in the STC while the other cooling rates at this mixing intensity have not? It is likely that the slow cooling rate has allowed the growing crystal units more time to equilibrate and therefore reject the impurity (23). Generally, the incorporation of the impurity is diffusion controlled, where the biuret moves both towards and away from the crystal surface in equal measure**.** At the slow cooling rate, the production of the bonds between the urea and biuret would be slow as the growth of urea crystals is slow. At faster cooling rates, faster growth rates are likely to increase the interactions and in turn the possibilities of impurity inclusions (15).

The previous paragraphs have offered some possible explanations as to why the STC appears to reject the impurity at some conditions but not at others. However, they do not explain why the OBC seems to be rejecting the impurity under all conditions. This is again likely to be related to the effect of mixing on the growing crystals. The visually better mixing in the

OBC throughout post-nucleation period provided more time for the impurity to move away from the crystal face before it becomes covered by other molecules. Another possible explanation would be that as the mixing internals (baffle and rod) in the OBC have a much larger surface area than that in the STC, smaller crystals and improved CSD are expected due to increased crystal breakage (40) when crystallizing at similar supersaturation levels (Table 7.6). These smaller crystals are constantly moving allowing biuret less time to bond to them before moving away.

7.3.1 Summary

So overall, what can be gathered from comparisons between the 0 and 1 % AI systems? As the retardation effect of the biuret on nucleation conditions affects both the supersaturation level upon nucleation and the corresponding nucleation temperature when the 1 % impurity is added, the higher supersaturation level and subsequently the lower nucleation temperature would have led to lower purity obtained at the 1 % AI level than that from the 0 % AI system.

The trend of higher purity crystals in the OBC than that in the STC obtained in a pure environment is still valid when 1 % impurity is added to the system.

7.4 5 wt. % Added impurity

The amount of impurity added has a significant effect on the crystal habit, with fatter and more 'block' like or cubic crystals (79) produced when the impurity level equals or exceeds 5 wt. %. For this reason, experiments with 5 wt. % added impurity were carried out.

The same experimental conditions and structure as 0 and 1 % AI were utilized, enabling direct comparisons between all impurity levels. The exact conditions and system components are presented in Section 3.4.1.

Table 7.11 shows the purity data along with both the standard deviation and the Kolmogorov-Smirnov statistical factor calculated using MATLAB®. Again all results shown are an average of 3 individual trials.

Table 7.11 – Average purity results for the 5 % AI trials

5 % AI		Cooling rate [°C min^{-1}]								
% Average purity ± SD		0.25			0.50			0.75		
		OBC	STC	P	OBC	STC	P	OBC	STC	P
Mixing intensity [W m^{-3}]	20							95.00 ± 0.15	94.83 ± 0.69	0.32
	170	93.08 ± 0.78	92.58 ± 0.42	0.32	94.00 ± 0.12	93.34 ± 0.48	0.32	93.53 ± 0.30	93.20 ± 0.15	0.32
	750							93.40 ± 0.18	93.15 ± 0.15	0.32

From Table 7.11 it can be seen that, similar to the other added impurity levels (0 and 1 % AI), the OBC is producing higher purity crystals than the STC at all investigated conditions, however, the results are statistically similar (P = 0.32).

Table 7.12 presents the supersaturation data at this added impurity, which are again statistically similar.

Table 7.12 – Average supersaturation values at nucleation for 5 % AI trials

Average supersaturation ± SD		Cooling rate (°C min^{-1})								
		0.25			0.50			0.75		
		OBC	STC	P	OBC	STC	P	OBC	STC	P
Mixing intensity (W m^{-3})	20							1.138 ± 0.036	1.195 ± 0.090	0.32
	170	1.191 ± 0.042	1.202 ± 0.117	0.32	1.136 ± 0.024	1.176 ± 0.045	0.32	1.130 ± 0.051	1.198 ± 0.012	0.32
	750							1.163 ± 0.063	1.300 ± 0.078	0.32

It should still be noted that the OBC nucleates at a lower level of supersaturation at all trialled conditions. This lower supersaturation level corresponds to a higher nucleation temperature in the OBC, as shown in Table 7.13, and implies that the work by Ni and Liao (70) still holds even with a higher impure starting environment.

Table 7.13 – Average nucleation temperatures for 5 % AI trials

Nucleation temperature ± SD [°C]		Cooling rate (°C min^{-1})								
		0.25			0.50			0.75		
		OBC	STC	P	OBC	STC	P	OBC	STC	P
Mixing intensity (W m^{-3})	20							22.76 ± 0.69	21.78 ± 0.24	0.03
	170	24.13 ± 0.30	23.15 ± 0.60	0.32	25.77 ± 0.06	22.68 ± 1.14	0.03	24.00 ± 0.27	23.61± 0.45	0.32
	750							22.57 ± 0.45	21.72 ± 0.12	0.03

At this added impurity level, both the rates of supersaturation generation and depletion are faster in the STC for all conditions, although some of the results are statistically different there is no consistency over the conditions investigated.

Table 7.14 lists the crystallization rate of biuret and in this case all rates produced are similar, suggesting that the levels of biuret incorporation were similar.

Table 7.14 – Average crystallization rate for biuret at 5 % AI trials; all values x10^{-6}

Average biuret crystallization rate ± SD (all x 10^{-6}) [g ml.s^{-1}]		Cooling rate (°C min^{-1})								
		0.25			0.50			0.75		
		OBC	STC	P	OBC	STC	P	OBC	STC	P
Mixing intensity (W m^{-3})	20							6.25 ± 1.02	4.59 ± 1.26	0.32
	170	6.35 ± 4.59	12.36 ± 2.82	0.06	7.49 ± 2.55	5.94 ± 0.54	0.32	6.42 ± 0.48	5.94 ± 2.67	0.32
	750							7.49 ± 0.99	8.03 ± 1.02	0.78

If these systems are still functioning in the manner suggested by Charmolue (25) and Givand (45), could agglomeration still be the main cause of the purity differences? Or alternatively, are they due to differences in impurity incorporation, as suggested by Scott and Black (79), even with the biuret depletion rates presented in Table 6.14?

Again CSD were obtained and the mean crystal size (D_{50}) and span were tabulated below in Table 7.15.

Table 7.15 – Average D_{50} and CSD span results crystals produced at 5 % AI in OBC and STC

Cooling rate (°C min^{-1})	Mixing intensity (W m^{-3})	OBC		STC		P(D_{50})
		D_{50} (µm)	Span	D_{50} (µm)	Span	
0.25	170	386.52 ± 19.2	1.86	496.31 ± 11.7	2.91	0.06
0.50	170	242.12 ± 17.0	1.82	616.53 ± 77.1	2.09	0.06
0.75	20	283.51 ± 80.1	2.47	627.61 ± 60.3	2.22	0.03
0.75	170	261.13 ± 25.1	1.95	690.26 ± 74.1	1.82	0.03
0.75	750	332.25 ± 20.3	1.62	390.99 ± 23.4	2.87	0.06

The D_{50} in the STC are much larger than in the OBC. This is supported by the CSD in Figure 7.5 where the curve from the STC is shifted to the right with a large tail.

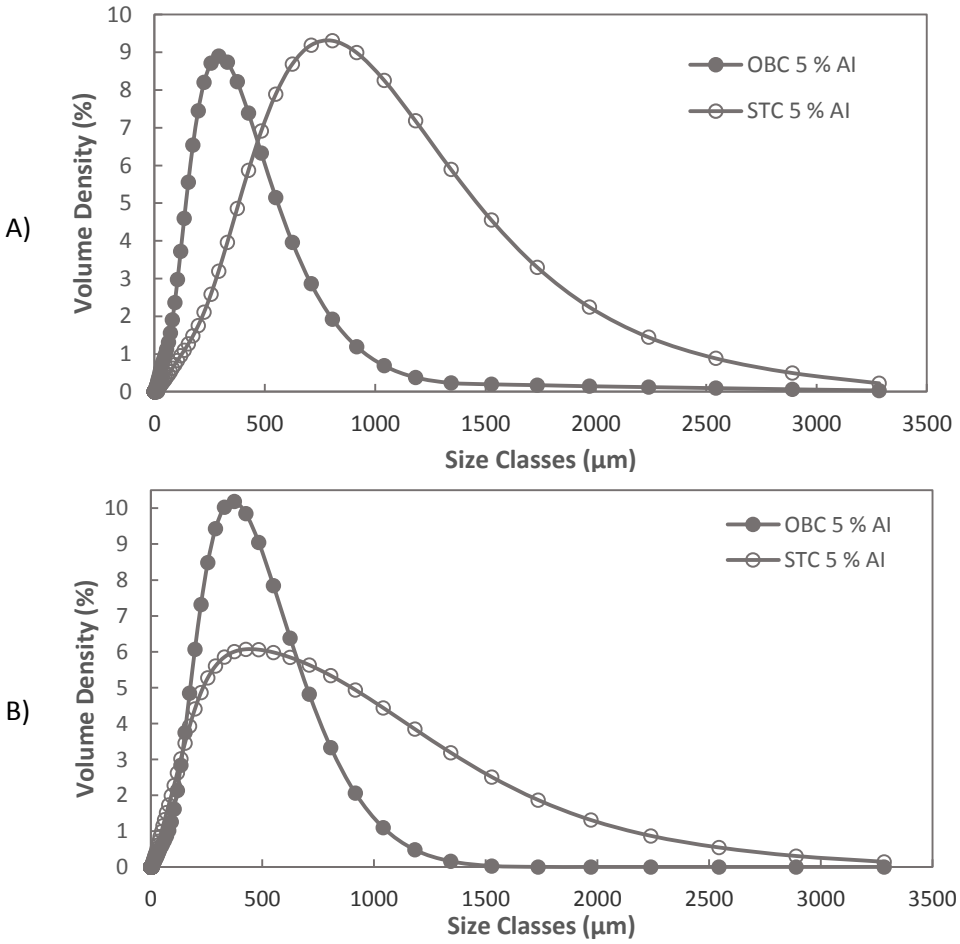

Figure 7.5 – CSD obtained from crystals from 5 % AI trials in OBC and STC at 0.75 °C min^{-1} with mixing intensity of A) 170 W m^{-3} and B) 750 W m^{-3}

The crystal images are displayed in Figure 7.6, all the crystals produced are thicker and in many cases, more cubic than at either the 'pure' or 1 % level, indicating impurity incorporation. When the image pairs are examined, it is apparent that the STC has a higher agglomeration at every condition. The cubic crystals are the direct result of incorporation of the biuret in both systems, but the STC shows more evidence of agglomeration. There are more small crystals in the OBC because of the larger mixing internals (OBC baffle area of 13320 mm^2 compared to the STC area of 3070 mm^2).

The aspect ratios in Table 7.16 again show that the OBC has a smaller value than the STC under every condition investigated, i.e. the STC is producing 'fatter' crystals than the OBC, if a similar length is assumed. As the imaging in Figure 7.6 suggests that both vessels and all conditions are subject to impurity incorporation, this difference is probably because of the higher agglomeration in the STC. This is confirmed by the agglomerates noted in the STC images in Figure 7.6, as well as the CSD results shown in Table 7.15 and Figure 7.3.

Table 7.16 – Aspect ratio results for crystals from the OBC and STC at 5 % AI

Cooling rate (°C min^{-1})	Mixing intensity (W $m^{-3)}$	OBC		STC	
		Number of crystals imaged	Aspect ratio	Number of crystals imaged	Aspect ratio
0.25	170	750	0.598 $\pm$ 0.15	423	0.623 $\pm$ 0.16
0.50	170	533	0.603 $\pm$ 0.16	506	0.618 $\pm$ 0.16
0.75	20	112	0.640 $\pm$ 0.17	107	0.580 $\pm$ 0.15
0.75	170	519	0.583 $\pm$ 0.15	557	0.641 $\pm$ 0.16
0.75	750	718	0.608 $\pm$ 0.15	380	0.655 $\pm$ 0.17

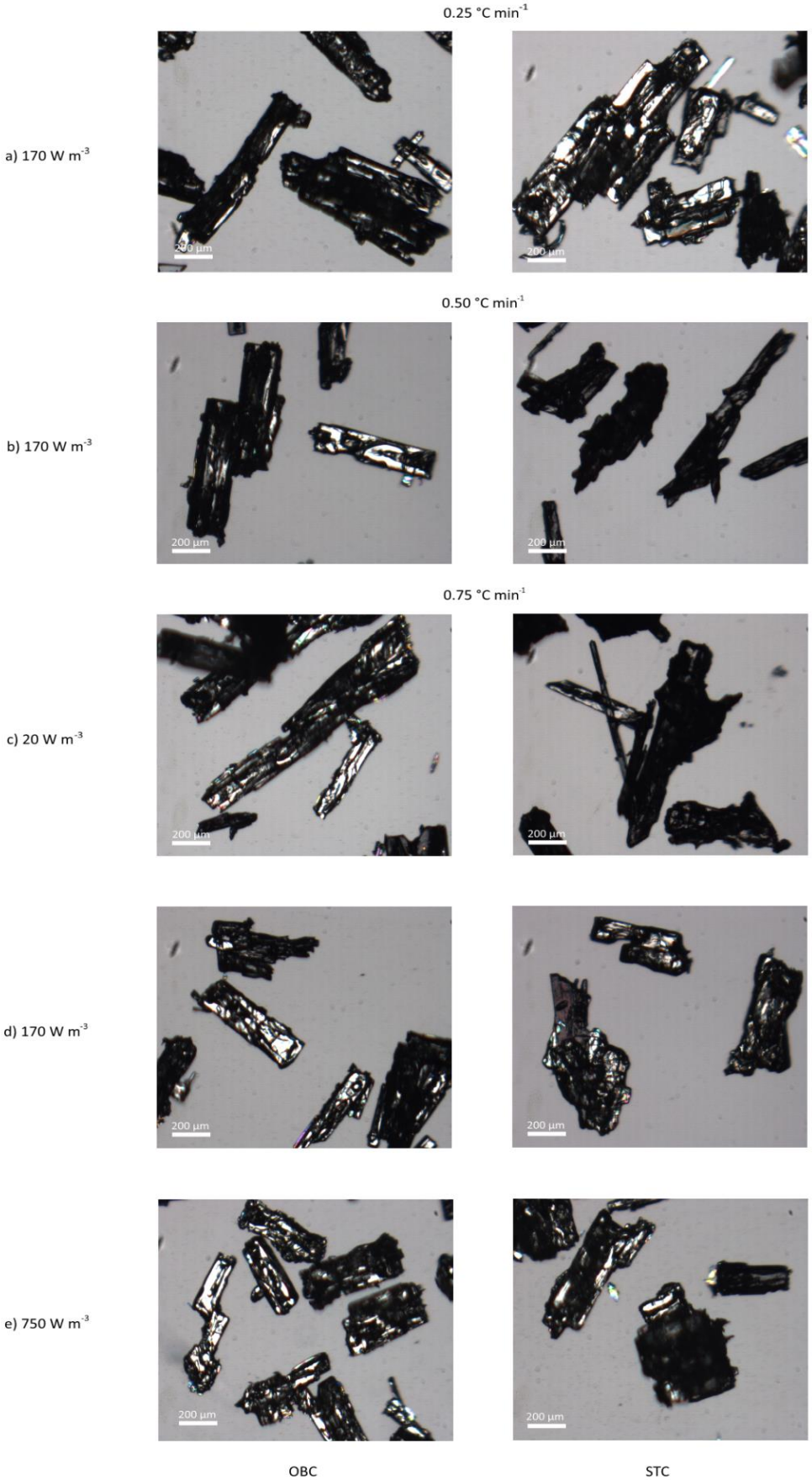

Figure 7.6 – Crystals from 5 % AI trials in OBC and STC

The crystallization rate of the urea can be calculated and compared between the two impurity levels (0 and 5 % AI), as shown in Table 7.17. Note the values obtained between the OBC and STC are similar.

Table 7.17 – Urea crystallization rates for 0 and 5 % AI in the OBC and STC systems (all x 10^{-5})

Urea crystallization rates ± SD [s^{-1}]		OBC			STC		
		0 % AI	5 % AI	P	0 % AI	5 % AI	P
0.25	170	3.18 ± 0.93	3.89 ± 0.78	0.32	3.26 ± 0.60	10.19 ± 4.08	0.10
0.50	170	5.41 ± 0.87	8.56 ± 1.86	0.06	4.38 ± 0.87	9.12 ± 3.27	0.03
0.75	20	5.80 ± 0.42	8.84 ± 3.03	0.06	4.17 ± 0.39	6.45 ± 2.49	0.03
0.75	170	7.16 ± 0.81	8.41 ± 1.02	0.32	4.67 ± 2.61	10.21 ± 1.35	0.06
0.75	750	5.91 ± 0.93	7.97 ± 1.35	0.06	6.12 ± 1.35	9.33 ± 3.24	0.06

From Table 7.17 it is clear that the 5 % AI rate is always faster than the 0 % AI at each comparable condition. This suggests that more small single crystals are produced at the 5 % level, as indicated by the mean crystal sizes above, these were more likely to agglomerate in the high supersaturation environment.

7.5 Conclusion

From the results presented, it is apparent that the OBC still produces crystals of a higher purity than the STC under comparable conditions and for all added impurity levels tested, although the difference is not always statistically significant with the increase of added impurity. The purity differences between the vessels appear to be related to the level of agglomeration obtained, with the STC always having a higher agglomeration, due to the visible poorer mixing environment together with the higher supersaturation level mentioned in the STC. In contrast, the crystals and agglomerates are more prone to break up in the OBC because of the increased surface area of the mixing internals as well as the mixing uniformity.

As the level of impurity added increases, the purity drops within both vessels and at each condition, which is expected.

Chapter 8 Comparison of impurity effect on selected conditions in each vessel

In the past chapter, the purity data were compared at two added impurity levels; in this chapter the comparison of parameters for all three impurity levels are made at two selected conditions as outlined in Table 8.1 and for simplicity they have been assigned identifying numbers. These conditions were chosen as they are representative of the remaining conditions and cover both of the 1 % added impurity trends noted and discussed in Chapter 7. AS

Table 8.1 – Experimental conditions and assigned identifying number

Condition number	Cooling rate (°C min^{-1})	Target mixing intensity (W m^{-3})
1	0.25	170
2	0.75	750

8.1.1 OBC at Condition 1

Figure 8.1, show the purity results obtained at all three impurity levels, with the Kruskal-Wallis statistical factor (P_{kw}) (114) as well as the Kolmogorov-Smirnov Statistical factors (P) relating all possible data pairings within the set. All data points are an average of 3 individual trials, the standard deviations are also given for each point.

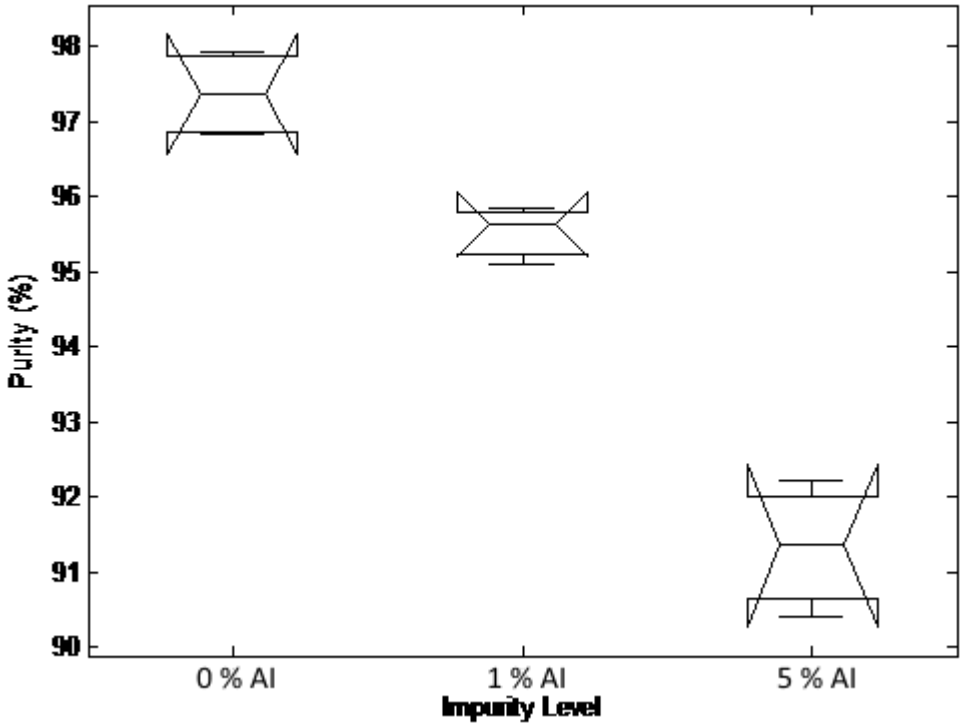

Figure 8.1 – Kruskal-Wallis box plot showing the purity from the OBC at condition 1

As expected, when the added impurity level (% AI) increases, the purity obtained decreases and is statistically different overall. The level of supersaturation obtained upon nucleation and the nucleation temperatures are shown in Table 8.2 and again are presented with the corresponding statistical analysis values.

Table 8.2 – Supersaturation levels and temperature at nucleation in the OBC system at condition 1

Average supersaturation level upon nucleation ± SD	0 % AI	1 % AI	5 % AI	P_{kw}
	1.080 ± 0.012	1.101 ± 0.012	1.191 ± 0.042	
Supersaturation KS test P values	0 – 1% AI	0 – 5 % AI	1 – 5 % AI	0.03
	0.03	0.03	0.03	
Average nucleation temperature ± SD [°C]	0 % AI	1 % AI	5 % AI	P_{kw}
	30.39 ± 0.30	27.77 ± 0.39	24.13 ± 0.30	0.03

Due to the aforementioned effect of impurity on crystal nucleation and growth (23), the level of supersaturation required at nucleation is seen to increase and the corresponding

nucleation temperature decreases as the level of impurity increases in Table 8.2. An increase in supersaturation leads to an increase in the rate of crystallization; the rates for both the urea and the biuret are presented in Table 8.3, where a high rate in the urea system indicates the production of more small crystals and a high rate in the biuret suggests impurity incorporation (15). The biuret crystallization rate values for the 0 % AI was determined from the trace amounts of biuret within the system, as no impurity had been added at this stage. It has been included to give an indication of the system parameters when no impurity has been added as comparison for the impure systems.

Table 8.3 – Crystallization rates of both urea and biuret from the OBC trials at condition 1

Rate of urea crystallization ($\times 10^{-5}$) $\pm$ SD [g ml.s^{-1}]	0 % AI	1 % AI	5 % AI	P_{kw}
	3.18 $\pm$ 0.93	3.77 $\pm$ 0.90	3.89 $\pm$ 0.78	
Urea KS test P values	0 – 1% AI	0 – 5 % AI	1 – 5 % AI	0.71
	0.32	0.32	0.98	
Rate of biuret crystallization ($\times 10^{-6}$) $\pm$ SD [g ml.s^{-1}]	0 % AI	1 % AI	5 % AI	P_{kw}
	2.78 $\pm$ 0.78	2.63 $\pm$ 1.26	6.35 $\pm$ 4.59	
Biuret KS test P values	0 – 1% AI	0 – 5 % AI	1 – 5 % AI	0.13
	0.98	0.06	0.06	

From Table 8.3 as the impurity level and subsequently the supersaturation level increases, the crystallization rates also increase for both compounds. However, the differences in the urea rates for 1 % and 5 % AI are essentially the same (P = 0.98). In contrast, the biuret crystallization rate obtained at the 5 % AI level is statistically higher than that of either of the lower impurity levels, which are similar to each other. This suggests the biuret is leaving the solution at a faster rate at the 5 % AI level compared to the lower levels.

The mean crystal size (D_{50}) and CSD span are given in Table 8.4, in conjunction with the full CSD profiles and the microscope images of the crystals, in Figures 8.2 and 8.3 respectively.

Table 8.4 – Average mean crystal size and span values for crystals from all impurity levels

Added impurity level	0 % AI	1 % AI	5 % AI	P_{KW}
Average D_{50} values ± SD [µm]	266.58 ± 32.4	195.05 ± 19.8	386.52 ± 19.2	0.03
CSD span	2.50	2.32	1.86	-

Mean crystal size KS test P values	0 – 1 % AI	0 – 5 % AI	1 – 5 % AI
	0.03	0.03	0.03

From Table 8.5 it is clear that the addition of impurity has an effect on the crystal size achieved; however, the mean crystal size does not increase consistently with the impurity level, which is supported by the CSD profiles in Figure 8.2.

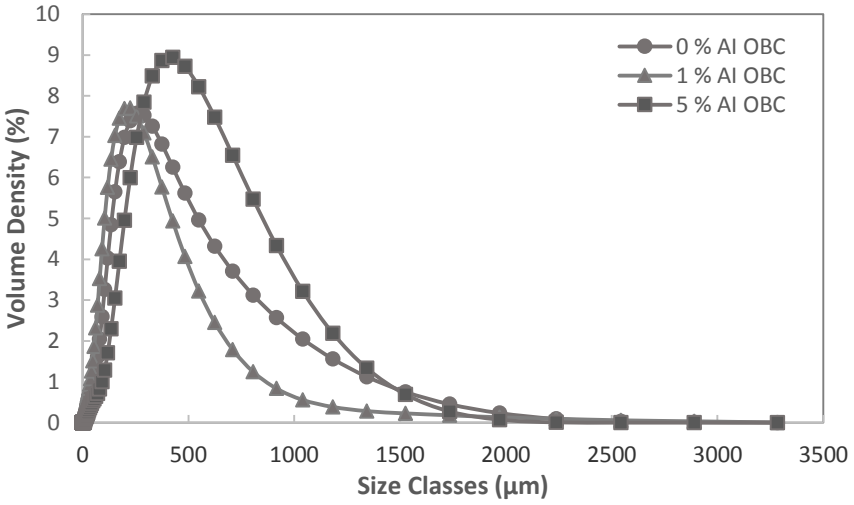

Figure 8.2 – Full CSD from crystals produced by condition 1 in the OBC at 0, 1 & 5 % AI

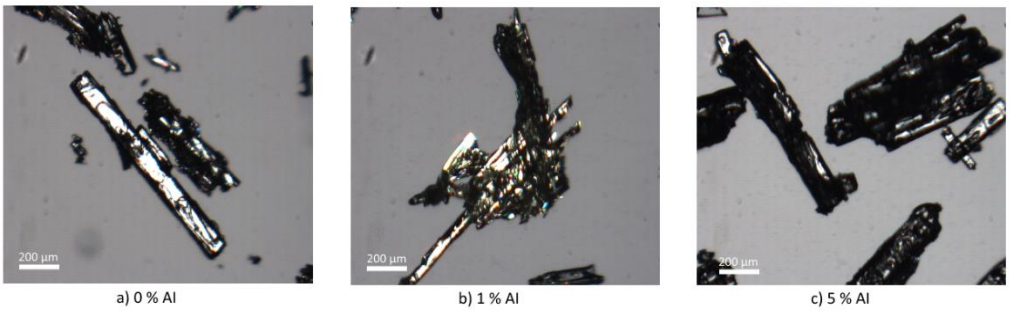

Figure 8.3 – Microscope images of crystals from the OBC using condition 1

at a) 0 % AI, b) 1 % AI and c) 5 % AI

The crystals imaged (Figure 8.3 (c)) for 5 % AI are more block-like and thicker looking crystals than those at the lower impurity levels. As previously discussed (76), this block-like or cubic habit is the fingerprint of biuret being incorporated into the growing crystal with the lower final purity. This impurity incorporation coincides with the higher biuret crystallization rate in Table 8.3, which gives support to the hypothesis that a high crystallization rate in the biuret is associated with impurity being incorporated. This incorporation is less observed at the lower impurity level (1 % AI) and here the lower purity obtained appears to be a consequence of additional agglomeration (Fig. 8.3 (b)). These agglomerates are shorter and more circular than at those at 0 % AI (Fig. 8.3 (a)) and the type of agglomeration has also changed from crystal 'twinning' at 0 % AI to more 'clumped' agglomeration at the 1 % level. This reduction in the agglomerate size is the likely cause of the apparent decrease in mean crystal size in Table 8.4.

Table 8.5 – Size characteristics of crystals obtained from Morpholgi G3 for the OBC at condition 1

Size characteristics $\pm$ SD	Number of crystals analysed	Length (µm)	Width (µm)	Circularity	Circle equivalent diameter (µm)
0 % AI	1353	701.5 $\pm$ 176.5	218.5 $\pm$ 54.1	0.728 $\pm$ 0.07	323.2 $\pm$ 85.0
1 % AI	577	764.5 $\pm$ 190.6	242.9 $\pm$ 57.3	0.711 $\pm$ 0.07	341.6 $\pm$ 89.1
5 % AI	750	765.5 $\pm$ 228.6	325.7 $\pm$ 91.1	0.738 $\pm$ 0.07	427.6 $\pm$ 129.7

From Table 8.5 as the level of impurity increases, the length, width, circularity and CED of the crystals increase, more so for crystals at the 5 % level.

8.1.2 STC at Condition 1

Following the analysis for the OBC, similar examinations were carried out for the STC at condition 1. All data points are an average of 3 individual trials, the standard deviations are also given for each point. When the added impurity level increases the purity attained decreases, as shown in Table 8.6 and this drop is statistically different between each impurity level.

Table 8.6 – Average % purity results from the crystals produced by the STC operating at condition 1

Average % purity $\pm$ SE	0 % AI	1 % AI	5 % AI	P_{kw}
	96.33 $\pm$ 0.09	94.29 $\pm$ 0.22	92.58 $\pm$ 0.14	
KS test P values	0 – 1% AI	0 – 5 % AI	1 – 5 % AI	0.03
	0.03	0.03	0.03	

Unlike the OBC results (Table 8.2) however, the supersaturation levels for the STC do not show the expected trend of increasing when the impurity level increases, shown in Figure 8.4. However, the nucleation temperatures in Table 8.7, follow a similar trend to the OBC at this condition as the nucleation temperature decrease as the impurity level increases.

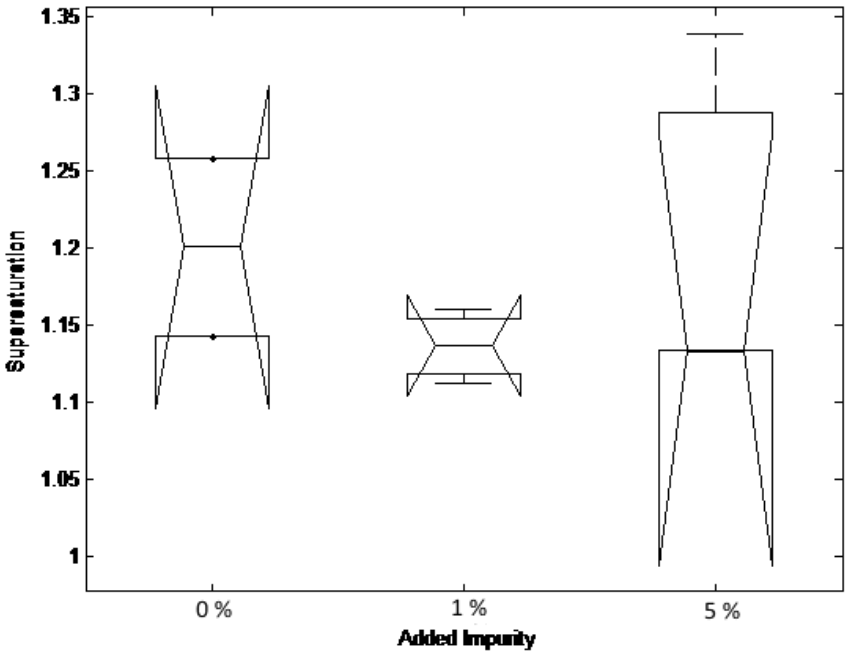

Figure 8.4 – Kruskal-Wallis box plot of supersaturation levels upon nucleation for the STC at condition 1

Table 8.7– Nucleation temperatures from the STC system at condition 1

Average nucleation temperature ± SE [°C]	0 % AI	1 % AI	5 % AI	P_{kw}
	29.64 ± 0.81	27.50 ± 0.33	23.18 ± 0.63	0.03

From Table 8.8 it can be seen that the urea crystallization rate increases statistically with increasing levels of impurity which is different to the OBC results under these conditions. In contrast, the biuret crystallization rate is similar between the 0 and 1 % results, while much higher for the 5 % AI.

Table 8.8 – Crystallization rates of urea and biuret from the STC trials at condition 1

Crystallization rate of urea (x 10^{-5}) ± SD [g $ml.s^{-1}$]	0 % AI	1 % AI	5 % AI	P_{kw}
	3.26 ± 0.60	5.22 ± 0.42	10.19 ± 4.08	
Urea KS test P values	0 – 1% AI	0 – 5 % AI	1 – 5 % AI	0.07
	0.06	0.09	0.06	
Crystallization rate of biuret (x 10^{-6}) ± SE [g $ml.s^{-1}$]	0 % AI	1 % AI	5 % AI	P_{kw}
	3.17 ± 0.00	2.15 ± 0.39	12.36 ± 2.82	
Biuret KS test P values	0 – 1% AI	0 – 5 % AI	1 – 5 % AI	0.12
	0.17	0.06	0.06	

Figure 8.5 presents the microscopy images of crystals from the STC and it is clear that the 5 % AI crystals (Fig. 8.5 (c)) are more cubic showing impurity incorporation, the 1 % AI crystals (Fig. 8.5 (b)) however suggest that agglomeration is the sole reason for the purity values obtained. The crystals produced at the 0 % AI level (Fig. 8.5 (a)) exhibit limited evidence of agglomeration but with a variety of crystal sizes.

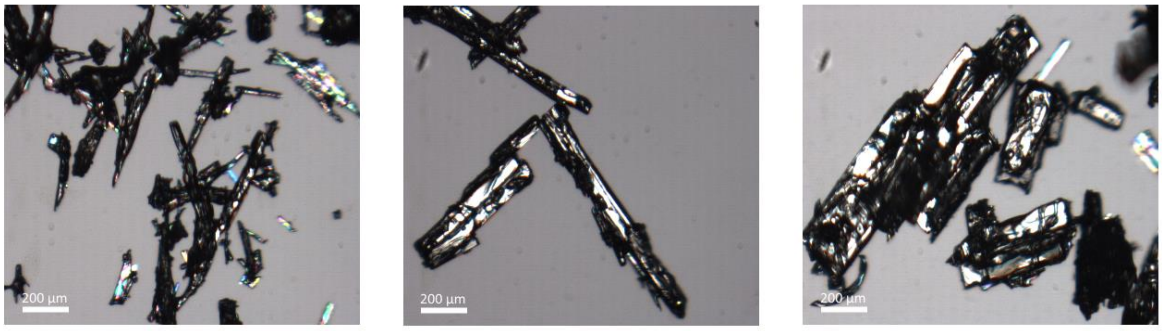

a) 0 % AI b) 1 % AI c) 5 % AI

Figure 8.5 - Microscope Images of crystals produced by the STC using Condition 1 at a) 0 % AI, b) 1 % AI and c) 5 % AI

The extracted CSD data is presented in Table 8.9 and shows an increase in the mean crystal size as the impurity level increases, agreeing with the CSD presented in Figure 8.6. This would be expected due to the apparent increase in both agglomeration and impurity incorporation evident at 1 % and 5 % AI respectively in Figure 8.5.

Table 8.9 – Average mean crystal size and span values for crystals produced at all impurity levels

Level added impurity	0 % AI	1 % AI	5 % AI	P_{KW}
Average D_{50} values ± SD [µm]	303.30 ± 80.7	376.66 ± 212.1	469.31 ± 11.7	0.28
CSD span	3.91	2.45	2.91	-

Mean crystal size KS test P values	0 – 1 % AI	0 – 5 % AI	1 – 5 % AI
	0.84	0.84	0.84

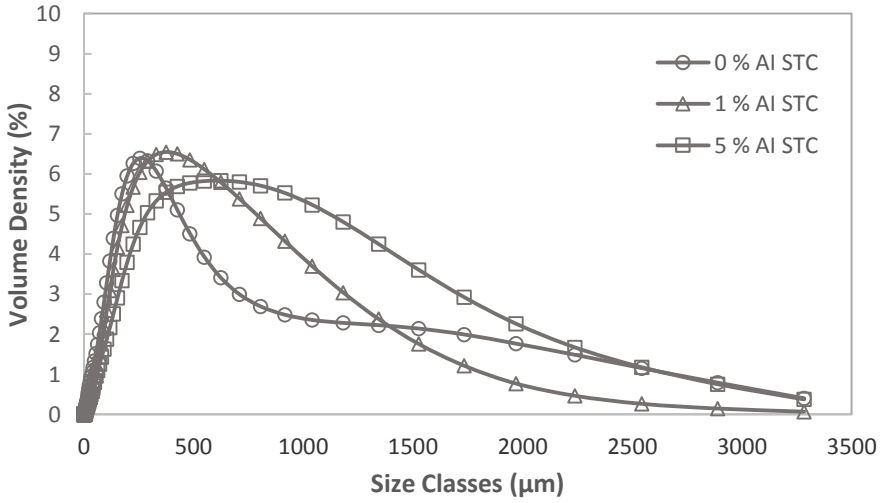

Figure 8.6 – Full CSD from crystals produced by condition 1 in the STC at 0, 1 & 5 % AI

Similar to the OBC analysis, Table 8.10 lists the length, width, circularity and circle equivalent diameter obtained from the Morphologi G3 system along with the calculated standard deviation (SD) values.

Table 8.10 – STC crystal characteristics from Morpholgi G3 at condition 1

Size characteristics ± SD	Number of crystals analysed	Length (µm)	Width (µm)	Circularity	Circle equivalent diameter (µm)
0 % AI	698	848.5 ± 205.5	247.8 ± 55.7	0.714 ± 0.07	376.8 ± 95.7
1 % AI	725	681.4 ± 190.6	208.6 ± 58.3	0.717 ± 0.07	316.1 ± 91.0
5 % AI	423	805.6 ± 216.4	446.6 ± 104.7	0.742 ± 0.07	551.8 ± 137.6

For all three impurity levels, only the circularity offers any overall trend, similar to the OBC results, i.e. there is an increase in circularity as the impurity level increases. The other two impurity levels (0 and 1 %) gave similar values probably due to the 'twinning' type of agglomeration.

8.2.1 OBC at Condition 2

The final condition to be analysed in this manner is the highest cooling rate (0.75 °C/min) and the fastest mixing intensity of 750 W/m^3. For the OBC, the results and the trends are similar to those noted in 8.1.1, see Fig. 8.7 for Kruskal-Wallis plot of the purity data at this condition. As the conditions studied are different, this indicates that the OBC is operating in a similar manner at all conditions investigated.

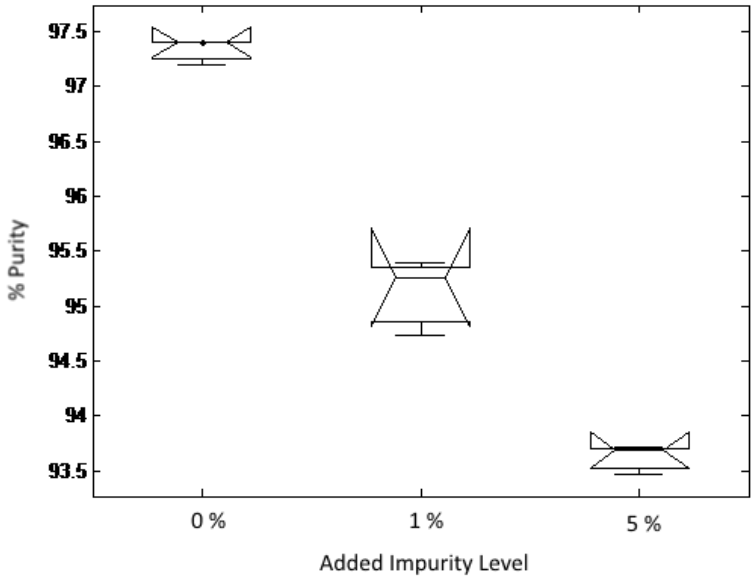

Figure 8.7 – Kruskal-Wallis plot of purity values from OBC operating at Condition 2

8.2.2 STC at Condition 2

In contrast to the OBC, the STC at this condition produces different results to those previously discussed in section 8.1.2; in particular the crystallization rates and CSD. The crystallization rate for urea (Table 8.11) is similar at the 1 and 5 % levels, while the 0 % AI value is statistically lower. This suggests that both of the added impurity systems could have produced greater amounts of small crystals which are more likely to agglomerate. The purity data for this condition and vessel are presented in Figure 8.8, to give an indication of the ranges of values obtained. All data points are an average of 3 individual trials, the standard deviations are also given for each point.

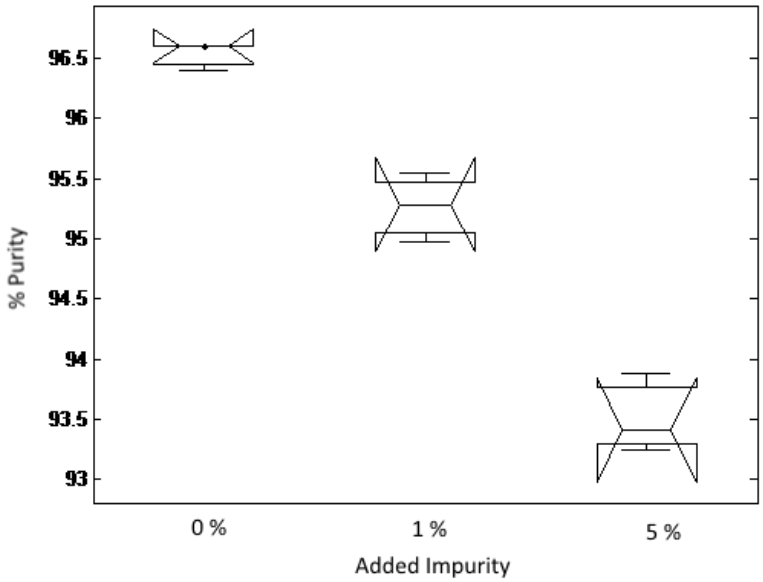

Figure 8.8 – Kruskal-Wallis box plot showing purity results from the STC at condition 2

Table 8.11 – Crystallization rates of urea and biuret from the STC operating at condition 2

Crystallization rate of urea (x 10^{-5}) $\pm$ SD [g $ml.s^{-1}$]	0 % AI	1 % AI	5 % AI	P_{kw}
	6.12 $\pm$ 1.35	8.57 $\pm$ 2.76	9.33 $\pm$ 3.24	
Urea KS test P values	0 – 1% AI	0 – 5 % AI	1 – 5 % AI	0.09
	0.06	0.06	0.84	
Crystallization rate of biuret (x 10^{-6}) $\pm$ SD [g $ml.s^{-1}$]	0 % AI	1 % AI	5 % AI	P_{kw}
	4.80 $\pm$ 3.90	10.53 $\pm$ 0.39	8.03 $\pm$ 1.02	
Depletion KS test P values	0 – 1% AI	0 – 5 % AI	1 – 5 % AI	0.37
	0.32	0.42	0.42	

The crystallization rate of biuret (Table 8.11) is high at both added impurity levels compared to 0 % AI, indicating that the system is incorporating the impurity at both added

impurity levels, unlike the previous condition. Both of these crystallization rate effects would have an effect on the crystal sizing and eventually purity. The mean crystal size and CSD span for all three impurity levels are given in Table 8.12.

Table 8.12 – Mean crystal size (D_{50}) and CSD span for the STC crystals from condition 2

Added impurity level	0 % AI	1 % AI	5 % AI	P_{KW}
Average D_{50} values $\pm$ SD [µm]	186.18 $\pm$ 7.32	366.88 $\pm$ 75.1	390.99 $\pm$ 23.4	0.11
CSD span	2.60	2.53	2.87	-

Mean crystal size KS test P values	0 – 1 % AI	0 – 5 % AI	1 – 5 % AI
	0.06	0.06	0.84

The results in Table 8.13 indicate that the crystals produced at 0 % AI are smaller than those at either 1 or 5 % AI, which are similar in mean size, supporting the suggestion that there may be impurity incorporation in both added impurity cases. Similar span values at all three impurity conditions imply the presence of agglomeration. The CSD shown in Figure 8.9 confirm the agglomeration, as well as impurity incorporation.

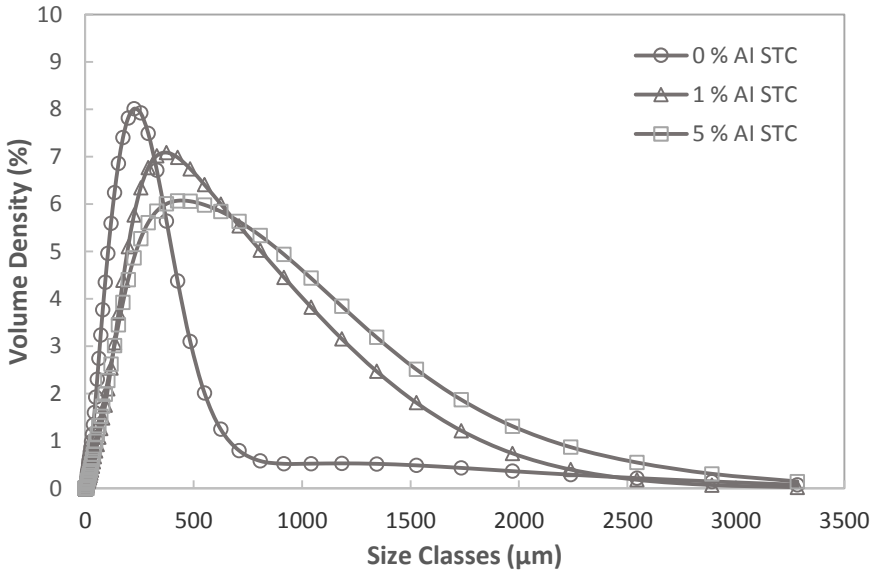

Figure 8.9 – CSD from STC crystals from condition 2 at all three added impurity (AI) levels

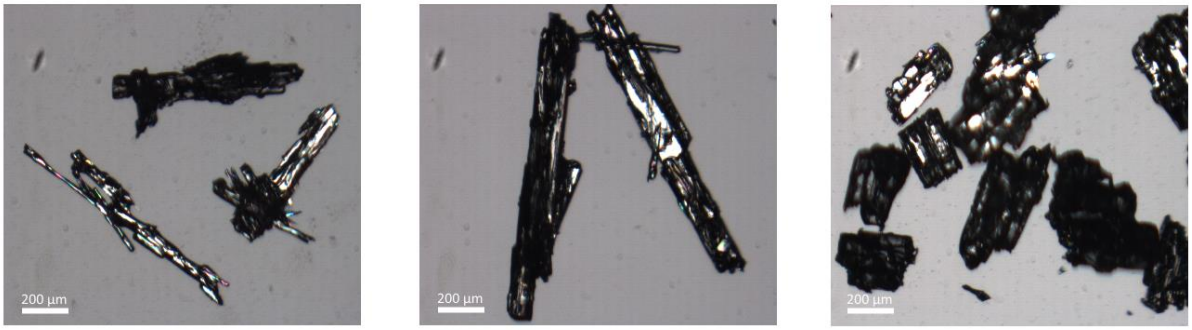

A) 0 % AI B) 1 % AI C) 5 % AI

Figure 8.10 – Microscope images of crystals from the STC system at condition 2 with A) 0 % AI, B) 1 % AI and C) 5 % AI

The crystals presented in Figure 8.10 (A) are thin needle-like crystals, at 1 % AI (Fig. 8.10 (B)), the crystal size increases becoming fatter. At the 5 % level the biuret is fully incorporation into the growing crystal, producing 'cubic' crystals (76), matched by the faster crystallization rates at this level in Table 8.11.

The Morphologi G3 data in Table 8.13 show that the results obtained at 1 % AI are very large compared to the other results under these conditions, the reasons for this are unclear but probable related to the high crystallization rates of both urea and biuret.

Table 8.13 – Size characteristics of crystals from Morpholgi G3 for the STC at condition 2

Size characteristics ± SD	Number of crystals analysed	Length (µm)	Width (µm)	Circularity	Circle equivalent diameter (µm)
0 % AI	1127	489.9 ± 137.4	166.9 ± 39.5	0.712 ± 0.07	221.7 ± 62.3
1 % AI	346	1284 ± 326.6	736.5 ± 131.8	0.724 ± 0.07	719.8 ± 174.7
5 % AI	380	744.6 ± 221.5	506.7 ± 139.5	0.747 ± 0.07	555.2 ± 159.6

8.3 Conclusions

From the comparisons presented, when the added impurity level increases, the purity of the crystals decreases as expected. In the OBC the purity drop at 1 % AI appears to be due to increased crystal size and agglomeration; while is due to the incorporation of the biuret into the growing crystals at 5 % AI. In the STC, certain conditions show impurity incorporation at 1 % and all conditions at 5 % AI.

Chapter 9 Conclusions and Future Work

9.1 Conclusions

It has been experimentally shown that the OBC produces crystals with a statistically higher purity than the STC, when obtained from a relatively pure starting environment under comparable conditions. The initial aim of this work was to confirm confidentially obtained results and this has been achieved through the experimental work completed. Investigations into the reasons behind this purity difference revealed that the level of supersaturation required to induce nucleation is statistically lower in the OBC, which corresponds to a higher nucleation temperature when compared to the STC. It has been proposed (120) that this higher level of supersaturation in the STC produces a higher rate of nucleation and lower growth rate, consequently, producing smaller single crystals. The effectiveness of mixing has been shown to be reduced due to the large amount of these small crystals in the STC leading in turn to the formation of more agglomerated crystals. The higher incidence of agglomeration in the STC is then the likely cause of the lower purity as larger amounts of mother liquor become trapped between the agglomerated single crystals.

It has also been demonstrated that this improvement in purity in the OBC is still apparent with 'impure' starting environments. This was examined with the addition of two levels of known impurity in both vessels under similar experimental conditions to those in the 'pure' work. When 1 wt. % biuret was added into both systems, the overall purity dropped compared to that obtained from the 'pure' experiments. The level of supersaturation and the MSZW required to induce nucleation was also increased. This was a result of the effect of impurity addition on the growth of both the nuclei and the crystals. As the crystals produced spent less time under the applied mixing at this lower nucleation temperature, an increase in agglomeration and crystal size are likely. The higher incidence of agglomeration was related to the higher supersaturation level, which produced more small crystals that are able to join together easier in the high supersaturation environment. This increase in agglomeration is associated with the reduction in purity when compared to 0 % AI. The crystal imaging also indicated that the crystals from the OBC had limited evidence of impurity incorporation at this impurity level with needle-like crystals being produced which had similar aspect ratios to the 'pure' crystals.

In contrast, the STC did not show such clear trends at 1 % AI as noted in the OBC. Both the lowest mixing intensity and the lowest cooling rate conditions in the STC produced crystals with increased agglomeration compared to the 'pure' system that were similar to the crystals in

the OBC at this added impurity level. It was also apparent that under these conditions the crystallization rates of both urea and biuret together with the supersaturation level upon nucleation were similar to those achieved in the OBC; indicating that these systems had crystallized in a similar manner. The other three conditions investigated in the STC showed statistically higher biuret crystallization rates compared to the OBC, indicating 'uptake' of the impurity that is supported by the crystal images and aspect ratios for these conditions; leading to statistically lower purities than the OBC.

When 5 wt. % of the biuret impurity was added, both systems have been shown to incorporate the impurity into the growing single crystals. This in turn lowers the purity of the crystals when compared to either 0 or 1 % added impurity. At this impurity level the crystallization rates of both urea and biuret are high in both vessels with similar purity and supersaturation data. However, the purity in the OBC is still slightly higher than that obtained in the STC under all conditions, with a wider variety of crystal sizes and more agglomeration noted in the STC.

The CSD obtained from the OBC is always narrower in span than that from the STC for all applied conditions and added impurity levels. It is thought that this is due to the combination of how mixing is generated, more uniform mixing and the larger mixing internals of the OBC which increases attrition of the crystals, producing smaller crystals and fewer agglomerates.

The initial purity of the solid also affects the system, with a lower purity compound increasing the metastable zone width thus requiring further cooling, which takes more energy and time.

9.2 Future Work

Due to constraints of time and equipment, a number of experiments could not be undertaken within the time of this PhD work. The following is a summary of the further work.

- To quantify the degree of agglomeration present within the systems would offer the ultimate support to our hypothesis regarding the differences of agglomeration. Possibly though modelling studies and further research work.
- Investigating the effect on purity using a moving-fluid oscillatory baffled crystallizer (mf-OBC) or a continuous OBC (COBC) would have direct impact in industry.
- The initial study on the effect of the starting purity of urea upon nucleation generated some interesting results, opening a new and exciting area of further research. There will be a significant amount of new science to be discovered within this area.
- The utilization of different materials of construction for both the OBC and STC could be an important subject for future investigations as work by other researchers has indicated that there were variations in the type of nucleation and in the rates of crystal breakage and growth, when materials other than stainless steel were employed.
- For experiments with different impellers it would be useful if the tests are repeated using the same RPM, instead of the same mixing intensity. In this way the effects of impeller shape and size on mixing and crystal characters could better be compared.
- This work could be repeated utilizing more compounds to verify and confirm the noted trends. Examining different compounds could provide more support to these results and expand the knowledge within this area of research.
- Another possible area of further work would involve expanding the range of experimental conditions tested. This could be completed by operating at both slower and faster linear cooling rates to examine their effect on the purity and crystal size. Also increased mixing intensities could be tested in order to find the optimum conditions for the production of high purity crystals. As purity improvement is a major factor within industrial research and pharmaceutical development.

Chapter 10 References

1. Takiyama H. Supersaturation operation for quality control of crystalline particles in solution crystallization. Advanced Powder Technology. 2012;23(3):273-8.
2. Dunuwila DD, Berglund KA. ATR FTIR spectroscopy for in situ measurement of supersaturation. Journal of Crystal Growth. 1997;179(1-2):185-93.
3. Myerson AS. Handbook of Industrial Crystallization. Second ed: Butterworth-Heinemann; 2002.
4. Bari SB, Kadam BR, Jaiswal YS, Shirkhedkar AA. Impurity profile: Significance in Active Pharmaceutical Ingredient. Eurasian Journal of Analytical Chemistry. 2007;2(1):32.
5. Saito N, Yokota M, Fujiwara T, Kubota N. A note of the purity of crystals produced in batch suspension crystallization. Chemical Engineering Journal. 2001;84(3):573-5.
6. Berkovitch-Yellin Z, van Mil J, Addadi L. Crystal morphology engineering by “tailor-made” inhibitors: a new probe to fine intermolecular interactions. Journal of the American Chemical Society. 1985;107:3111-22.
7. Amanullah A, Serrano-Carreon L, Castro B, Galindo E, Nienow AW. The Influence of Impeller Type in Pilot Scale Xanthan Fermentations. Biotechnology And Bioengineering. 1998;57(1):95-108.
8. Baird MHI, Stonestreet P. Energy Dissipation in Oscillatory Flow within a Baffled Tube. Chemical Engineering Research And Design. 1995;73(5):503.
9. Ni X, Mackley MR, Harvey AP, Stonestreet P, Baird MHI, Rao NVR. Review Paper: Mixing Through Oscillations and Pulsations—A Guide to Achieving Process Enhancements in the Chemical and Process Industries. Chemical Engineering Research and Design. 2003;81:373-83.
10. Mackley MR, Tweddle GM, Wyatt ID. Experimental heat transfer measurements for pulsatile flow in baffled tubes. Chemical Engineering Science. 1990;45(5):1237-42.
11. ltd NTS. Report - Crystallisation of pharmaceutical compounds for industiral companies. 2010.
12. Paul EL, Tung H-H, Midler M. Organic crystallization processes. Powder Technology. 2005;150(2):133-43.
13. Widenski DJ, Abbas A, Romagnoli JA. A model-based nucleation study of the combined effect of seed properties and cooling rate in cooling crystallization. Computers & amp; Chemical Engineering. 2011;35(12):2696-705.
14. Davey R, Garside J. From Molecules to Crystallizers: An Introduction to Crystallization. First ed. Oxford: Oxford University Press; 2000 2006. 79 p.
15. Mullin JW. Crystallization - Thrid Eddition. 3 ed. Oxford: Butterworth-Heinimann; 1997. 521 p.
16. Sarkar D, Rohani S, Jutan A. Multi-objective optimization of seeded batch crystallization processes. Chemical Engineering Science. 2006;61(16):5282-95.
17. Doki N, Kubota N, Sato A, Yokota M. Effect of cooling mode on product crystal size in seeded batch crystallization of potassium alum. Chemical Engineering Journal. 2001;81(1-3):313-6.
18. Kim K-J, Mersmann A. Estimation of metastable zone width in different nucleation processes. Chemical Engineering Science. 2001;56(7):2315-24.
19. Revalor E, Hammadi Z, Astier J-P, Grossier R, Garcia E, Hoff C, et al. Usual and unusual crystallization from solution. Journal of Crystal Growth. 2010;312(7):939-46.
20. Cockrem MCM. Crystallization Technology Handbook. Edited by A. Mersmann. Chemical Engineering Science. 1996;51(5):839.
21. McCabe WL. Crystal growth in aqueous solutions I-Theory. Industrial and Engineering Chemistry. 1929;21(1):30-3.
22. Vekilov P. Nucleation. Crystal Growth and Design. 2010;10(12):5007-19.

23. Ulrich J, Strege C. Some aspects of the importance of metastable zone width and nucleation in industrial crystallizers. Journal of Crystal Growth. 2002;237–239, Part 3:2130-5.
24. Davey RJ, Schroeder SLM, ter Horst JH. Nucleation of Organic Crystals—A Molecular Perspective. Angewandte Chemie International Edition. 2013;52(8):2166-79.
25. Charmolue H, Rousseau RW. L-serine obtained by methanol addition in batch crystallization. AIChE Journal. 1991;37(8):1121-8.
26. Kobari M, Kubota N, Hirasawa I. Computer simulation of metastable zone width for unseeded potassium sulfate aqueous solution. Journal of Crystal Growth. 2011;317(1):64-9.
27. Strickland-Constable RF. The Breeding of Crystal Nuclei - A review of the Subject. Crystallization from Solution: Nucleation Phenomena in Growing Crystal Systems. 1972;68(121):1 - 7.
28. Aamir E, Nagy ZK, Rielly CD. Optimal seed recipe design for crystal size distribution control for batch cooling crystallisation processes. Chemical Engineering Science. 2010;65(11):3602-14.
29. Kubota N, Doki N, Yokota M, Sato A. Seeding policy in batch cooling crystallization. Powder Technology. 2001;121(1):31-8.
30. Callahan CJ, Ni X-W. Probing into Nucleation Mechanisms of Cooling Crystallization of Sodium Chlorate in a Stirred Tank Crystallizer and an Oscillatory Baffled Crystallizer. Crystal Growth and Design. 2012;12(5):2525-32.
31. Ni X, Liao A. Effects of mixing, seeding, material of baffles and final temperature on solution crystallization of L-glutamic acid in an oscillatory baffled crystallizer. Chemical Engineering Journal. 2010;156:226-33.
32. Funakoshi K, Takiyama H, Matsuoka M. Influences of seed crystals on agglomeration phenomena and product purity of m-chloronitrobenzene crystals in batch crystallization. Chemical Engineering Journal. 2001;81(1-3):307-12.
33. Doremus. Growth and perfection of crystals: international conference 1958: Wiley, 1958.; 1958.
34. Chianese A, Di Luozzo M, Kubota N. Effect of pyrogallol additive on the growth rate and the habit of hydroquinone crystals. Crystal Growth and Design. 2003;3(3):425-30.
35. Kubota N, Yokota M, Mullin JW. The combined influence of supersaturation and impurity concentration on crystal growth. Journal of Crystal Growth. 2000;212(3-4):480-8.
36. Mohameed HA, Abu-Jdayil B, Al Khateeb M. Effect of cooling rate on unseeded batch crystallization of KCl. Chemical Engineering and Processing: Process Intensification. 2002;41(4):297-302.
37. Lerond L, Muhr H, Plasari E, Hassoun M, Valery E, Ludemann-Hombourger O. Optimization of the cooling profile to improve the filterability of crystals isolated during an optical resolution by diastereomeric salt formation. Powder Technology. 2009;190(1-2):236-41.
38. Vega A, Díez F, Alvarez JM. Programmed cooling control of a batch crystallizer. Computers & Chemical Engineering.19, Supplement 1(0):471-6.
39. Hojjati H, Rohani S. Cooling and seeding effect on supersaturation and final crystal size distribution (CSD) of ammonium sulphate in a batch crystallizer. Chemical Engineering and Processing: Process Intensification. 2005;44(9):949-57.
40. Jones AG, Mullin JW. Programmed cooling crystallization of potassium sulphate solutions. Chemical Engineering Science. 1974;29(1):105-18.
41. Bohlin M, Rasmuson AC. Application of Controlled Cooling and Seeding in Batch Crystallization. Canadian Journal of Chemical Engineering. 1992;70(1):120-6.
42. Qu H, Pöllänen K, Louhi-Kultanen M, Kilpiö T, Oinas P, Kallas J. Batch cooling crystallization study based on in-line measurement of supersaturation and crystal size distribution. Journal of Crystal Growth. 2005;275(1–2):e1857-e62.
43. Martini S, Herrera ML, Hartel RW. Effect of cooling rate on nucleation behavior of milk fat-sunflower oil blends. Journal of Agriculture and Food Chemistry. 2001;49(7):3223 - 9.

44. Mayrhofer B, Nývlt J. Programmed cooling of batch crystallizers. Chemical Engineering and Processing: Process Intensification. 1988;24(4):217-20.
45. Givand JC, Teja AS, W. Rousseau R. Manipulating crystallization variables to enhance crystal purity. Journal of Crystal Growth. 1999;198-199, Part 2(0):1340-4.
46. Saito N, Yokota M, Fujiwara T, Kubota N. Liquid inclusions in crystals produced in suspension crystallization. Chemical Engineering Journal. 2000;79(1):53-9.
47. Poornachary SK, Chow PS, Tan RBH. Impurity Effects on the Growth of Molecular Crystals: Experiments and Modeling. Advanced Powder Technology. 2008;19(5):459-73.
48. Kubota N, Mullin JW. A kinetic model for crystal growth from aqueous solution in the presence of impurity. Journal of Crystal Growth. 1995;152(3):203-8.
49. Kubota N, Yokota M, Mullin JW. Supersaturation dependence of crystal growth in solutions in the presence of impurity. Journal of Crystal Growth. 1997;182(1–2):86-94.
50. Rauls M, Bartosch K, Kind M, Kuch S, Lacmann R, Mersmann A. The influence of impurities on crystallization kinetics – a case study on ammonium sulfate. Journal of Crystal Growth. 2000;213(1-2):116-28.
51. Brunsteiner M, Jones AG, Pratola F, Price SL, Simons SJR. Toward a Molecular Understanding of Crystal Agglomeration. Crystal Growth & Design. 2004;5(1):3-16.
52. Sangwal K. Kinetic effects of impurities on the growth of single crystals from solutions. Journal of Crystal Growth. 1999;203(1-2):197-212.
53. Nie Q, Wang J, Wang Y, Bao Y. Effects of Solvent and Impurity on Crystal Habit Modification of 11α-Hydroxy-16α, 17α-epoxyprogesterone. Chinese Journal of Chemical Engineering. 2007;15(5):648-53.
54. Pamplin. Crystal Growth.
55. Lawton S, Steele G, Shering P, Zhao L, Laird I, Ni X-W. Continuous Crystallization of Pharmaceuticals Using a Continuous Oscillatory Baffled Crystallizer. Organic Process Research & Development. 2009;13:1357-63.
56. Frobese D-H, Bohnet M. Heat transfer to liquids and suspensions in agitated narrow vessels. Chemical Engineering & Technology. 1989;12(1):324.
57. Matthews HB, Rawlings JB. Batch crystallization of a photochemical: Modeling, control, and filtration. AICHE Journal. 1998;44(5):1119-27.
58. Lodaya KD, Lahti LE, Jones ML. An Investigation into the Nucleation Kinetics of Urea Crystallization in Water by Means of Crystal-Size Distribution Analysis. Industrial & Engineering Chemistry Process Design and Development. 1977;16(3):294-7.
59. Nagata S. Mixing: principles and applications: Kodansha/Wiley, 1975.; 1975.
60. Nienow AW, Miles D. Impeller Power Numbers in Closed Vessels. Industrial & Engineering Chemistry Process Design and Development. 1971;10(1):41-3.
61. LeCaptain DJ, Berglund KA. The applicability of second harmonic generation for in situ measurement of induction time of selected crystallization systems. Journal of Crystal Growth. 1999;203(4):564-9.
62. Su Q, Nagy ZK, Rielly CD. Pharmaceutical crystallisation processes from batch to continuous operation using MSMPR stages: Modelling, design, and control. Chemical Engineering & Processing: Process Intensification. 2015;89:41-53.
63. Ristic RI. Oscillatory Mixing for Crystallization of High Crystal Perfection Pharmaceuticals. Chemical Engineering Research and Design. 2007;85(7):937-44.
64. Oliveira MSN, Ni X-W. Effect of hydrodynamics on mass transfer in a gas–liquid oscillatory baffled column. Chemical Engineering Journal. 2004;99(1):59-68.
65. Stonestreet P, Van Der Veeken PMJ. The Effects of Oscillatory Flow and Bulk Flow Components on Residence Time Distribution in Baffled Tube Reactors. Chemical Engineering Research and Design. 1999;77(8):671-84.
66. Ni X, Gélicourt YSd, Neil J, Howes T. On the effect of tracer density on axial dispersion in a batch oscillatory baffled column. Chemical Engineering Journal. 2002;85(1):17-25.
67. Mackley MR, Ni X. Experimental fluid dispersion measurements in periodic baffled tube arrays. Chemical Engineering Science. 1993;48(18):3293-305.

68. Mackley MR, Stonestreet P. Heat transfer and associated energy dissipation for oscillatory flow in baffled tubes. Chemical Engineering Science. 1995;50(14):2211-24.
69. Coulson JM, Richardson JF. Coulson & Richardson's Chemical Engineering. Vol. 1, Fluid Flow, Heat Transfer and Mass Transfer: Elsevier; 1999. 932p. p.
70. Ni X, Liao A. Effects of Cooling Rate and Solution Concentration on Solution Crystallization of L-Glutamic Acid in an Oscillatory Baffled Crystallizer. Crystal Growth & Design. 2008;8(8):2875 - 81.
71. Brown CJ, Adelakun JA, Ni X-w. Characterization and modelling of antisolvent crystallization of salicylic acid in a continuous oscillatory baffled crystallizer. Chemical Engineering & Processing: Process Intensification. 2015.
72. Armenante PM, Mazzarotta B, Chang G-M. Power consumption in stirred tanks provided with multiple pitched-blade turbines. Industrial & Engineering Chemistry Research. 1999;38(7):2809-16.
73. Baird MHI, Stonestreet P. Energy dissipation in oscillatory flow within a baffled tube. Trans IChemE. 1995;73(5):503-11.
74. Pinck LA, Kelly MA. The solubility of urea in water. J Am Chem Soc. 1925;47:2170-2.
75. Schnidman L, Sunier AA. The solubility of urea in water. J Phys Chem. 1932;36:1232-40.
76. Davey R, Fila W, Garside J. The influence of biuret on the growth kinetics of urea crystals from aqueous solutions. Journal of Crystal Growth. 1986;79(1-3, Part 2):607-13.
77. Zha M, Franzosi P, Zanotti L, Zuccalli G, Paorici C, Capelletti R, et al. Crystal growth and characterisation of urea by physical vapour transport in semi-open cells. Journal of Crystal Growth. 1995;146(1–4):29-36.
78. Mougin P, Wilkinson D, Roberts KJ. In situ ultrasonic attenuation spectroscopic study of the dynamic evolution of particle size during solution-phase crystallization of urea. Crystal Growth & Design. 2003;3(1):67 - 72.
79. Scott C, Black S. In-Line Analysis of Impurity Effects on Crystallisation. Organic Process Research and Development. 2005;9(6):890-3.
80. Acros-Organics. Saftey Data Sheet - Biuret 2011 [cited 2011]. Available from: https://extranet.fisher.co.uk/chemicalProductData_uk/wercs?itemCode=10190252&lang=EN.
81. Information NCfB. PubChem Compound Database Summary for CID 7913 - Biuret 2010 [cited 2015 Oct. 16, 2015]. Solubility data biuret]. Available from: https://pubchem.ncbi.nlm.nih.gov/compound/7913.
82. Lee F-M, Lahti LE. Solubility of urea in water-alcohol mixtures. Journal of Chemical & Engineering Data. 1972;17(3):304-6.
83. Gron H, Mougin P, Thomas A, White G, Wilkinson D, Hammond RB, et al. Dynamic in-process examination of particle size and crystallographic form under defined conditions of reactant supersaturation as associated with the batch crystallization of monosodium glutamate from aqueous solution. Industrial and Engineering Chemistry Research. 2003; 42(20):4888 - 98.
84. Technologies P. FlexIR Hollow Waveguide Accessory Installation and User Guide. In: Technologies P, editor. 1 ed. Madison, Wisconsin, USA: Pike; 2008. p. 1 -10.
85. Rouessac F, Rouessac A. Chemical Analysis : Modern Instrumentation Methods and Techniques: John Wiley; 2007. 601p. p.
86. Elmer P. FT-IR Spectroscopy Attenuated Total Reflectance (ATR) Technical Note. Technical Note FT-IR Spectroscopy [Internet]. 2005 25/05/2015 [cited 2015 01/07/2015]:[1 -5 pp.].
87. Van Overbeke A, Baeyens W, Van den Bossche W. Quantitative Fourier transform infrared/attenuated total reflectance analysis of ketoprofen in some pharmaceutical formulations. Vibrational Spectroscopy. 1995;9(2):121-30.
88. Rajalakshmi T, Fareed RSQ, Dhanasekaran R, Ramasamy P, Thomas J, Srinivasan K. Characterization of urea single crystals. Materials Science and Engineering: B. 1996;39(2):111-5.

89. Nasr-El-Din HA, Mac Taggart RS, Masliyah JH. Local solids concentration measurement in a slurry mixing tank. Chemical Engineering Science. 1996;51(8):1209-20.
90. Hlozny L, Sato A, Kubota N. (Short Communications) On-Line Measurement of Supersaturation during Batch Cooling Crystallization of Ammonium Alum. Journal of Chemical Engineering of Japan. 1992;25(5):604.
91. Togkalidou T, Fujiwara M, Patel S, Braatz RD. Solute concentration prediction using chemometrics and ATR-FTIR spectroscopy. Journal of Crystal Growth. 2001;231(4):534-43.
92. Scientific T. Application Note: 50730 - HIgh-Speed, High-Sensitivity Detectors for Use in the Mid-Infrared Spectral Range 2007 [cited 2014 03-12-2014]. Types of IR Dectors Explanation]. Available from: http://mmrc.caltech.edu/FTIR/Nicolet/Nicolet%20Tech%20Notes/MCT%20detector%20Thermo.pdf.
93. Christian. Analytical chemistry: Wiley, 1994.5th ed.; 1994.
94. Groen, H, Roberts, K J. An Examination of the Crystallization of Urea from Supersaturated Aqueous and Aqueous-Methanol Solutions as Monitored In-Process Using ATR FTIR Spectroscopy. Crystal Growth and Design. 2004;4(5):930-6.
95. Wülfert F, Kok WT, Smilde AK. Influence of Temperature on Vibrational Spectra and Consequences for the Predictive Ability of Multivariate Models. Analytical Chemistry. 1998;70(9):1761-7.
96. Pöllänen K, Häkkinen A, Reinikainen SP, Louhi-Kultanen M, Nyström L. A Study on Batch Cooling Crystallization of Sulphathiazole: Process Monitoring Using ATR-FTIR and Product Characterization by Automated Image Analysis. Chemical Engineering Research and Design. 2006;84(1):47-59.
97. Heigl N, Koller DM, Glasser BJ, Muzzio FJ, Khinast JG. Quantitative on-line vs. off-line NIR analysis of fluidized bed drying with consideration of the spectral background. European Journal of Pharmaceutics and Biopharmaceutics. 2013;85(3, Part B):1064-74.
98. Groen. On-line monitoring and control of supersaturation in batch crystallisers for organic fine chemical products using ATR FTIR spectroscopy / by Heidi Groen: Heriot-Watt University, 2001.; 2001.
99. Mukhopadhyay SM. Sample Preparation for Microscopic and Spectroscopic Characterization of Solid Surfaces and Films. 2003 [cited 08/10/2015]. In: Sample Preparation Techniquies in Analytical Chemistry [Internet]. John Wiley & Sons, [cited 08/10/2015]; [337 - 411]. Available from: http://www.spectroscopynow.com/userfiles/sepspec/file/specNOW/Tutorials/sample_prep_mitra_377-412.pdf.
100. Tachibana M, Horiuchi S, Wang JS, Kojima K. - Dislocation-Structures in Urea Single-Crystals by X-RAY Topography. Journal of Physics D - Applied Physics. 1993;- 26(- 8B):B145 - B8.
101. Instruments M. Morphologi G3 User Manual. 5 ed2013 2013. 1 - 284 p.
102. Adams S. The essential concepts of statistics. 1995. In: Principles of Statistics [Internet]. Available from: http://www.graphpad.com/guides/prism/6/statistics/index.htm?stat_the_essential_concepts_of_stat.htm.
103. Britannica EoE. Normal distribution. Encyclopedia Britannica2014.
104. Liu C. Lab 8: z-score and Normal Distribution [cited 2015 05/02/2015]. Available from: http://people.hofstra.edu/Cong_Liu/PSY40/8_Lab.html.
105. StatSoft I. How to Analyze Data with Low Quality or Small Samples, Nonparametric Statistics. 2013 [cited 12/12/2014]. In: Electonic Statistics Textbook [Internet]. Tulsa, [cited 12/12/2014]. Available from: http://www.statsoft.com/Textbook/Nonparametric-Statistics.
106. Hoskin T. Parametric and Nonparametric: Demystifying the Terms[cited 2015:[5 p.]. Available from: http://www.mayo.edu/mayo-edu-docs/center-for-translational-science-activities-documents/berd-5-6.pdf.
107. Trek S. Null Hypothesis 2015 [cited 2015 30/01/2015]. Available from: http://stattrek.com/statistics/dictionary.aspx?definition=null_hypothesis.

108. Department P. ANOVA: ANalysis Of VAriance between groups: College of Saint Benedict & Saint John's University; [cited 2015 30/01/2015]. Available from: http://www.physics.csbsju.edu/stats/anova.html.
109. Department P. Student's *t*-Tests: College of Siant Benedict and Siant John's University; [cited 2015 02/02/2015]. Available from: http://www.physics.csbsju.edu/stats/t-test.html.
110. Britannica EoE. Student's t-test. 2015 ed2014.
111. Zaiontz C. Wilcoxon Rank Sum Test for Independent Samples 2014 [cited 2015 02/02/2015]. Available from: http://www.real-statistics.com/non-parametric-tests/wilcoxon-rank-sum-test/.
112. Measuring Usability L. Fundamentals of Statistics 1: Basic Concepts:: Nominal, Ordinal, Interval and Ratio [cited 2015 02/02/2015]. Available from: http://www.usablestats.com/lessons/noir.
113. Physics Do. Kolmogorov-Smirnov Test 2015 [cited 2015 28/01/2015]. Available from: http://www.physics.csbsju.edu/stats/KS-test.html.
114. Lowry R. The Kruskal-Wallis Test for 3 or More Independent Samples. 2013. In: Inferential Statistics [Internet]. [1 - 6]. Available from: www.vassarstats.net/textbook/.
115. Callahan CJ, Ni XW. An investigation into the effect of mixing on the secondary nucleation of sodium chlorate in a stirred tank and an oscillatory baffled crystallizer. CrystEngComm. 2014;16(4):690 - 7.
116. Baldi G, Conti R, Gianetto A. Concentration profiles for solids suspended in a continuous agitated reactor. AIChE Journal. 1981;27(6):1017.
117. Mullin JW, Raven KD. Influence of Mechanical Agitation on the Nucleation of Some Aqueous Salt Solutions. Nature. 1962;195(4836):35.
118. Yu ZQ, Tan RBH, Chow PS. Effects of operating conditions on agglomeration and habit of paracetamol crystals in anti-solvent crystallization. Journal of Crystal Growth. 2005;279(3–4):477-88.
119. Qu H, Louhi-Kultanen M, Kallas J. In-line image analysis on the effects of additives in batch cooling crystallization. Journal of Crystal Growth. 2006;289(1):286-94.
120. Yuan Y, Leng Y, Huang C, Yue M, Tan Q. Effects of cooling rate, saturation temperature, and agitation on the metastable zone width of DL-malic acid-water system. Russian Journal of Physical Chemistry. 2015;89(9):1567.

Appendix A – Effect of Mixing on FTIR Probe

Table A.1 – Average concentration values and standard deviations for OBC and STC

Vessel	Trial number	Un-mixed system		Mixed system	
		Average concentration (g ml^{-1})	Standard deviation	Average concentration (g ml^{-1})	Standard deviation
OBC	1	1.339	0.013	1.344	0.008
	2	1.364	0.059	1.340	0.006
STC	1	1.321	0.008	1.342	0.007
	2	1.373	0.043	1.338	0.007

Table A.2 – Average supersaturation values for un-mixed and mixed systems in the OBC and STC

Vessel	Trial number	Un-mixed system		Mixed system	
		Average supersaturation	Standard deviation	Average supersaturation	Standard deviation
OBC	1	0.872	0.009	0.869	0.005
	2	0.889	0.038	0.866	0.004
STC	1	0.861	0.005	0.867	0.004
	2	0.908	0.027	0.868	0.005

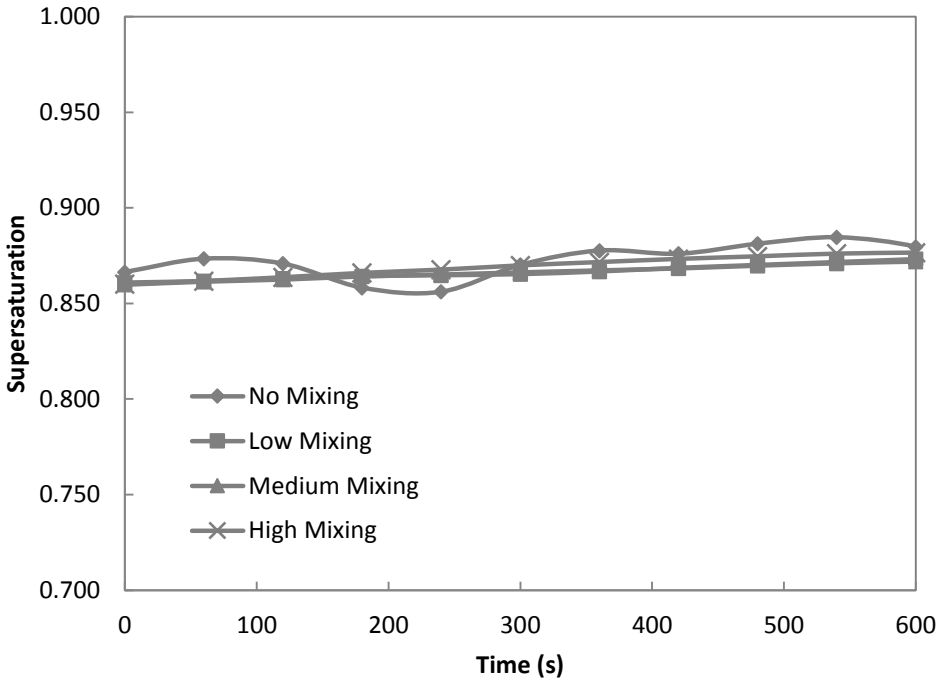

Figure A.1 – Supersaturation curves for OBC with varying levels of mixing

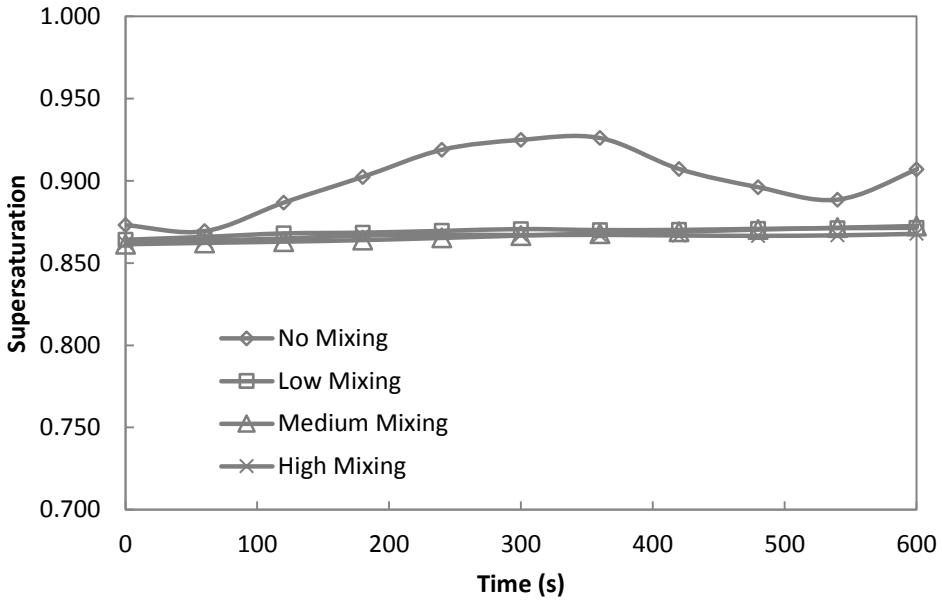

Figure A.2 – Supersaturation curves for STC with varying levels of mixing